Design and Analysis of Active Fluid-and-Cellular Solid Composites
for Controllable Stiffness Robotic Elements

by

Nadia G. Cheng

B.S. Aerospace Engineering
University of California, San Diego, 2007

Submitted to the Department of Mechanical Engineering
in Partial Fulfillment of the Requirements for the Degree of
Master of Science in Mechanical Engineering

at the

Massachusetts Institute of Technology

May 2009
[JUNE]

Signature of Author.....
Department of Mechanical Engineering
May 22, 2009

Certified by.....
Karl Iagnemma
Principal Research Scientist of Mechanical Engineering
Thesis Supervisor

Accepted by.....
David E. Hardt
Professor of Mechanical Engineering
Graduate Officer

Design and Analysis of Active Fluid-and-Cellular Solid Composites
for Controllable Stiffness Robotic Elements

by

Nadia G. Cheng

Submitted to the Department of Mechanical Engineering
on May 22, 2009 in Partial Fulfillment of the
Requirements for the Degree of Master of Science in
Mechanical Engineering

ABSTRACT

The purpose of this thesis is to investigate the use of a new class of materials for realizing soft robots. Specifically, meso-scale composites—composed of cellular solids impregnated with active fluids—were be designed to have controllable stiffness to take the form of a continuous body of a soft robot. This represents an improvement compared to past efforts in soft robotics, which often involved modifying the infrastructure of current, rigid robots to yield softer ones. This latter approach often faced the challenges of developing actuators that were "soft" but still discrete, and were limited in performance. In contrast, the controllable-stiffness composites proposed in this thesis eliminate the need for multiple actuators; a single structure can transition between various states to serve as both rigid, load-bearing components as well as morphable, compliant ones. While the vast range of fluid-foam combinations for such an application have yet to be explored, the work presented here focuses on a specific composite: open-cell polyurethane foam impregnated with wax. This type of composite can be thermally activated to exhibit both solid and nearly fluid states (while the wax can be melted to become a fluid, the foam holds the composite together as a pseudo-solid). This thesis discusses the research that has been conducted to 1) characterize the mechanical properties of wax-foam composites as well as 2) investigate possible ways in which the composites can be used as robotic components.

Thesis Supervisor: Karl Iagnemma
Title: Principal Research Scientist of Mechanical Engineering

ACKNOWLEDGMENTS

I am very grateful to the National Defense Science and Engineering Graduate Fellowship program, whose funding continues to allow me to pursue invaluable research opportunities. Thank you to the DARPA ChemBots program, whose vision and funding made the work presented in this thesis possible.

Dr. Karl Iagnemma, Professor Anette Hosoi, Professor Gareth McKinley, and Professor Martin Culpepper—I truly appreciate you all for being such great leaders on SQUISHbot and for always having the students' interests in mind. Dr. Iagnemma, thank you for all the time you have invested into helping me strive for my personal best. To Dr. Iagnemma and Prof. Hosoi, your patience, enthusiasm, and sound advice have helped me grow substantially as a researcher. Thank you, Prof. Culpepper, for welcoming me into your lab space and for always making yourself available as a mentor. Mr. Pierce Hayward, thank you for being so generous with your time; you have greatly contributed to the experimental work presented in this thesis as well as my learning experience. My talented and inspiring colleagues—Maria Telleria, Sarah Bates, Randy Ewoldt, and Dr. Arvind Gopinath—you have largely contributed to making SQUISHbot a wonderful and enjoyable experience. I am extremely lucky to be part of such a great team of people and researchers.

To my family, friends, and especially Max, your everyday support and encouragement have given me the drive and resilience to make this thesis something that I am proud of. Thank you, Mom, Dad, and Lara, for all the years of unbounded and unwavering love and support. Through demonstration, you have taught me that happiness and fulfillment come from being thankful for and making the most of all that I am given. And for that, I am eternally grateful.

CONTENTS

Abstract 2

Acknowledgments 4

Contents 6

Figures 9

Tables 13

1 Introduction 14

1.1 Proposed approach: tunable continuous structures 15

1.2 SQUISHbot: Its role in the development of novel composites for soft robotics 16

1.3 Research and development of wax-filled foams 17

2 Mechanical characteristics of active fluid-foam composites 19

2.1 Testing equipment descriptions 20

2.1.1 Zwick/Roell Z2.5 20

2.1.2 TA-XTplus Texture Analyzer 22

2.2 Selection process for composite combination 24

2.2.1 Fluid class selection 24

2.2.1.1 Magnetorheological (MR) fluid 24

2.2.1.2 Solder 26

2.2.1.3 Hot glue 28

2.2.1.4 Wax 29

2.2.2 Wax-foam combination selection 29

2.2.2.1 Waxes and foams considered 29

2.2.2.2 Sample preparation method 31

2.2.2.3 Test method 33

2.2.2.4 Results and conclusions 34

2.3 Basic composite characterization 37

2.3.1 Compression test data 38
2.3.1.1 Foam only 38
2.3.1.2 Wax only 43
2.3.1.3 Composites 56
2.3.2 Volume fraction dependent tests for 1 cm diameter samples 61
2.3.2.1 Sample preparation: use of adapted tweezers 61
2.3.2.2 Results and analysis 63
2.3.3 Experimental validation of theoretical model for composites with small volume fractions 67
2.3.3.1 Model description 67
2.3.3.2 Sample preparation process 71
2.3.3.3 Test results 73
2.3.3.4 A comparison between the test data and the predicted data 76
2.4 Future work for composite characterization 77
2.4.1 Cyclic testing 77
2.4.2 Bending tests 80
2.4.3 Acquire temperature-dependent data 83
2.4.4 Developing and validating predictive models using 3D-printed foams 83
2.4.4.1 Using 3D-printed foam as platform for developing predictive models 84
2.4.4.2 Designing anisotropy into foam structures 85

3 Robotic applications for wax-foam composites 91
3.1 To-date case studies 91
3.1.1 Universal joints 91
3.1.2 Three-legged mechanism modeled after Boston Dynamics robot 93
3.1.3 Spine proof-of-concept 97
3.2 Future work 101
3.2.1 Thermal activation challenges 101
3.2.2 Development of a functioning spine 102
3.2.3 Implementation of a functioning compression module 102

4 Conclusions 105

References **107**

FIGURES

Figure 2.1: Blown-up photo of sample, labeled "10," under compression between two platens. 21
Figure 2.2: Stiffness calibration test for Zwick testing machine using a 2.5 kN load cell. 22
Figure 2.3: Blown-up photo of sample, labeled "8," under compression between a moving platen and a fixed platform on the Texture Analyzer. 23
Figure 2.4: System calibration test for Texture Analyzer using 5 kg load cell. 24
Figure 2.5: Schematic of basic principle of how MR fluid operates between activated and non-activated. 25
Figure 2.6: Images from tests to determine stiffness capabilities of MR fluid-filled foams. 26
Figure 2.7: A solder droplet on a foam surface to demonstrate that the wetting angle $\theta > 90^{\circ}$ means that the solder does not preferentially wick into the foam 27
Figure 2.8: Foam samples, after being cut into cylinders, before being saturated with wax. Starting from the black-colored samples going clockwise: quick-recovery PU (black), slow-recovery (2) (green) PU, slow-recovery (1) (bright yellow) PU, super absorbent PU (white), [dime], unknown PU (dull yellow). 32
Figure 2.9: Stress vs. strain data for 20 different wax-foam composites 35
Figure 2.10: Image of PU (2) foam taken under optical microscope 38
Figure 2.11: Image of foam-cutting set-up. 40
Figure 2.12: Stress vs. strain data for PU (2) foam cylinders. 41
Figure 2.13: Modulus vs. diameter data for foam cylinders. 42
Figure 2.14: Images of select steps from the wax sample preparation process described in Table 2.11 45
Figure 2.15: Stress vs. strain data from compression tests performed on wax cylinders that were 10 mm tall and had varying diameters of 10 mm (black), 20 mm (green), 30 mm (blue), and 40 mm (red) 47
Figure 2.16: Effective modulus vs. aspect ratio data from compression tests performed on wax cylinders that were 10 mm tall and had varying diameters of 10 mm, 20 mm, 30 mm, and 40 mm. 48

Figure 2.17: Stress vs. strain data from compression tests performed on wax cylinders that were 22 mm tall and had varying diameters of 10 mm (black), 15 mm (green), 20 mm (blue), and 25 mm (red)..... 51
Figure 2.18: Effective modulus vs. aspect ratio data from compression tests performed on wax cylinders that were 22 mm tall and had varying diameters of 10 mm, 15 mm, 20 mm, and 25 mm. 52
Figure 2.19: Effective modulus vs. aspect ratio data for two sets of wax samples made from polymer molds. 53
Figure 2.20: Effective modulus vs. diameter data for two sets of wax samples made from polymer molds. 54
Figure 2.21: Effective modulus vs. diameter data for three sets of wax samples: two sets made from polymer molds and one set made from boring cylinders out of a wax slab..... 55
Figure 2.22: Stress vs. strain data for 25.4 mm-tall fully saturated cylindrical composites with varying diameters of 10 mm (black), 15 mm (green) 20 mm (blue), and 25 mm (red)..... 57
Figure 2.23: Stress vs. strain data for 38.1 mm-tall fully saturated cylindrical composites..... 58
Figure 2.24: Effective modulus vs. aspect ratio data for both composites and wax samples..... 59
Figure 2.25: Effective modulus vs. diameter data for both composites and wax samples. 60
Figure 2.26: 3D-printed tweezers fittings used to limit the distance a pair of tweezers could be compressed to. Fittings were made to limit the compression height to 0.375", 0.25", and 0.125" (the initial height of each composite sample was 0.5"). 61
Figure 2.27: Images showing steps for producing composites with controlled volume fractions.62
Figure 2.28: Mass vs. compressed height (of saturated foam sample before being removed from wax bath) of final composite. Foam cylinder samples (12.7-mm height, 10-mm diameter) were with of super absorbent PU (1). 63
Figure 2.29: Stress vs. strain data for composites with varying volume fractions. The data is color coded as follows: fully saturated composite (black), composite compressed to 0.375" in wax bath (green), composite compressed to 0.25" in wax bath (blue), and composite compressed to 0.125" in wax bath (red). 65
Figure 2.30: Effective modulus vs. volume fraction for foam cylinder samples (12.7 mm height, 10 mm diameter) made with super absorbent PU (1). 66
Figure 2.31: Images of PU (2) foam, in various states, taken under an optical microscope. 69

Figure 2.32: Tongs used to prepare minimally saturated composite samples. 72
Figure 2.33: Select images from sample preparation process for making minimally saturated wax-foam composites. 73
Figure 2.34: Effective modulus vs. volume fraction data for composites with low volume fractions 74
Figure 2.35: Effective modulus vs. volume fraction for composites with low volume fractions. Sample sizes were 25 mm in diameter and 25 mm tall 75
Figure 2.36: Effective modulus vs. volume fraction for composites with low volume fractions to compare empirical data with predicted values. 76
Figure 2.37: Stress vs. strain data for a single composite sample compressed for 6 complete cycles 78
Figure 2.38: The ratio of plastic strain/elastic strain vs. cycle; data was obtained from Figure 2.37 79
Figure 2.39: Test set-up on Zwick for bending tests on beam samples. A fully saturated wax-foam composite is shown here, with L = 38.4 mm. 81
Figure 2.40: Force vs. displacement curves from several preliminary bending tests performed on fully saturated wax-foam composite beams. All the beams were roughly 13 mm tall, 10 mm wide, and 38.4 mm long (the latter of which was defined by the test jig). 82
Figure 2.41: Examples of 3D-printed foams 84
Figure 2.42: Two open-cell 3D-printed foams that respond differently to the same applied force. 85
Figure 2.43: Two different anisotropic modules—one that shears and another that compresses when the same normal force is applied—are joined in series 86
Figure 2.44: 3D sphere design used to demonstrate anisotropic stiffness. 87
Figure 2.45: 3D-printed anisotropic sphere. 88
Figure 2.46: Compression tests results for a 3D-printed sphere. 89
Figure 3.1: A wax-filled cylindrical beam, 10 mm in diameter, in its non-actuated (to left) and actuated (top right) states. A series of images also shows the beam during the activation process, during which the joint transformed from being a rigid to compliant via resistive heating 92
Figure 3.2: Boston Dynamics version of 3-legged robot (CAD model). Image courtesy of Boston Dynamics. 94

Figure 3.3: 3-legged mechanism with fluid-foam composites acting as bending joints..... 95
Figure 3.4: 3-legged mechanism with composite bending joints in its maximally compressed state during a test. 96
Figure 3.5: Concept for single-actuator, multiple-activators spine..... 98
Figure 3.6: Proof-of-concept demonstration of spine. 100
Figure 3.7: Proof-of-concept spine shown in a series of configurations. 101
Figure 3.8: CAD model for compression module that can be integrated into spine mechanism. 103
Figure 3.9: A demonstration of a prismatic element that can be integrated into the single-actuator spine concept..... 104

TABLES

Table 2.1: Select specifications of the Zwick materials testing machine 20
Table 2.2: Select specifications of the Texture Analyzer materials testing machine 22
Table 2.3: Dynamic viscosities of hot glue 28
Table 2.4: Dynamic viscosities of wax 29
Table 2.5: Waxes considered for composites 30
Table 2.6: Foams considered for composites 31
Table 2.7: Sample preparation method for composite selection process 32
Table 2.8: Specifications for compression tests performed on Zwick testing machine 34
Table 2.9: Effective compression moduli for twenty wax-foam composites in units of GPa. 36
Table 2.10: Select properties of the batik wax 37
Table 2.11: Preparation process for cylindrical wax samples 44
Table 2.12: Procedure for producing composites with controlled volume fractions 62
Table 2.13: Description of variables introduced in the predictive model 68
Table 2.14: Steps for producing minimally saturated composites. 72

CHAPTER 1

INTRODUCTION

The term "soft robot" is difficult to define because the concept, for many people, exists only in the imagination. Perhaps taking a traditional robot and making all its rigid components "soft" makes a soft robot. But if one looks beyond the conventional concept of robotics, a more radical definition exists. The notion that a continuous, controllable "flesh" can be designed to perform tasks—ones that modern-day robots might not even be capable of—is the inspiration for the type of soft robots that the work in this thesis strives to develop a foundation for.

Because many challenges inhibit the creation of a truly soft robot, gradual efforts have been made to transform traditional robots into "softer" ones to perform tasks or operate in environments that current robots are unable to. As industrial and service robots become more common, one main motivation for developing soft robots has been to make robots safe for humans to work alongside. A common approach for achieving this has been to make robots more sensitive to their environments using technologies such as smart skins impregnated with sensors [1] or light-weight and flexible limbs with powerful torque sensing capabilities [2]. Similarly, another need for soft robotic components has been prompted by the increasing use of wearable devices that require relatively large actuators, for instance in medical applications [3]. In addition to external devices, soft robots can even be designed to traverse and interact with the internal organs of humans, reducing the risks and complications of invasive procedures. Even robots that do not interact with humans, such as rovers that traverse rough terrains, might benefit from being deformable and soft [4] to be more adaptable to their surroundings rather than having rigid and unyielding components that limit a robot's capabilities.

The potential applications for soft robotics extend beyond the aforementioned areas, but existing efforts have yet to realize the possibilities. In the meantime, most of the work in soft

robotics has involved replacing discrete, rigid components with softer, more tunable ones. Soft artificial actuators—such as those based on polymeric, piezoelectric, magnetostrictive, and electrostatic principles—have been developed to mimic muscle elements [5]. Some work has even been done to integrate natural, living muscles into robots for actuation [6], [7]. While these soft actuator technologies are impressive, traditional robotics components overwhelmingly outperform them in areas like position accuracy and bandwidth [4].

Not only have actuators been developed to resemble natural muscles, but entire robots have been biologically inspired; scientists and engineers attempt to design systems to exploit mechanisms that are used by creatures in nature to improve the functionality of robots. To achieve the dexterity and "softness" of species such as octopuses [8] and snakes [10], engineers have often implemented many actuators in a system rather than utilizing continuous, tunable structures. Consequently—and even though some of these robots exhibit very smooth, fluid motion—their bodies are limited in their overall compliance. One example of a squishy robot that has many actuators is a caterpillar-inspired one, whose multiple SMA actuators can be considered to be very compliant and passively conformable [9]. While this type of robot might present one kind solution for actualizing soft robotics, the work in this thesis proposes to approach the problem by moving away from the need to utilize many discrete actuators and, instead, develop novel, smart composites that can be used as a robot's tunable and continuous flesh.

1.1 Proposed approach: tunable continuous structures

The purpose of this thesis is to investigate and encourage the development of tunable materials with locally controllable stiffness to be utilized as functional robotics components. Specifically, the proposed structures are meso-scale composites made of cellular solids containing active fluids that can exhibit drastic changes in stiffness.

An excellent example of a controllable-stiffness composite is a magnetorheological (MR) elastomer, which is a rubbery polymer that contains magnetizable particles. When a magnetic field is applied to this material, its bulk properties change as the particles align along the direction of the magnetic field; the material can go from being isotropic to exhibiting directional stiffness. However, because an MR elastomer does not undergo drastic changes in modulus

when it is activated, it is mostly used in activated dampening mechanisms such as tunable automotive suspensions [11].

Other applications that might benefit from similar materials include morphing aircraft, adaptive prosthetics and orthotics, and shock-absorbing structures. A broad range of techniques have been used in attempt to realize such applications, including: thermally responsive materials such as shape-memory polymers, ionic gels, magneto- and electrorhelological fluids and gels, piezoelectric and magnetostrictive ceramics, and electroactive polymers, to name a few. These novel technologies rely on chemical and physical mechanisms to achieve actuation or changes in mechanical properties. By utilizing these mechanisms in meso-scale composites, components can be designed to optimize the performance of the overall structure [12].

1.2 SQUISHbot: Its role in the development of novel composites for soft robotics

Though the larger goal of the work presented here was to contribute to developing a platform for soft robotics, it was initially inspired by and is part of a project called SQUISHbot. The project team consists of researchers from Boston Dynamics and a group of researchers from MIT led by Prof. Martin Culpepper, Prof. Anette Hosoi, Dr. Karl Iagnemma, and Prof. Gareth McKinley (Robert Playter of Boston Dynamics and Prof. Anette Hosoi are co-PIs of the project). SQUISHbot is funded by a DARPA program called Chemical Robots (ChemBots), whose aim was to "create a new class of soft, flexible, meso-scale mobile objects that can identify and maneuver through openings smaller than their dimensions and perform various task." While DARPA wanted researchers to develop this new class of soft robots to improve the capabilities of unmanned platforms to help "warfighters... gain access to denied spaces and perform tasks safely, covertly, and efficiently" [13], one can imagine how the science and technology behind these novel, morphable systems can contribute to broader applications in society.

The ChemBots program uses a set of metrics to determine the success of the research during Phase I, which was slated to be 18 months long (at the time this thesis was written, eight months still remained in Phase I). The required milestones for the Phase I are as follows: "Demonstrate a ChemBot, approximately the size (but not necessarily the form-factor) of a regulation softball (i.e., 30 cm circumference; 10 cm diameter; 500 cm^3 volume), that can:

a) travel a distance of 5 meters at a speed of 0.25 meters/minute;
b) achieve a 10-fold reduction in its largest dimension; and
c) traverse through a 1 cm opening of arbitrary geometry and reconstitute its original size and shape, in 15 seconds"

It was also desirable for the robot to be capable of carrying and manipulating an arbitrary payload [13].

Creating a robot that can change dimensions was not the primary challenge for SQUISHbot, as many robots have been designed to mechanically expand and contract; robots with telescoping mechanisms are a good example of this [21], [22]. The difficult and interesting research problem inferred by the overall goal of the project was to create a morphable soft robot. The approach that was chosen to accomplish this, as previously mentioned, was to develop a novel class of smart, tunable materials that could take the form of functional robots.

In addition to the aforementioned DARPA-specified Phase I milestones, the SQUISHbot team of researchers also wanted its robot to be capable of climbing walls, drawing inspiration from an earlier robot, named Robosnail, that had been developed under the guidance of Professors Hosoi and McKinley in the Hatsopoulos Microfluidics Laboratory at MIT. Robosnail was a robot designed to mimic the way snails locomote using a phenomenon called adhesive locomotion. This is how snails use their excreted pedal mucus to travel on a wide range of substrates, including inverted ones [23], [24]. The focus of the work presented in this thesis does not concern adhesive locmotion; however, some of the technologies considered during the development of the tunable materials were influenced by the research that was being conducted in parallel to develop an adhesive locomotion-based platform for SQUISHbot.

1.3 Research and development of wax-filled foams

Largely motivated by the functional requirements of SQUISHbot, wax-filled foams were selected as the active-fluid-and-cellular-solid composites to be developed and studied in detail. The tunable material for the soft robot had to be capable of morphing while having adequate stiffness to act as a load-carrying structure. Specifically, flexible open-cell polyurethane foams and batik wax were used; other wax-foam combinations that are more appropriate might be realized in future work. A thorough description of the materials selection process is in 2.2.2.

The benefit of studying these meso-scale composites is that both waxes and foams are widely commercially available; they can create countless combinations, providing a vast design space that can be readily realized in the laboratory. The unique concept of using a "fluid" (this term is used loosely, as wax has a solid state) like wax as a structural component is that it can be thermally-activated to undergo drastic changes in viscosity and stiffness. Foams—or, more generally, cellular solids—exist both synthetically and in nature because of their unique capabilities as functional, light-weight structures [14]. The open-cell flexible polyurethane foams used in this research were selected for their compliance and excellent wicking capabilities.

Significant research continues to be conducted to model and predict the behavior of many different types of cellular solids [14]. Constitutive models for fluid-filled foams have been developed to predict the mechanical behavior of certain foods like vegetables, whose structures are essentially fluid-filled, closed-cell foams [15], [16]. With relevance to the thermal-activation required to alter the state of the wax in the composites, research has also been conducted to characterize the thermal properties of foams with fluids in them. However, this area of research mostly concerns metal foams, as they are widely utilized for thermal-insulation purposes [17], [18].

With the flexible foam acting as a scaffold in which the wax can be passively stored and flow throughout, the composite can transition from being a high-modulus structural element to a compliant one when the wax is melted. A large portion of this thesis is concerned with characterizing and understanding the mechanical properties of wax-foam composites. Mostly, composites have been studied in their rigid states; future work will involve studying the composites in their compliant states.

Finally, several patents that involve wax-filled foams—for example, a type of gasket [19] and a new material for toy or model sets [20]—have been issued in years past. However, the pairing of these two seemingly disparate materials has never been used in robotics applications.

CHAPTER

2

MECHANICAL CHARACTERIZATION OF ACTIVE FLUID-FOAM COMPOSITES

The overall challenge of SQUISHbot was to develop a novel mechanism to enable fabrication of a wall-climbing, payload-carrying soft robot. Therefore, it was desirable to have a single structure that could achieve desired configurations to locomote and apply necessary loads but did not employ rigid mechanical components. One concept for accomplishing this was to develop a structure with controllable stiffness, i.e., one that allows the same part of the robot can be rigid at one moment and then compliant the next. For instance, rather than utilizing traditional ball-and-socket joints to create a universal joint, the robot could have a continuous beam-like structure—one that has the potential to be highly compliant—that can bend in arbitrary locations and maintain arbitrary configurations, just as an octopus arm appears to do.

To achieve such controllable stiffness, the concept of using a lattice structure to store a controllable-stiffness medium was developed. A simple implementation of this could use a cellular solid, or foam, containing a fluid that can actively vary its rheological properties. Favorable properties of foam include: "shape memory" (like a kitchen sponge, some foams can return to their original shapes after being externally deformed) and wickability (also like a kitchen sponge, some foams absorb certain fluids very well). Both of these properties are important because they would allow the foam-fluid composite to be self-restoring after being deformed.

While the general class of active-fluid-and-cellular-solid composites can include an overwhelming number of combinations, the bulk of this chapter focuses on a small group of composites that can be readily produced with commercially available fluids and foams. Though different composites' mechanical properties and modes of operation can differ greatly from one

another, understanding and exploiting their individual capabilities can open new possibilities for designers of soft robotics.

To understand how utilizing a fluid-foam composite as a structural component contributes to a design space, a thorough understanding of the composite's structural properties is required. This chapter describes several fluid-foam combinations that have been considered as well as the testing and analysis performed to characterize a specific wax-foam composite.

2.1 Testing equipment descriptions

Two materials testing machines were used to perform various compression and bending tests. Zwick/Roell's Z2.5 was used during tests that required large applied loads, while Stable Micro Systems' TA-XTplus Texture Analyzer was used for tests that required small applied loads.

2.1.1 Zwick/Roell Z2.5

Select specifications of the Zwick testing machine are listed in Table 2.1. An image of the Zwick machine during a compression test is shown in Figure 2.1.

Table 2.1: Select specifications of the Zwick materials testing machine

Measurable force range	10 N—2.5 kN
Force resolution	0.01 N
Crosshead displacement resolution	0.01 mm

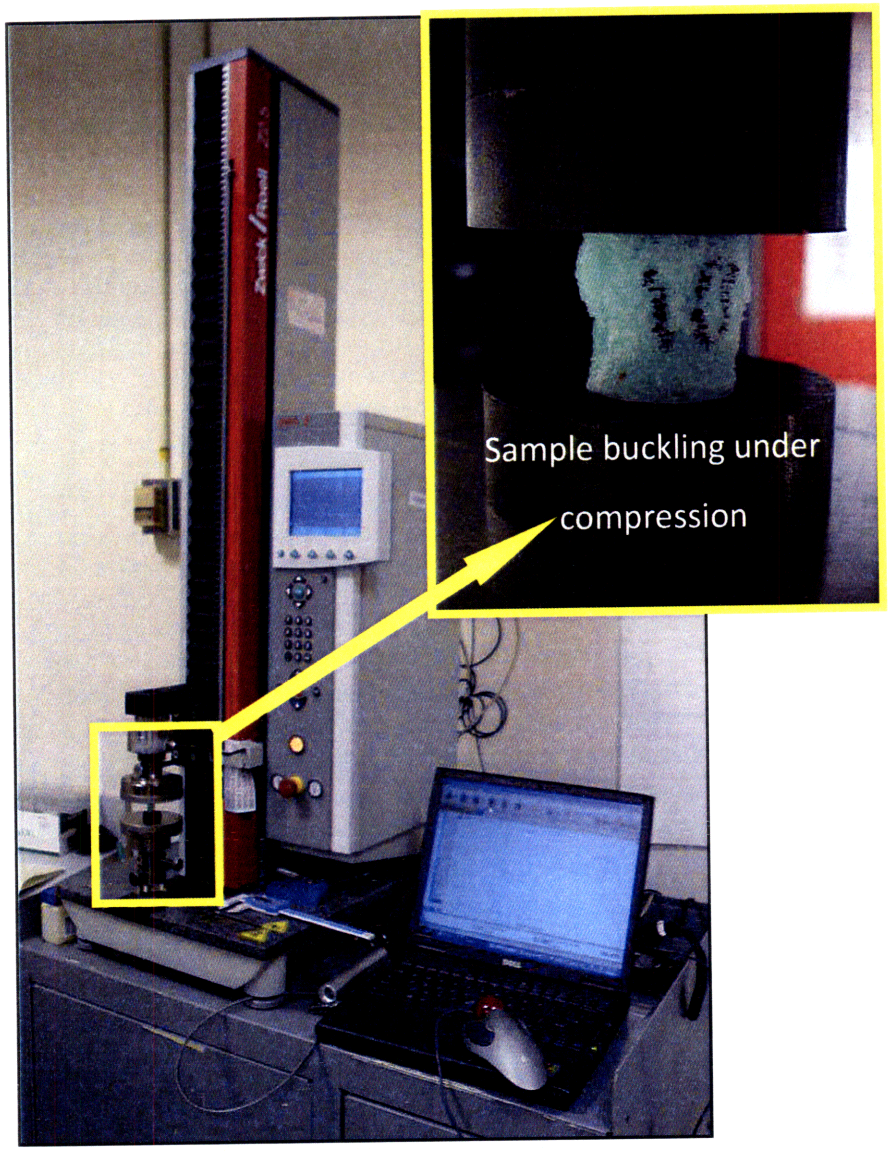

Figure 2.1: Blown-up photo of sample, labeled "10," under compression between two platens.

The machine has an internal system compliance, which effectively produces apparent displacement values that are different from the actual amount a sample is deformed. To compensate for the system compliance, the stiffness of the machine was determined by performing a compression test with the machine platens flush against each other. A force vs. displacement test, whose data is shown in Figure 2.2, determined that the stiffness of the machine was 5328.773 N/mm. This value for the machine stiffness was factored into the apparent stiffness of each test sample by treating the machine as a spring in series with a test sample.

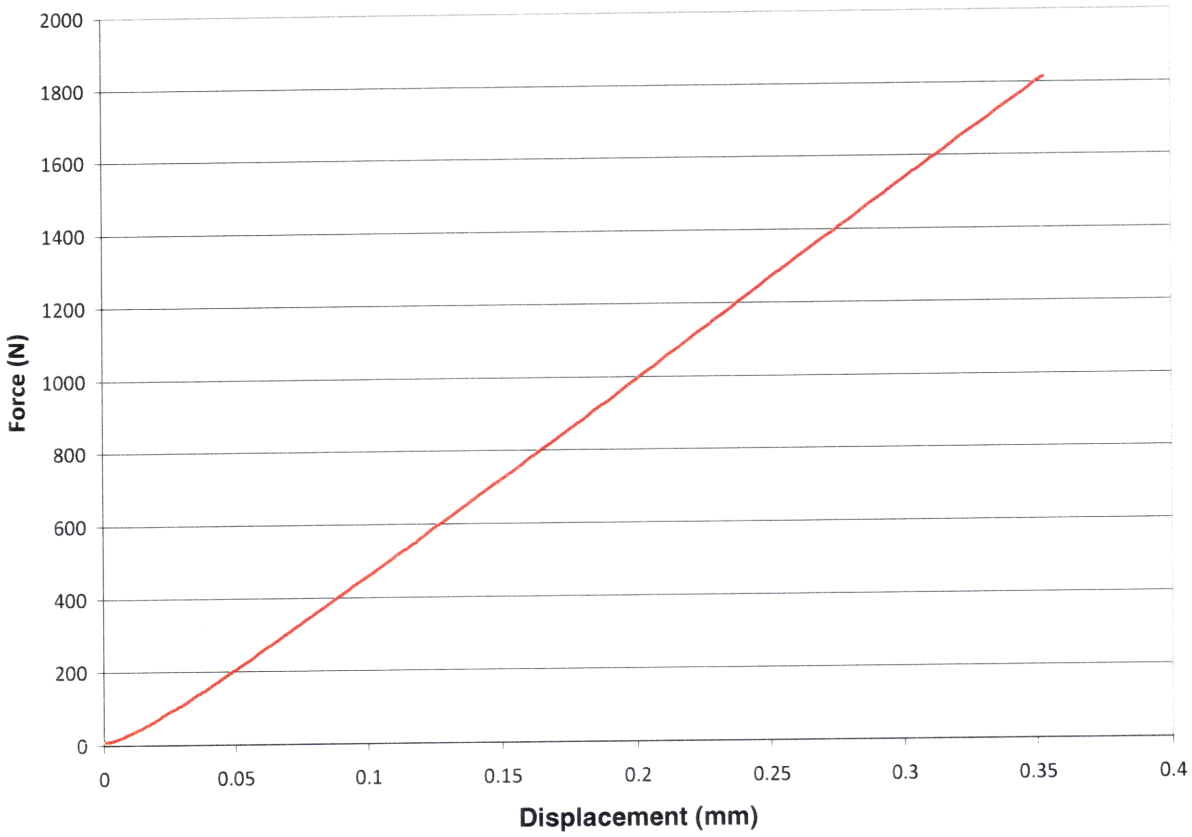

Figure 2.2: Stiffness calibration test for Zwick testing machine using a 2.5 kN load cell.

2.1.2 TA-XTplus Texture Analyzer

Select specifications of the Texture Analyzer are listed in Table 2.2. An image of the Texture Analyzer during a compression test is shown in Figure 2.3.

Table 2.2: Select specifications of the Texture Analyzer materials testing machine

Measurable force range	0—250 N
Force resolution	0.01 N
Crosshead displacement resolution	0.01 mm

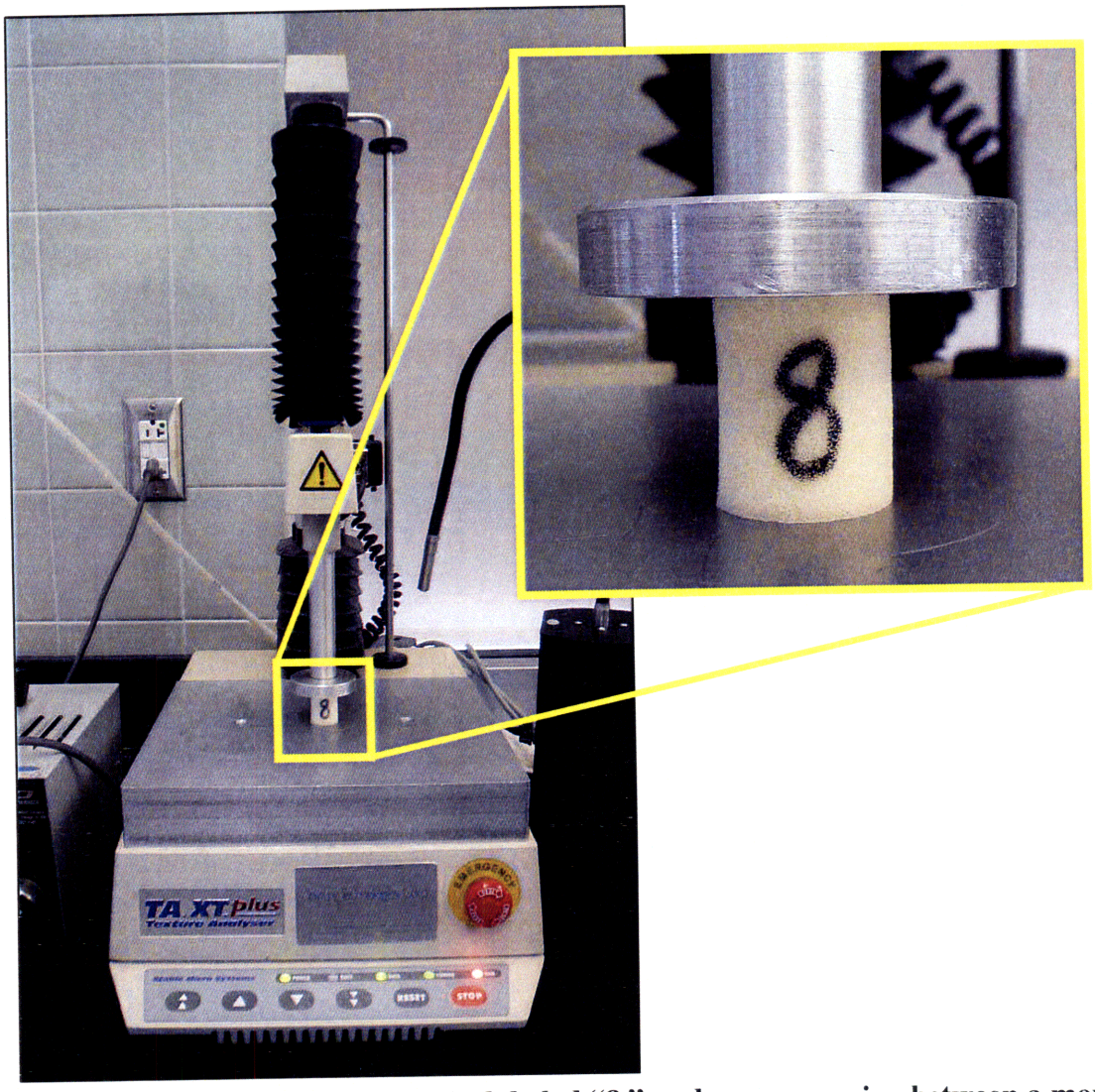

Figure 2.3: Blown-up photo of sample, labeled "8," under compression between a moving platen and a fixed platform on the Texture Analyzer.

Similar to the Zwick machine, the Texture Analyzer has an internal system compliance. The same type of compression test that was performed with the Zwick, in which two compression platens were pushed against each other, was conducted using the Texture Analyzer to determine its system compliance. A force vs. displacement test, whose data is shown in Figure 2.2, determined that the stiffness of the machine was 125.8 N/mm. This value for the machine stiffness was factored into the apparent stiffness of each test sample by treating the machine as a spring in series with a test sample.

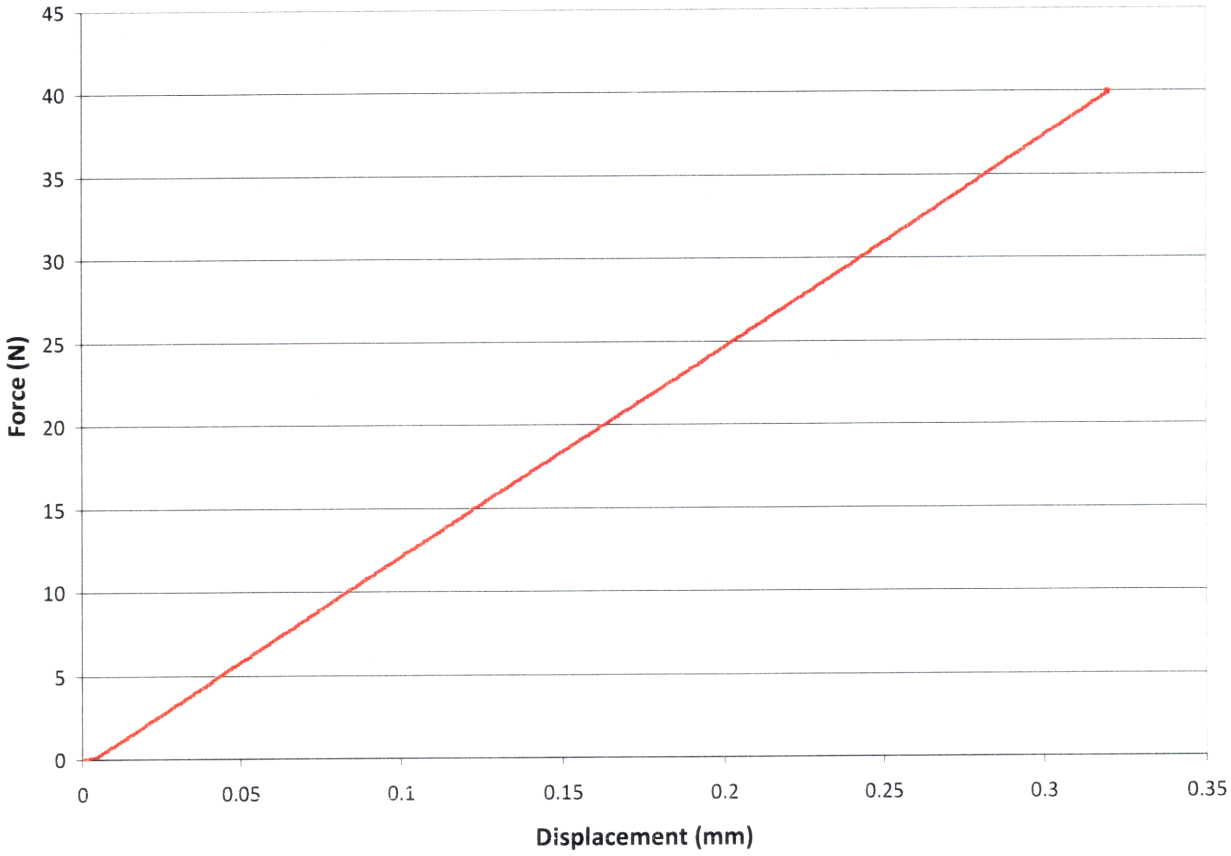

Figure 2.4: System calibration test for Texture Analyzer using 5 kg load cell.

2.2 Selection process for composite combination

2.2.1 Fluid class selection

In selecting a variable stiffness or variable rheology material to store in a foam, four types of "fluids" were considered (the term "fluid" is used loosely here, as three of these items can achieve non-fluid states): magnetorheological (MR) fluid, solder, hot glue, and wax, the latter three of which are thermorheological (TR) fluids.

2.2.1.1 Magnetorheological (MR) fluid

An MR fluid consists of a fluid medium—usually water or oil—that has micron-sized magnetizable particles, such as iron filings, suspended in it [25]. When a magnetic field is

applied to an MR fluid, the magnetizable particles arrange along the direction of the field. The basic principle of how an MR fluid reacts to an applied magnetic field is illustrated in Figure 2.5.

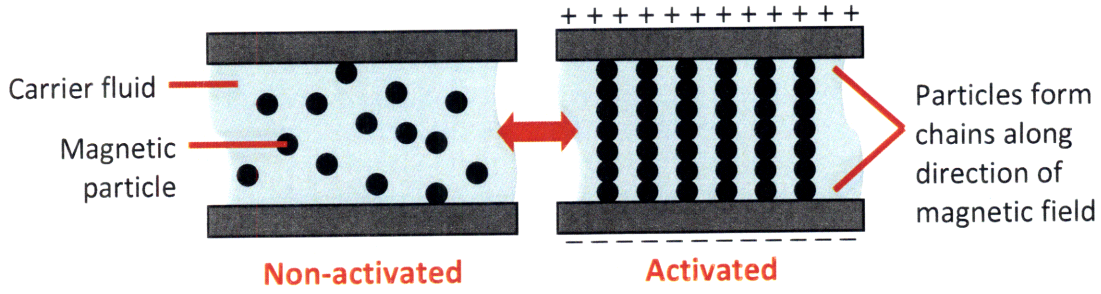

Figure 2.5: Schematic of basic principle of how MR fluid operates between activated and non-activated.

In its non-activated state, an MR fluid's behavior can be characterized using constitutive equations for Newtonian fluids. However, in the presence of a magnetic field, the fluid becomes non-Newtonian and has a yield shear stress. It requires more force to break the chains and shear the activated fluid than it would to shear a non-activated fluid the same amount. In contrast to a non-activated MR fluid's viscosity of 0.10—1.0 Pa-s, an activated MR fluid can exhibit a dynamic yield stress up to 50 kPa [27].

MR fluid was originally considered as a candidate for an adhesive locomotion fluid because its yield shear stress can be actively controlled. In addition to exploiting this unique capability of MR fluid, significant work in industry has been done to utilize foams saturated with MR fluid for shock absorption purposes [26]. When a foam impregnated with MR fluid is compressed along the direction of the length of the particle chains at a high strain rate, the chains provide initial resistance against the high impact. While an MR-impregnated foam does become noticeably "stiffer" when a magnetic field is applied to it, the composite's stiffness is highly dependent on the rate at which the it is strained.

Several qualitative tests were performed to determine whether MR fluid-filled foams would provide adequate stiffness, in its activated state, to act as load-bearing structures for SQUISHbot. The set-up for these tests is shown in Figure 2.6.

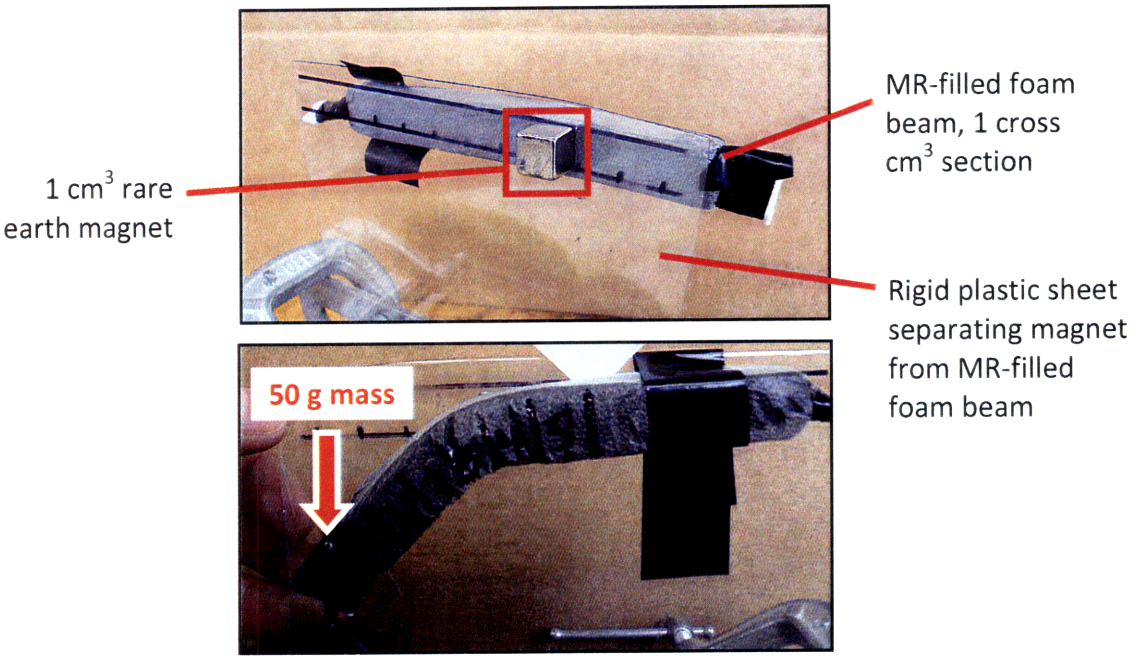

Figure 2.6: Images from tests to determine stiffness capabilities of MR fluid-filled foams.

The test samples were composed of saturated MR fluid-foam beams (approximately 1 cm^2 cross section) wrapped in cellophane. A 1 cm^3 permanent magnet was applied to a portion of the beam to create a locked "joint," and masses were hung from an end of the beam to quantify the amount of torque the activated joint could support. Different sized rare earth magnets were used, with the hypothesis that large magnets would create stiffer joints to support higher loads. The conclusion was that the MR fluid did not provide enough stiffness as a load-carrying structure, as the 50 gram masses the beams were limply supporting—even with large rare earth magnets that would be infeasible to include in the robot given the size constraints—were much less than the anticipated loads SQUISHbot needed to carry.

2.2.1.2 Solder

Unlike an MR fluid that is capable of an anisotropic change in particle distribution, solder is a thermorheological (TR) fluid that has an isotropic change in viscosity when its melting temperature is exceeded. Solder is a metal alloy that is commonly used in electronics applications; it is a solid in its cooled state and a low viscosity fluid in its heated state. Therefore, solder appeared to be a strong candidate as part of a variable stiffness element, with the caveat that it wicks well only with certain materials. Because it is known that solder wicks well with some metals, metals foams were considered for use as the "foam" portion of the

composite. However, the metal foams that were investigated were too stiff to be used as a compliant structure of a soft robot.

Since SQUISHbot could supply only a limited amount of on-board stored energy, it was desirable to identify low-temperature solders that required minimal power to heat and activate, or transition from its solid state to its liquid state. To test how well a low-temperature alloy could be wicked into an open-cell polyurethane foam, Field's metal, with a melting temperature of 62°C, was experimented with. It was immediately apparent that the melted alloy would not easily wick into the foam sample, as it was much more likely for the alloy to form droplets on the surface of the foam than to be wicked into the foam pores. Figure 2.7 demonstrates how the droplets on the foam formed wetting angles that were greater than 90°, meaning that the alloy would not preferentially wick into the foam. After using a soldering iron to melt and laboriously force the alloy into the foam, a rigid solder-foam composite was produced. It proved to be significantly more appropriate as a load-carrying element than MR fluid did. However, once a portion of the composite was heated again with a soldering iron, the melted alloy would quickly leave the foam pores and preferentially sit on the outer surface of the foam.

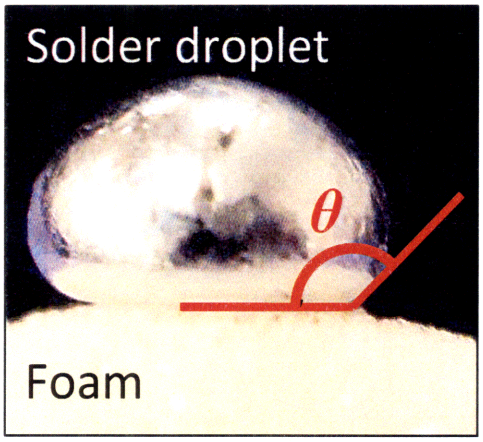

Figure 2.7: A solder droplet on a foam surface to demonstrate that the wetting angle θ > 90° means that the solder does not preferentially wick into the foam.

Despite the desirable stiffness change that solder is capable of, preliminary tests with Field's metal and generic solders indicated that the general class of alloys did not work well with the synthetic foams that were being considered for the controllable-stiffness composite elements. Even though solder was not selected as the "fluid" to be used in the composite structures that are

later characterized and analyzed in this chapter, it might be further investigated in future work. Ideas for redesigning the composite to accommodate solder include initially coating the foam with flux (though the feasibility of this has not yet been tested), and obtaining a compliant metal foam that is compatible with solder, such as electroplated steel wool.

2.2.1.3 Hot glue

Hot glue is another TR material, and like MR fluid, it was introduced to SQUISHbot as a potential adhesive locomotion fluid. In its cooled state, hot glue is rigid and often rubbery. Commonly used in applications like arts and crafts, hot glue becomes viscous when heated and can bond to many surfaces. In its melted state, hot glue has the consistency similar to that of a thick syrup. The dynamic viscosities of several melted hot glues are listed in Table 2.3 (the data was collected by Randy Ewoldt using a rheometer in the Hatsopoulos Microfluidics Laboratory at MIT).

Table 2.3: Dynamic viscosities of hot glue

Hot glue type	Melting temperature (°C)	Dynamic viscosity (Pa-s)
Fabric-use	77	377
High temperature	129	268
Carton-sealing	76	360
Jewelry-use	75	419

Hot glue-foam composites were prepared by melting the glue on a hot plate and forcing it into an open-cell polyurethane foam using a pair of tweezers. While saturating the foam with liquid glue was easier than saturating a foam with solder, the former task was still difficult because the glue was very viscous and did not naturally wick into the foam. Also, unlike with solder, once the hot glue was in the foam pores, it naturally stayed there because of its adhesion capabilities. Even though the stiffness change of hot glue is favorable (though not was drastic as that of solder's), its inability to easily wick into a foam made it a sub-par option as the fluid component of the composite being designed for SQUISHbot.

2.2.1.4 Wax

The fourth "fluid" considered was wax, which is another TR material. Like both solder and hot glue, wax is a solid at room temperature and becomes a fluid when heated beyond its melting temperature. Preliminary experiments suggested that wax had advantages over solder and hot glue because its low viscosity and high wettability allowed it to wick into the open-cell polyurethane foam very well. It also preferentially stayed in the foam after it was absorbed and is relatively stiff in its cooled state. Table 2.4 lists the dynamic viscosities of two liquid waxes (the data was collected by Randy Ewoldt using a rheometer in the Hatsopoulos Microfluidics Laboratory at MIT).

Table 2.4: Dynamic viscosities of wax

Wax type	Melting temperature (°C)	Dynamic viscosity (Pa-s)
Adhesive	71	4.63
Hair removal	56.9	19.89

Because wicking time (or the time it takes for a fluid to be drawn into another material) is directly proportional to viscosity, comparing the values in Table 2.3 and Table 2.4 indicate that wax can wick into foams at least two orders of magnitude faster than hot glue can. This makes wax a much more favorable candidate than hot glue because the wickability of the fluid might largely influence the speed of the robot.

After surveying four "fluid" classes—magnetorheological fluid, solder, hot glue, and wax—to be used in a controllable-stiffness fluid-foam composite, wax was selected because of its favorable properties for further study. The next section, 2.2.2, describes the process used to select a specific wax-foam combination that is characterized and analyzed in detail later in this chapter.

2.2.2 Wax-foam combination selection

2.2.2.1 Waxes and foams considered

Section 2.2.1 discussed why wax was chosen as the "fluid" component of a controllable-stiffness fluid-foam composite. Open-cell polyurethane (PU) foam was selected as the foam

component because it is readily available, can be very absorbent and compliant, and can be isotropic (i.e., the foam is composed of a unit cell repeated many times in three dimensions), which would simplify the modeling and characterization that is later discussed in this chapter.

Several waxes and open-cell polyurethane foams were selected as candidates for the composites based on their availability. It is important to keep in mind that the selected composite serves the primary purpose of developing a foundation for understanding a general class of composites that can be used in soft robotics. Significant future research, development, and experimentation can be conducted to select materials—that might lie outside the realm of waxes and generic foams—to optimize the performance of the composite.

Table 2.5 and Table 2.6 list the waxes and foams considered, respectively.

Table 2.5: Waxes considered for composites

Wax type	Brief description of wax
Batik wax cake	Typical candle wax
Adhesive wax	Compliant and moldable
Crayon	Typical crayon
Paraffin wax cake	Slightly softer than wax cake; had longer cooling/heating time than other waxes did

Table 2.6: Foams considered for composites

Polyurethane type	Bulk density (vendor-specified)	Brief description of foam
Unknown	N/A	Relatively large pores, very compliant
Quick-recovery, super-resilient	15 lbs/cu. ft.	Skin layer on top and bottom, very firm
Super absorbent	1.8 lbs/cu. ft.	Very soft like slice of bread
Slow-recovery (1), softest available of this type	5 lbs/cu. ft.	Very soft like slice of bread
Slow-recovery (2), firmest available of this type	5.8 lbs/cu. ft.	Very soft (slightly firmer than previous one, therefore recovers shape quicker than previous one does)

The mechanical properties of the wax-foam combinations were quantitatively compared to each other by performing compression tests on wax-filled foam samples. Compression moduli were obtained from the test data, providing a metric to use to compare the different combinations. It was assumed that the compression modulus was indicative of the overall strength of the composite, though bending and tensile tests need to be conducted in the future to gain a comprehensive characterization of the composite. Observations taken during the sample-preparation process were also important because certain materials could be identified as easier to work with than others.

2.2.2.2 Sample preparation method

Steps for preparing the wax-filled foam samples are listed in Table 2.7. All the foam sheets were purchased with 0.5-inch thickness, resulting in samples with the same height. The samples were also chosen to be 10 mm in diameter to be an appropriate size for SQUISHbot. Figure 2.8 shows the foam samples between Step 1 and Step 2 (i.e., after the foam was cut into cylinders and before it was saturated with wax). With four different types of waxes and five

different types of foams, each wax type was paired with each foam type, resulting in twenty different composite combinations that were tested.

Table 2.7: Sample preparation method for composite selection process

Step no.	Description
1	Cut the foam into cylinders using a 10 mm-diameter circular hole punch on a drill press (the shaft of the hole punch can be fit into the chuck of a drill press). Resulting foam cylinder dimensions: 0.5 inches (12.7 mm) height, 10 mm diameter.
2	Saturate the foam cylinder samples with wax by immersing the foam samples in a molten wax bath (in a glass beaker on a hot plate). With the foam still in the bath, use tweezers to force as much air out of the foam as possible (check that no more air bubbles are leaving the foam).
3	Carefully remove the wax-filled foam samples from the bath with a pair of tweezers or a paddle. Place the samples on a flat surface to cool, with the samples standing tall like columns.

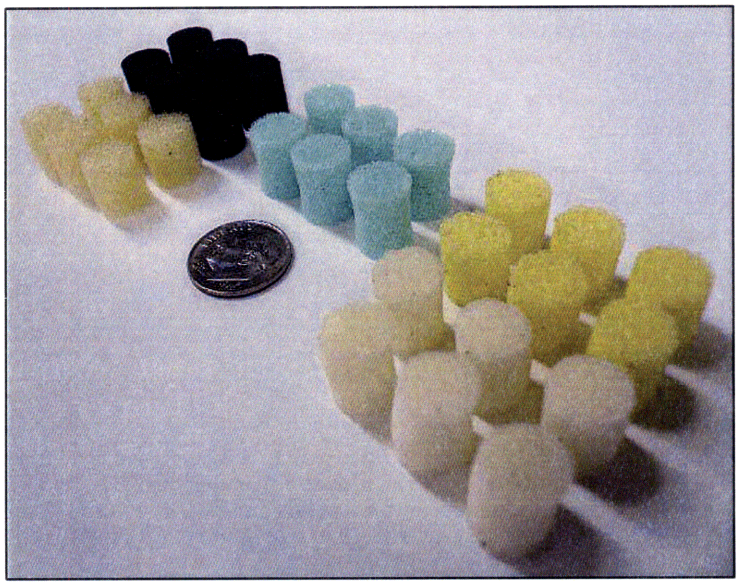

Figure 2.8: Foam samples, after being cut into cylinders, before being saturated with wax. Starting from the black-colored samples going clockwise: quick-recovery PU (black), slow-recovery (2) (green) PU, slow-recovery (1) (bright yellow) PU, super absorbent PU (white), [dime], unknown PU (dull yellow).

Some observations were made during the sample-preparation process: the quick-recovery foam samples did not absorb the wax well, most likely because these foams were too dense. All of the other foam types appeared to naturally wick the wax. Also, the slow-recovery (1) showed signs of tearing when tweezers were used to compress them during the saturation process.

2.2.2.3 Test method

Compression tests were performed on the wax-foam composite samples using the Zwick/Roell machine described in 2.1.1. Compression moduli were extracted from the test data. Compression tests, rather than tensile or bending tests, were conducted because they were the simplest and most reliable of the three in terms of sample preparation and test set-up. For example, it would be more difficult to prepare consistent beam-like samples for tensile and bending tests because the beams have a much larger volume of foam to saturate than the compression samples do. In addition, the foams would be relatively long and slender, so the combination of the compliant foam and the liquid wax tends to make the beams sag as they are removed from the wax bath. This makes placing the wet samples on a cooling surface a cumbersome process. However, as previously mentioned, it will be important to perform bending and tensile tests on the composites in the future to fully understand the limitations of the composites as functional structural components.

Select specifications and test parameters from the tests are listed in Table 2.8. Figure 2.1 showed a blown-up picture of a test sample buckling during a compression test. A numbering system was used to keep track of the samples, thus the label "10" on this specific sample.

Table 2.8: Specifications for compression tests performed on Zwick testing machine

Specification	Detail
Load cell range	2500 N
User-specified preload *The test does not begin until the machine detects that this load is being applied on the test sample.*	1 N
User-specified test speed	5 mm/min
User-specified test distance *The test automatically ends when the sample has been compressed by this amount*	2.5 mm
Displacement detection *How the displacement of the platens is determined*	Platen crosshead location
Output	Force vs. displacement

2.2.2.4 Results and conclusions

This section presents a comparison of compression test results of the different wax-foam composites introduced in 2.2.2.1, and it discusses why batik wax and super absorbent polyurethane foam were selected as the components of the composites to be characterized and analyzed later in this chapter.

Figure 2.9 shows a plot of stress vs. strain for the twenty different wax-foam composites. Each of the four wax types was paired with each of the five foam types, resulting in twenty wax-foam composite combinations. The plot also includes data for an additional sample—an empty (no wax) quick-recovery foam (the firmest foam type of all the foam types tested)—to show how the data for the composites compare with that of an unfilled foam.

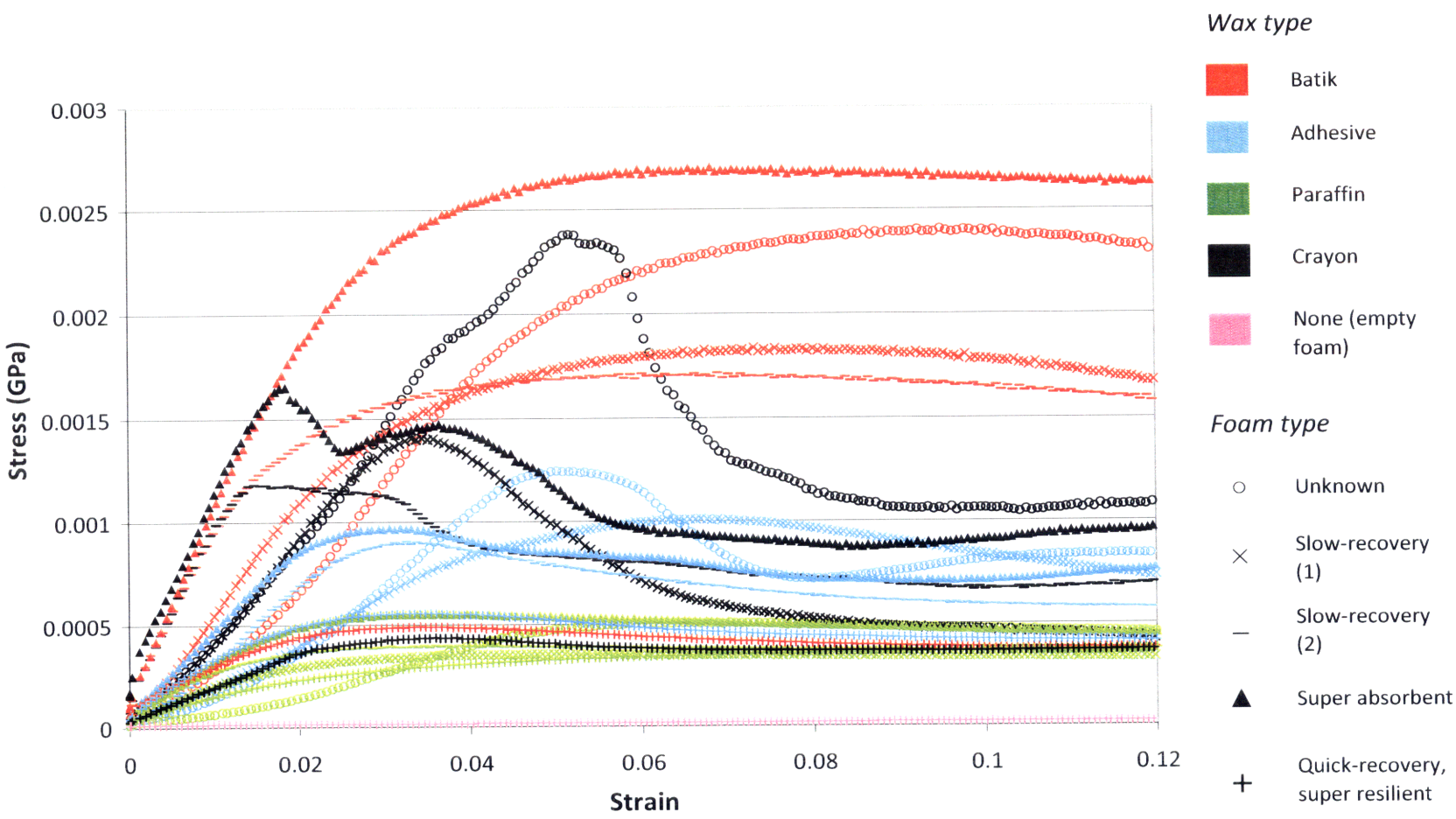

Figure 2.9: Stress vs. strain data for 20 different wax-foam composites.

The effective compression modulus for each composite was extracted from the data as the slope of the initial linear stress vs. strain portion (the elastic regime, by definition). The moduli, in units of GPa, for all twenty wax-foam composites are presented in Table 2.9.

Table 2.9: Effective compression moduli for twenty wax-foam composites in units of GPa.

		Wax type				
		Batik	Crayon	Paraffin	Adhesive	None
PU foam type	Unknown	0.0502	0.0534	0.0332	0.0129	--
	Slow-recovery (1)	0.0511	0.0486	0.0233	0.0139	--
	Slow-recovery (2)	0.0737	0.0827	0.0372	0.0202	--
	Super absorbent	0.0826	0.0862	0.0418	0.0251	--
	Quick-recovery, super resilient	0.0181	0.0164	0.0257	0.0106	0.0759 e-3

It is desirable for the composite to have both a large modulus and large yield stress in order to act as a load-carrying structure, as anticipated in SQUISHbot. The values in Table 2.9 indicate that the waxes that produced the highest moduli were batik wax and adhesive wax. The polyurethane foams that produced the highest moduli were the slow-recovery (2) PU (the firmest of this type available) and the super absorbent PU. Because SQUISHbot is still in the early stages of development, the required strength of the composites are not yet well-defined. Therefore, while several of these composites might fulfill future requirements, the one with the best combination of modulus and yield strength was selected for current studies.

Because the composites containing super absorbent PU resulted in relatively large yield stresses and slightly higher moduli than the slow-recovery (2) PU did, it was selected as the foam to be used in the composites that are later characterized and analyzed in this chapter. Another reason the super absorbent PU was favorable over the slow-recovery PU was that the latter foam was susceptible to tearing during sample preparation. The composites containing the unknown PU foam achieved large yield stresses, though it would have been difficult to obtain large

quantities of an identical foam, as the samples used were ones the laboratory already had but had no information about.

The density for two different super absorbent PU foams—designated (1) and (2), respectively—were 29.758 kg/ m^3 and 31.609 kg/ m^3, respectively. There were two versions of the super absorbent PU because the internet supplier whom the foams were purchased from had apparently changed their foam stock between purchases. The supplier confirmed that this was most likely because the vendor they had received the foams from had changed their stock. Therefore, information for both super absorbent PU foams needs to be included here because both types were used in experiment data presented in this chapter.

The modulus data in Table 2.9 indicated that composites containing the crayon wax generally had the largest moduli, with composites containing batik wax resulting in slightly smaller moduli. However, composites that contained batik wax consistently produced higher yield stresses than composites with other waxes did, which is an important consideration in selecting a material for load-carrying structures. Therefore, batik wax was selected as the wax component of the composites used throughout the rest of this chapter. Select properties for the batik wax are presented in Table 2.10. To determine the density of the cooled wax, the volume of a sample with known mass was measured using a gas pycnometer, courtesy of the Bioinstrumentation Laboratory at MIT.

Table 2.10: Select properties of the batik wax

Melting temperature	72 °C
Density (when cooled)	918 ± 5 kg/ m^3

2.3 Basic composite characterization

Batik wax and super absorbent polyurethane were selected as the wax and foam components, respectively, to be used in the composites studied throughout the rest of this chapter. It is important to understand the structural behavior of the composites for several reasons: for one, a designer must be familiar with a material's properties to meet given specifications. Also, while studying this specific composite does not necessarily characterize the entire performance space of all wax-foam composites—let alone active-fluid-and-cellular-solids

composites in general—it will help designers begin to understand the capabilities and possibilities of combining unrelated materials to create novel and functional structures.

2.3.1 Compression test data

This section describes the compression tests that were performed on rigid (cooled) wax-foam composites as well as the individual wax and foam components. Cylindrical samples were prepared with varying aspect ratios (i.e., the ratio of diameter to height) to determine whether the composites have dimension-dependent characteristics, as it is already known that the modulus of fluid-filled foams depends on cross section and strain rate.

2.3.1.1 Foam only

A flexible polyurethane foam was selected as the scaffold in which the wax would be stored in for the composite. The foams tested in this section were PU (1), as this was the foam used in the composites studied in subsequent sections. Even though the wax was expected to provide most of the compression strength of the composite, it is still useful to perform compression tests on the empty foams, as their behavior might affect the behavior of the overall composite. Figure 2.10 shows an image of the PU (2) foam taken under an optical microscope. Both PU (1) and PU (2) have the same cellular structure; the difference between them is that PU(2) has larger cells.

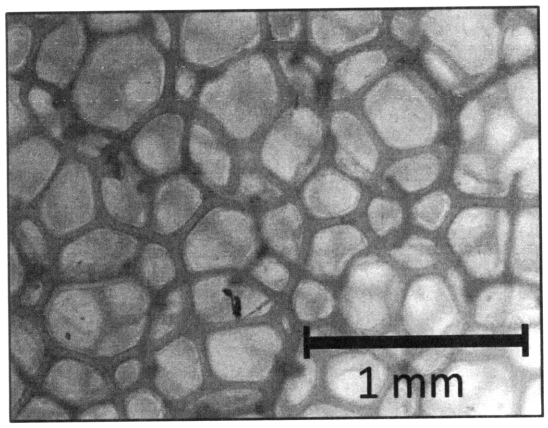

Figure 2.10: Image of PU (2) foam taken under optical microscope.

Flexible open-cell foams undergo several distinct stages during compression: a linear elastic one, a plateau, and densification. During the elastic regime, the individual struts that make the foam's cells bend as beams do, after which they buckle during the plateau regime. The foam undergoes densification when the struts impinge on each other and structure exhibits the behavior of a solid material rather than a porous one [29]. This section is mostly concerned with the linear elastic regime to determine a compression modulus for the material. The cylindrical foam samples that were tested were cut out of sheets of foam using circular cutters that were rotated using a drill press. An image of several hole cutters, including one set up in the chuck of a drill press, is shown in The samples' dimensions were selected to be the same as some of those used in later compression tests for the wax-foam composites. Figure 2.12 presents a stress vs. strain plot for foam samples with different dimensions, which were varied by using hole cutters with varying radii and foams of different thicknesses. The modulus for each sample was extracted from these curves as the slope of the linear elastic regime; Figure 2.13 is a plot of modulus vs. the diameter of each sample.

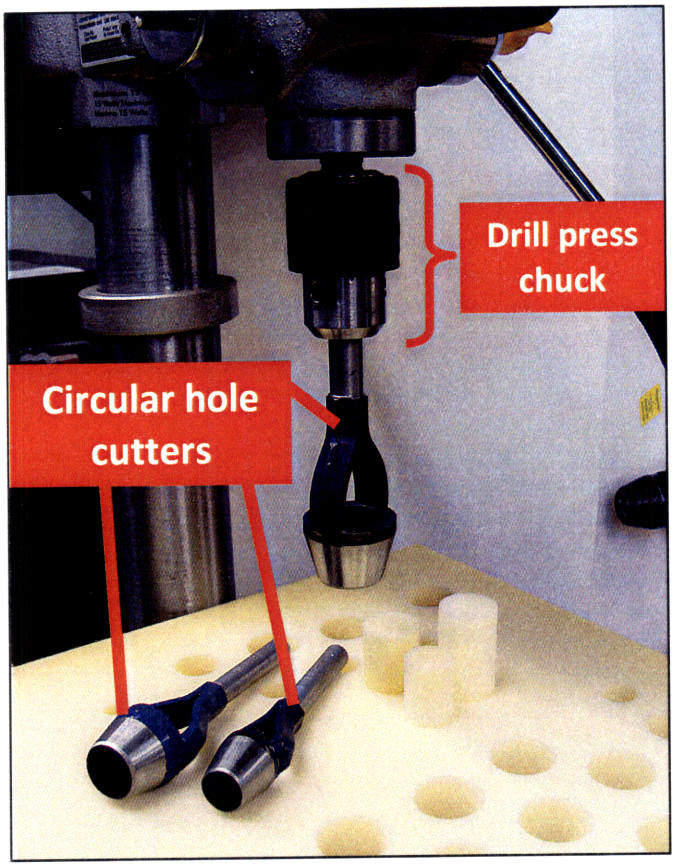

Figure 2.11: Image of foam-cutting set-up.

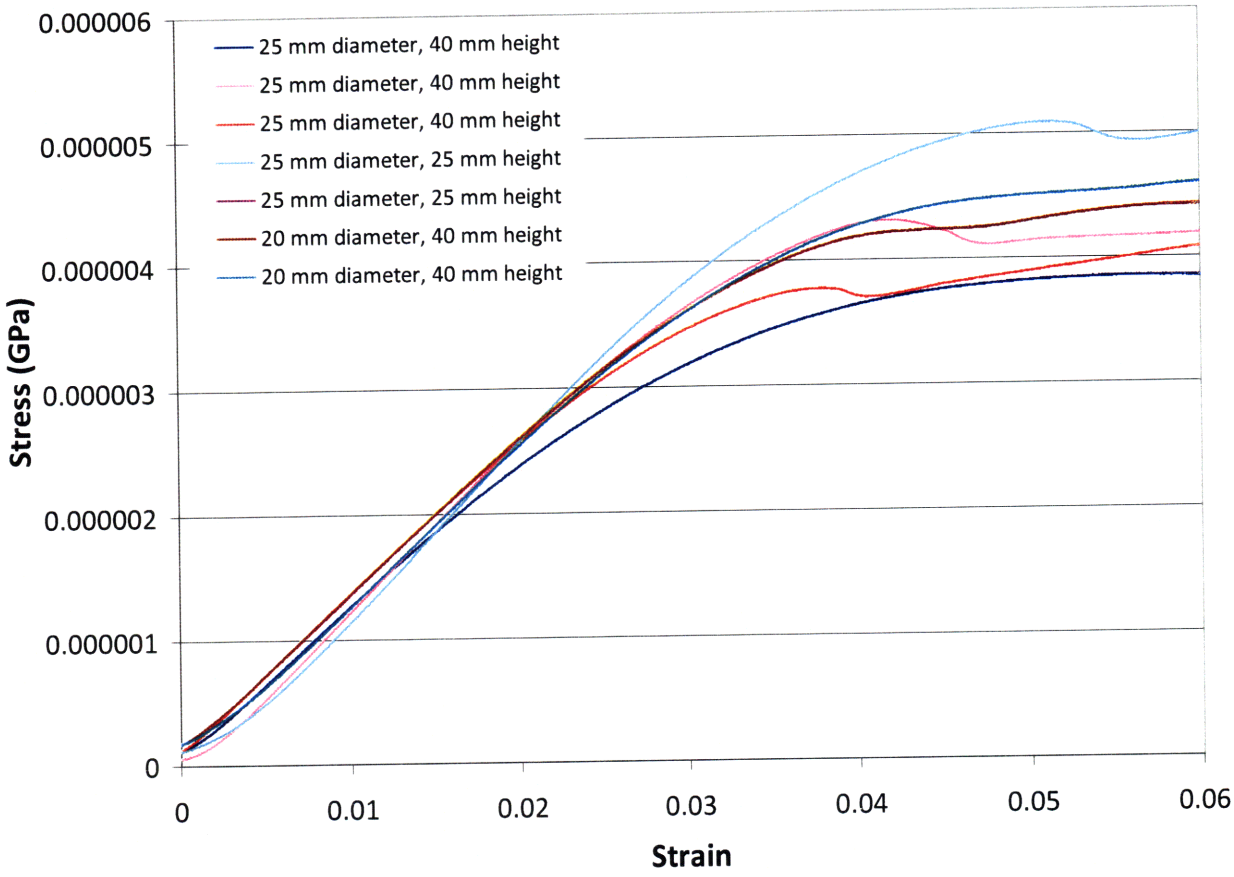

Figure 2.12: Stress vs. strain data for PU (2) foam cylinders.

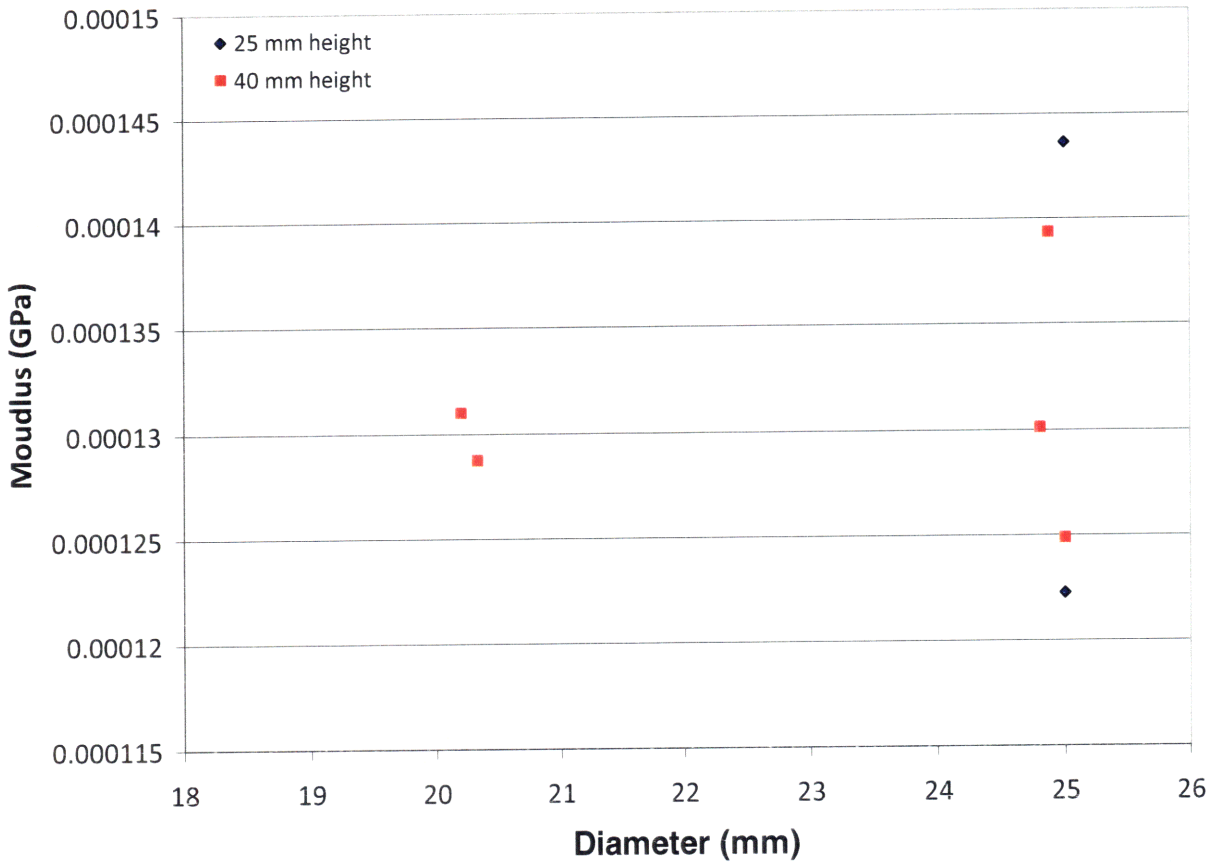

Figure 2.13: Modulus vs. diameter data for foam cylinders.

Several of the stress vs. strain curves have a slight kink in them after the proportionality limit. This might be due to some of the weaker struts of the foam breaking—hence, plastically deforming—during the initial compression, after which the intact struts buckle within the plateau regime. For instance, because of the way the foam is cut, the outer surfaces of the foam have many partial cells with dangling struts. Cyclic compression tests performed on the foams confirmed that there is slight plastic deformation occurring even when the test appears to be operating in the elastic regime. This is further investigated in 2.4.1, as the wax-foam composites exhibit a similar behavior during cyclic tests. Finally, the plot in Figure 2.13 indicates that the modulus of the foam is 0.13±0.01 MPa. The variation between samples is insignificant compared to the modulus of the wax or the composite, as will be indicated in subsequent sections.

2.3.1.2 Wax only

It was important to understand the properties of the wax in its cooled state, since the strength of the wax is the dominating factor in determining the strength of a wax-foam composite. It was hypothesized that the bulk properties of the wax, including compression modulus, would be consistent for any sample independent of its geometry. Therefore, it was expected that little to no variation would be observed between compression moduli for samples with different aspect ratios. However, initial test results indicated otherwise, leading to subsequent iterations of tests, as will be explained throughout this section.

To prepare consistent test samples, the batik wax was made into cylinders using flexible, 3D-printed polymer molds. Table 2.11 lists the steps involved in making these wax samples, with photos accompanying select steps shown in Figure 2.14.

Table 2.11: Preparation process for cylindrical wax samples.

Step no.	Description
1	3D-print polymer molds. The molds must be taller than the final wax samples to accommodate the concave surface of the sample—caused by surface tension during cooling—that will be removed later. This is to ensure that the surfaces that contact the compression platens are flat and parallel.
2	Submerge a mold in a wax bath and fill it with molten wax. Note that it is important for the temperature of the bath to be consistent for a set of samples; the temperature of the molten wax can significantly affect how the sample cools, potentially affecting the final sample's structural properties.
3	Carefully remove the mold from the bath so that no wax spills out of it, and place the sample on a flat surface to cool.
4	3D-print a second set of polymer molds. These molds should have the same diameters as in the first set but with the desired heights of the final samples.
5	Remove the cooled wax sample from its original mold and place it in one of the new molds so that the sample's concave surface is exposed.
6	Place the sample, in its new mold, on a hot plate so that the concave surface is in direct contact with the plate. Use the hot plate to remove the concave portion of the sample by melting it off until the height of the sample is the same as that of the mold (the sample should be melted until the rim of the mold is flush with the hot plate).
7	Remove the sample from the hot plate and allow the exposed surface to cool before removing the sample from the mold.

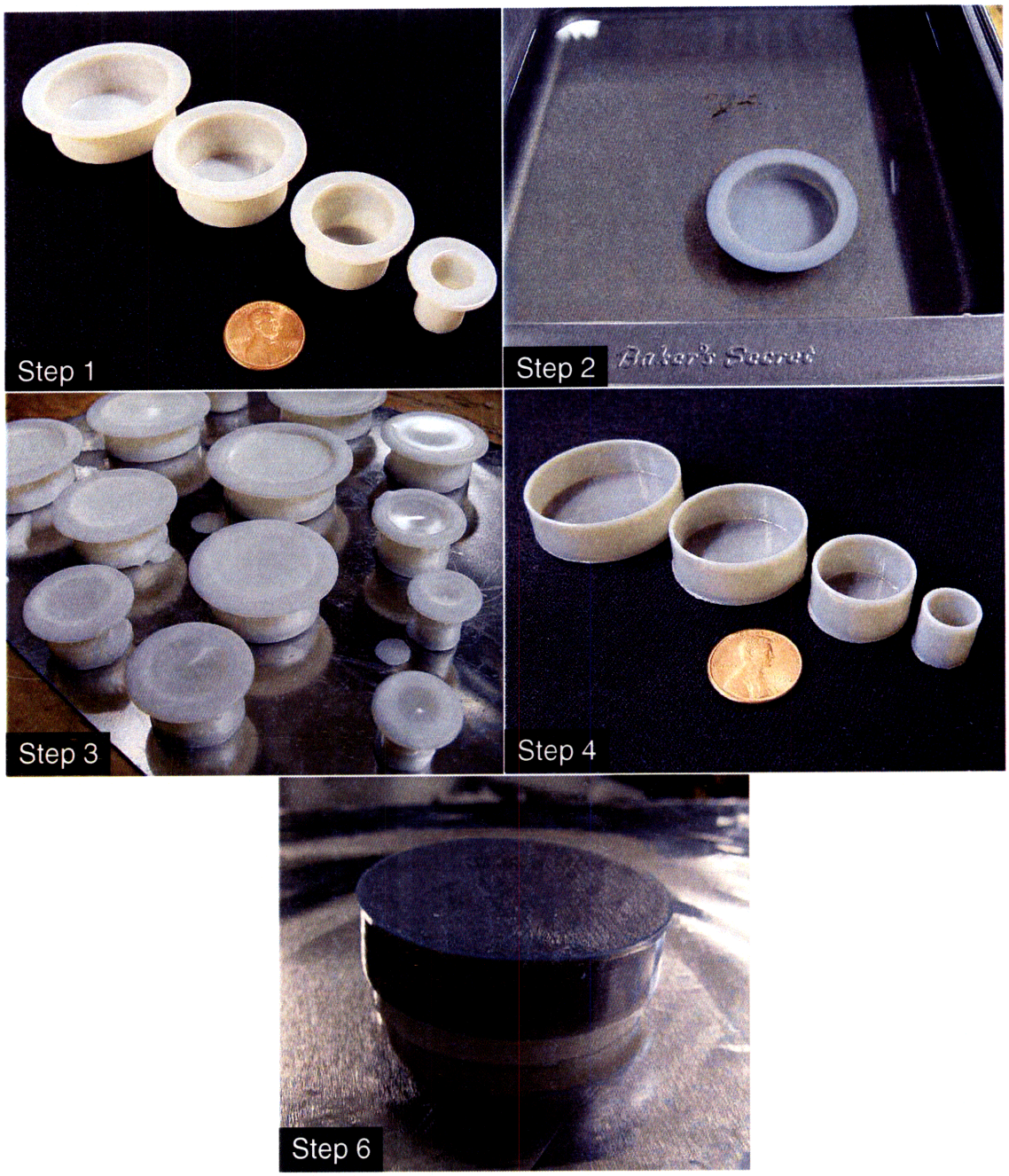

Figure 2.14: Images of select steps from the wax sample preparation process described in Table 2.11.

An initial set of compression tests was performed on wax samples that were 10 mm tall with varying diameters of 10 mm, 20 mm, 30mm, and 40mm, resulting in aspect ratios of 1:1, 2:1, 3:1, and 4:1, respectively. These dimensions were selected so that the samples would be relatively short and squat to avoid buckling during compression. This set of samples is shown in Figure 2.14.

The samples were prepared from a molten wax bath whose temperature was 82±1°C. It was important to make samples using a consistent bath temperature because the temperature affects how the wax cools, which potentially affects the structural properties of the final sample. For example, observations indicated that samples made from higher temperature wax baths resulted in taller concave surfaces than samples prepared in lower temperature baths did. When the wax cools at room temperature, the outer perimeter of the cylindrical samples cooled first, and because wax shrinks as it cools, the central portion of the wax shrank the most by the time the whole sample solidified. These concave surfaces were melted off on a hot plate at 72±1°C, resulting in cylindrical samples with flat, parallel end faces.

Compression tests were performed on these samples using the Zwick machine. The test parameters were the same as those listed in Table 2.8, with the exception of the test distance being 2.5 mm instead of 5 mm.

The raw data for stress vs. strain and effective modulus vs. aspect ratio are presented in Figure 2.15 and Figure 2.16, respectively.

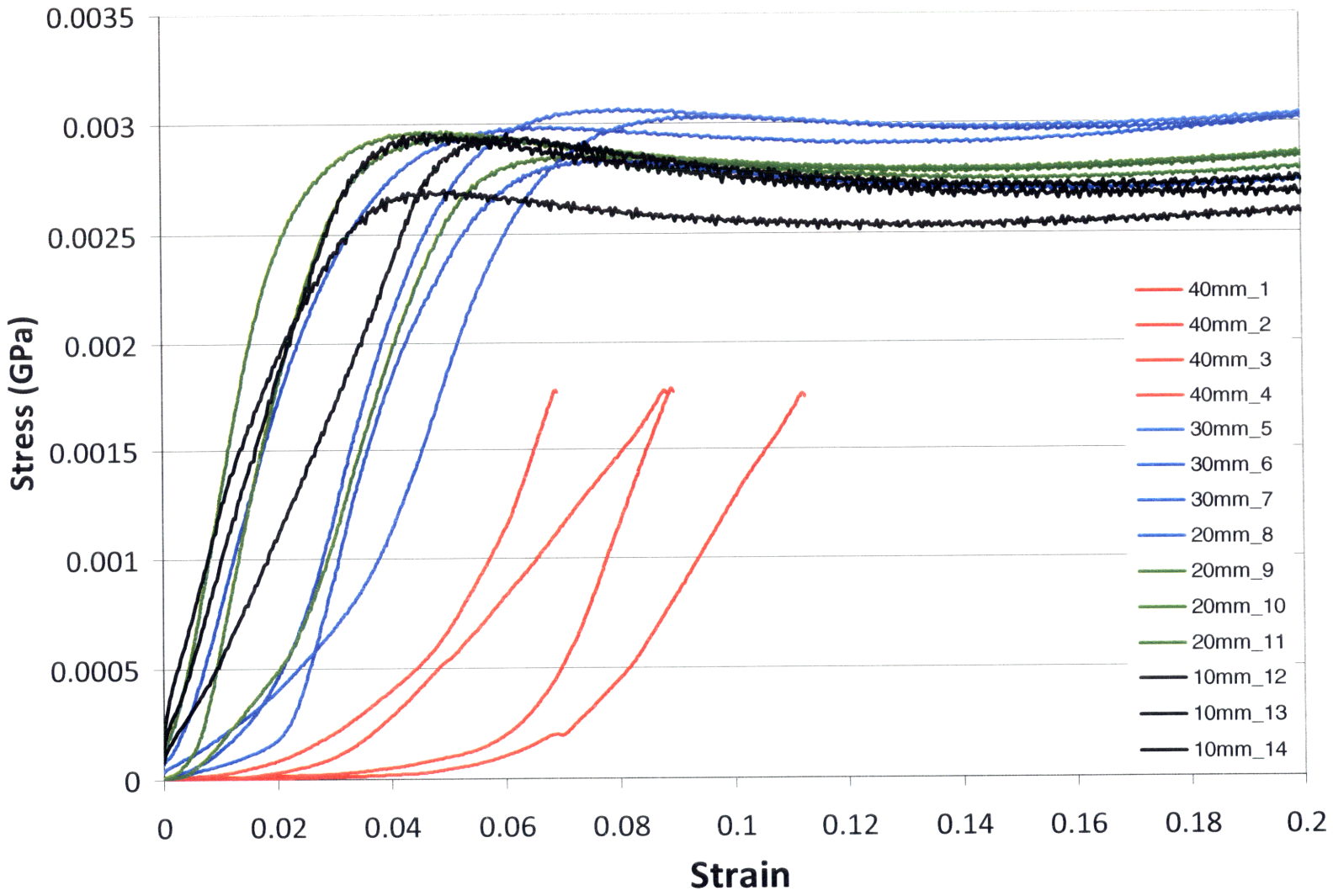

Figure 2.15: Stress vs. strain data from compression tests performed on wax cylinders that were 10 mm tall and had varying diameters of 10 mm (black), 20 mm (green), 30 mm (blue), and 40 mm (red).

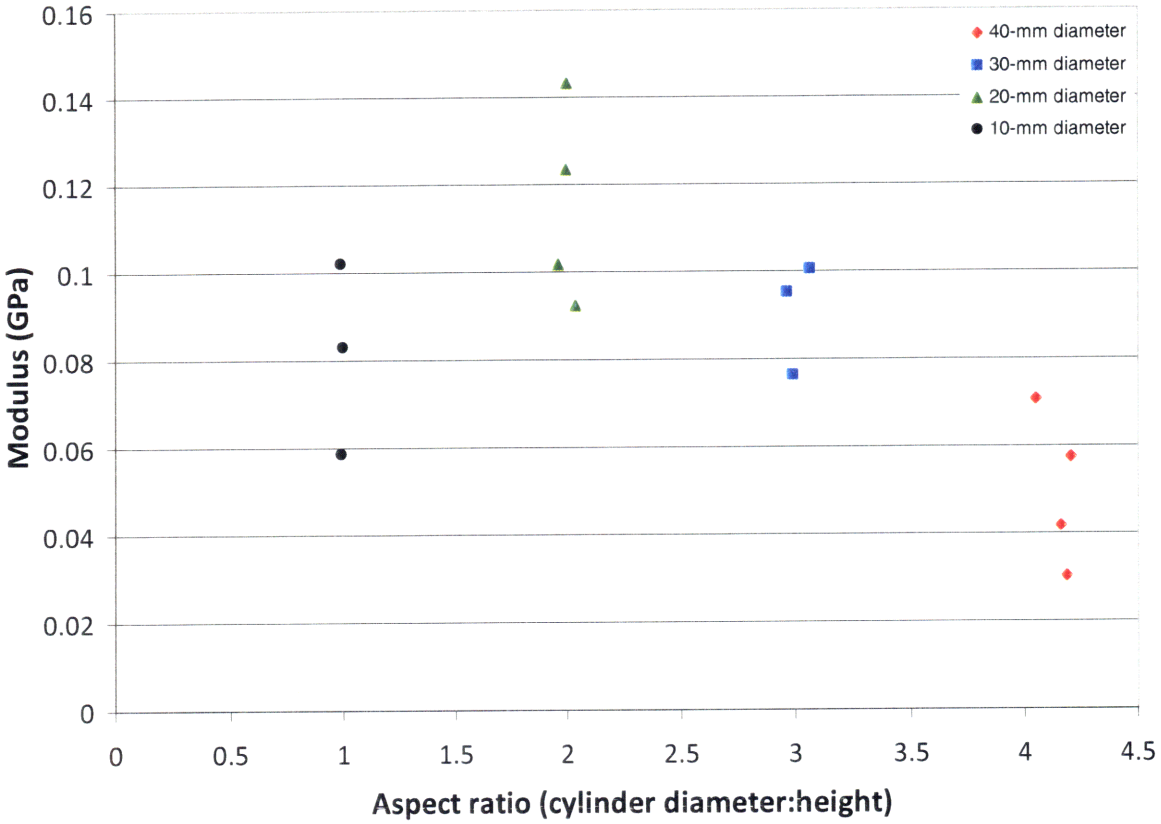

Figure 2.16: Effective modulus vs. aspect ratio data from compression tests performed on wax cylinders that were 10 mm tall and had varying diameters of 10 mm, 20 mm, 30 mm, and 40 mm.

The modulus for each sample was computed as the slope of the linear portion of the stress vs. strain curve within the elastic regime. For the 40 mm-diameter samples, the elastic regime was not considered to begin until ~0.06—0.1 strain; the initial "lag" in these curves most likely is a result of the platens were flattening the top surfaces of the samples, which had slight streaks and bumps of extruded wax that was not perfectly leveled after Step 6 in Table 2.11 (i.e., when the concave surfaces of the samples were melted off on the hot plate). The lag seen on the curves is more drastic for the larger diameter samples because these samples had more surface area, and hence potential, for there to be impurities.

As previously mentioned, it was expected that the modulus of the wax would be constant across all aspect ratios, but the results shown in Figure 2.16 did not support this hypothesis. While several data points representing each of the four aspect ratios had modulus values that fell within the range of 0.05—0.09 GPa, the moduli for samples with aspect ratios of 2, 3, and 4

appeared to increase with decreasing aspect ratio. This was surprising because even if modulus did vary with aspect ratio, intuition might lead one to assume that samples with smaller cross sections would be more prone to buckling, hence resulting in smaller moduli.

A hypothesis for why the shorter, squatter samples with aspect ratios of 4 were producing smaller moduli was that friction between the surfaces in contact prevented samples' end faces from expanding radially as they normally would under compressive loads. This would result in non-uniform stress distributions throughout a sample. For more squat samples (or the samples with large aspect ratios), the lateral distance these non-uniform stress distributions propagated might have been large relative to the total height of the sample, causing the overall structure to weaken. Conversely, samples with smaller aspect ratios were relatively slender so that the non-uniform stress distributions near the end faces did not affect a central portion of the sample, which experienced more uniform stress distributions. Therefore, the response to loading in the central portion of a more slender sample might dominate the no-slip effects near the end faces, resulting in a larger modulus. However, this is not entirely reflected in the data, as the moduli for samples with aspect ratios of 1 were generally smaller than those with aspect ratios of 2.

Because these unexpected results led to the suspicion that the wax samples had inappropriate dimensions for materials testing, ISO and ASTM testing standards for polymers—which was thought to be the general category of materials that best represented wax—were studied to identify the dimensions that should have been used. As a lower bound, ISO 604 stated that cylindrical samples for polymer compression tests should have aspect ratios no less than 0.08, or even 0.4 for some materials, to avoid buckling. All the samples tested had aspect ratios that were significantly above these lower bounds. ASTM D695 stated that cylindrical polymer samples should have an aspect ratio of 1:2; specifically, cylinders should be 12.7 mm (0.5 in) in diameter and 25.4 mm (1.0 in) tall. Using these standards as guidelines, a second set of tests was performed on samples with ≤ 1 aspect ratios, with a range of dimensions to cover those specified in ASTM standards. The hypothesis was that the moduli for this new set of samples would be more consistent across various aspect ratios.

For the second set of wax compression tests, samples were prepared to be approximately 20 mm tall with varying diameters of 10 mm, 15 mm, 20 mm, and 25 mm, resulting in aspect ratios of 1:2, 3:4, 1:1, and 5:4, respectively. It was intended for the samples to be ~25 mm tall to match ASTM standards, but the height of the concave surfaces of the cooled wax samples were

larger than estimated, so more wax had to be removed than expected to arrive at cylindrical samples with flat, parallel end faces. The samples were prepared under the same conditions as they were for the first set of tests: they were prepared from a molten wax bath whose temperature was 82±1°C, and their resulting concave surfaces were melted off on a hot plate surface at 72±1°C. The raw data for stress vs. strain and modulus vs. aspect ratio are presented in Figure 2.17 and Figure 2.18, respectively.

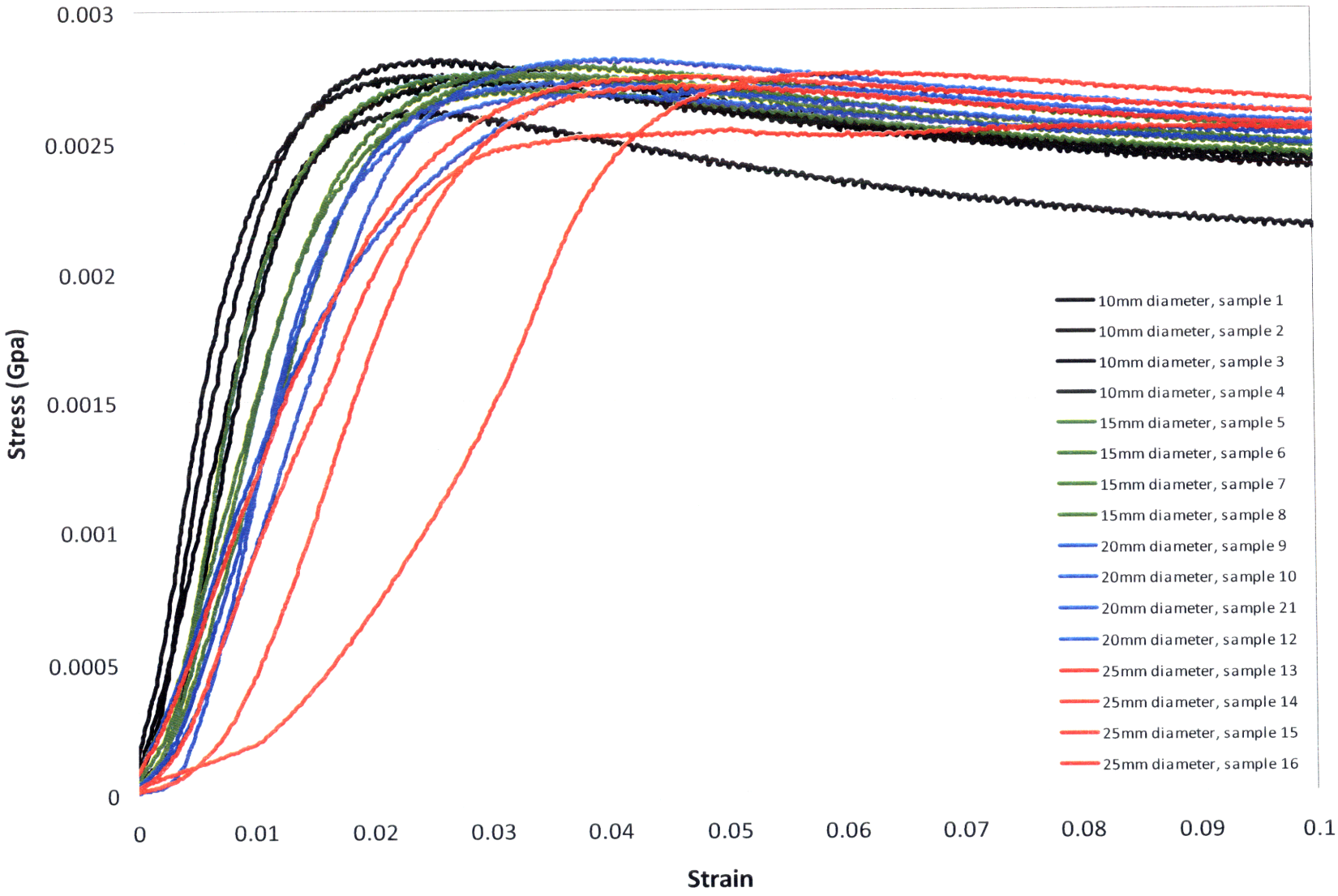

Figure 2.17: Stress vs. strain data from compression tests performed on wax cylinders that were 22 mm tall and had varying diameters of 10 mm (black), 15 mm (green), 20 mm (blue), and 25 mm (red).

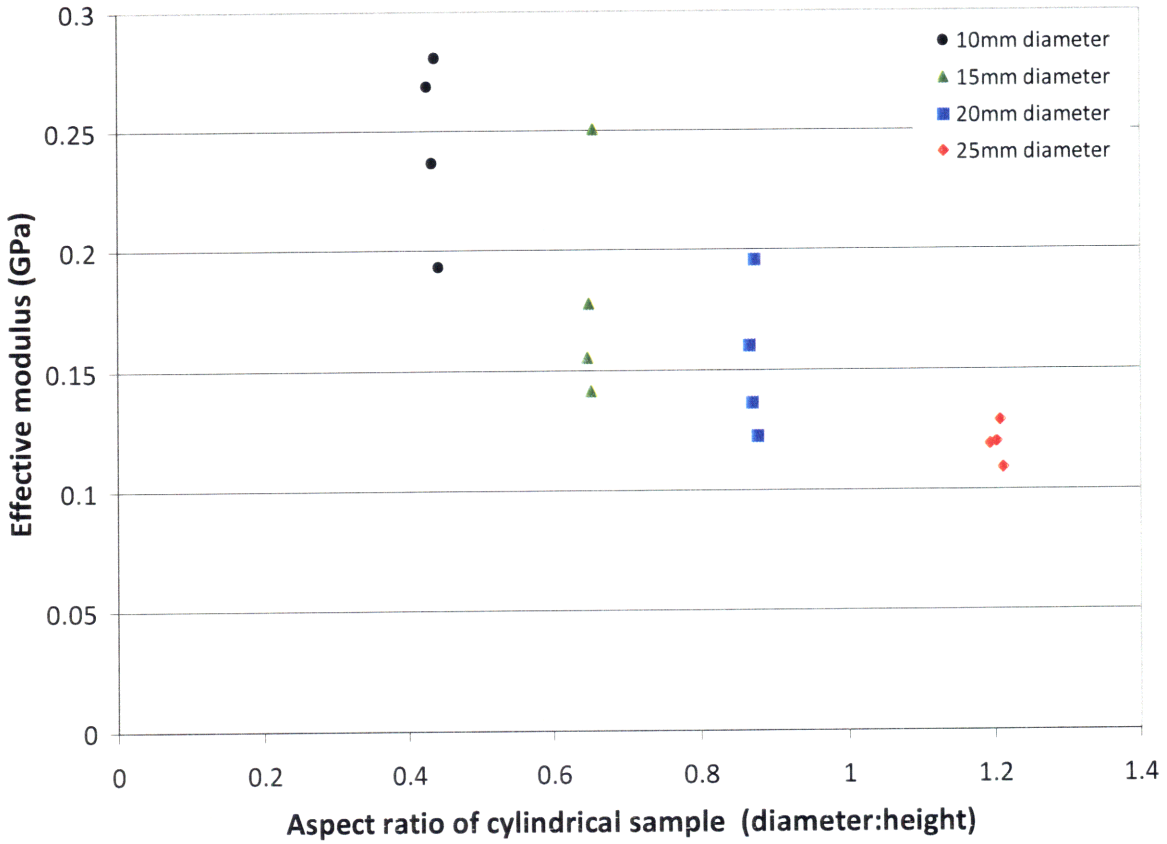

Figure 2.18: Effective modulus vs. aspect ratio data from compression tests performed on wax cylinders that were 22 mm tall and had varying diameters of 10 mm, 15 mm, 20 mm, and 25 mm.

The results shown in Figure 2.18 did not prove the hypothesis that the modulus values would converge for aspect ratios ≤1. In fact, the range of moduli produced by the second set of samples was larger than the range from the first set. There was also a more obvious trend of modulus values increasing with decreasing aspect ratios. This is shown in Figure 2.20, where the modulus vs. aspect ratio data from both sets of tests are presented in a single plot.

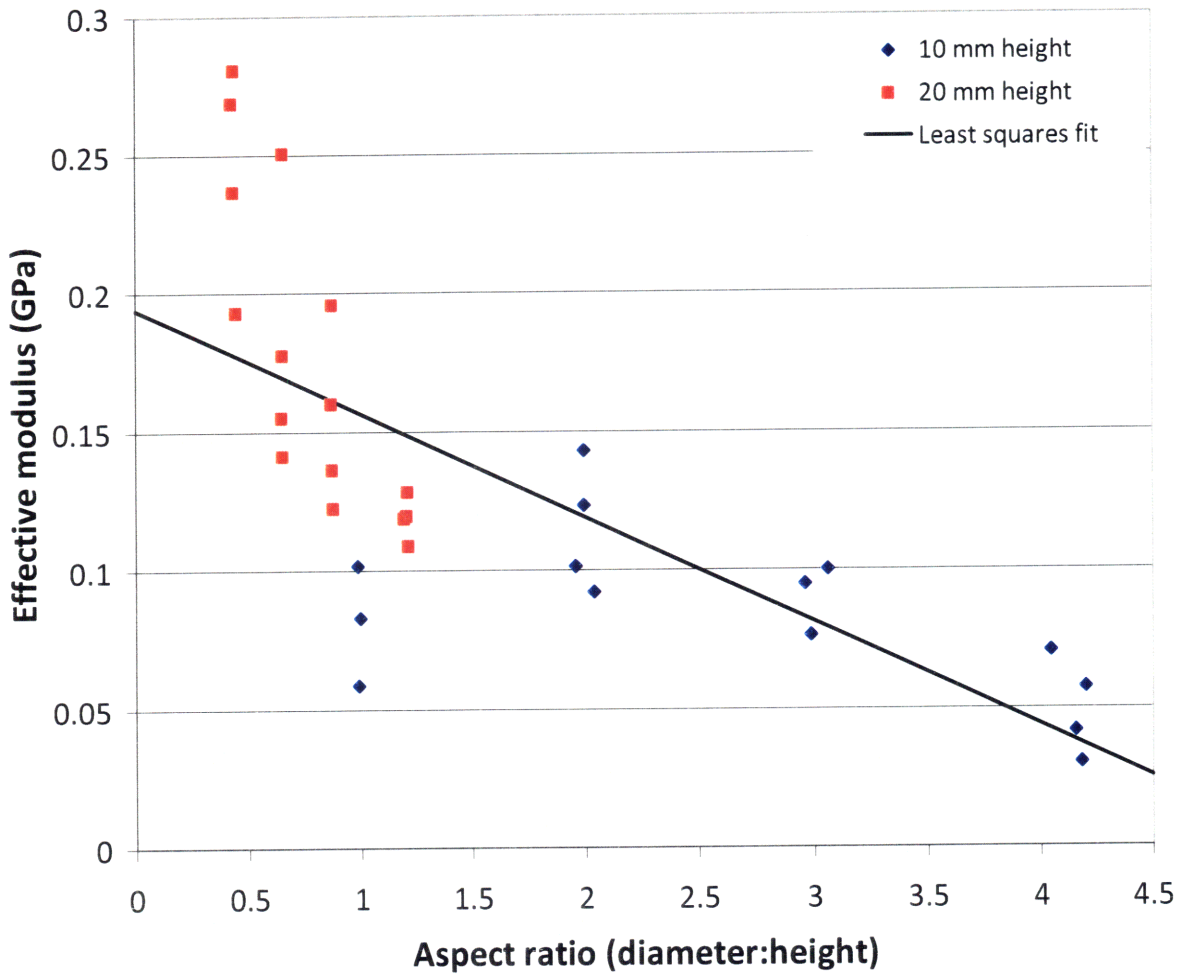

Figure 2.19: Effective modulus vs. aspect ratio data for two sets of wax samples made from polymer molds.

This plot suggests a correlation between modulus and aspect ratio, but the reasons for this are not obvious. A possible explanation for this dimension-dependence was that the modulus is cross-section dependent; because of the way the samples were individually prepared and cooled at room temperature, there might have been significant internal stresses occurring during cooling. If this was true, a sample's micro-structure would weaken during the cooling process, causing a sample to have a smaller modulus than if there was no internal pre-strain. Accordingly, samples with larger diameters would have more internal straining than samples with smaller cross sections because the latter would cool more uniformly. Modulus was plotted as a function of sample diameter in Figure 2.20 to determine if there was an obvious correlation between these two parameters.

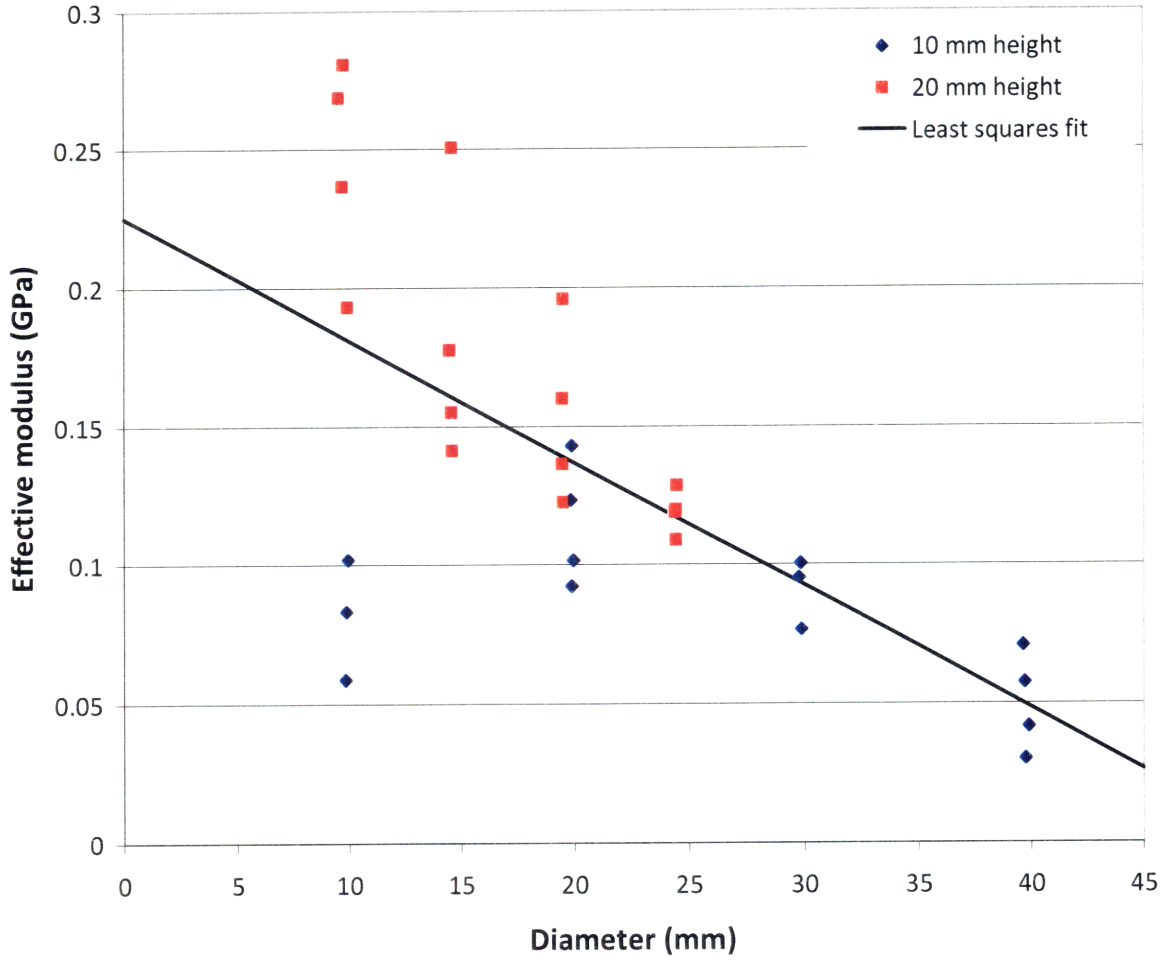

Figure 2.20: Effective modulus vs. diameter data for two sets of wax samples made from polymer molds.

Once again, the results were inconclusive, as demonstrated by comparing the data points representing samples that were 10 mm in diameter: although all seven of these samples had the same diameter, their modulus values fell within two distinct ranges according to each sample's height. In contrast, samples that were 20 mm in diameter produced a narrow range of modulus values. In fact, if the data for the 10 mm-diameter samples were ignored, there appears to be a strong correlation between sample diameter and modulus.

To further investigate the possibility that internal pre-straining induced during the cooling process had a significant effect on the samples' moduli, compression tests should be performed on wax samples that are annealed and/or cut out of a large sheet of wax to minimize the internal-

strain variation across samples with different cross sections. While a complete set of these tests will be conducted in future work, Figure 2.21 presents preliminary tests results—plotted with the results from Figure 2.19—for cylindrical wax samples that were bored out of 9" x 9" slabs of wax. These slabs were made by cooling a molten wax bath in an aluminum baking pan. Cylinders were bored out of the wax using circular cutters that were turned using a drill press. To minimize the variation between samples, cylinders were cut out along a constant radius from the center of the wax slab.

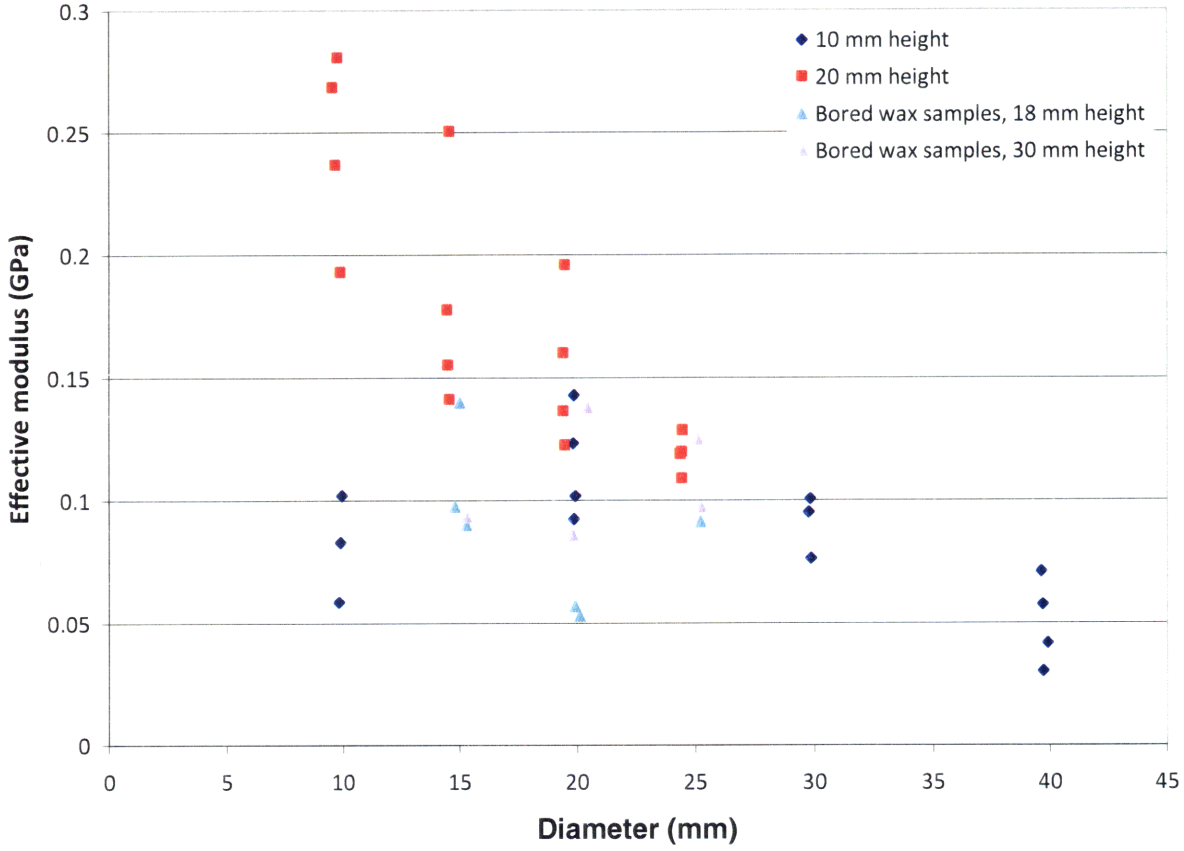

Figure 2.21: Effective modulus vs. diameter data for three sets of wax samples: two sets made from polymer molds and one set made from boring cylinders out of a wax slab.

These results are promising in that they reflect no obvious correlation between cross section and modulus. This suggests that the modulus of individual samples might be highly dependent on sample preparation. Even though this might lead to the conclusion that previous samples had not been prepared appropriately to determine the bulk modulus of the wax, the data is still useful in predicting the behavior of wax-foam composites as functional robotic

components. The way the individual wax samples were cooled at room temperature might be similar to how wax-foam composites would cool on a robot, therefore suggesting that the solid mechanics of the composites might depend on their geometries rather than a bulk property.

2.3.1.3 Composites

Composites were made by saturating PU (1) foams with batik wax. Because the fully saturated composites were mostly composed of wax, by volume, their structural properties were expected to be comparable to those of the waxes studied in the previous section.

The samples were selected to have two different heights of 25.4 mm (1 inch) and 38.1 mm (1.5 inches) based on ASTM standards (discussed in the previous section) and foam thicknesses that were commercially available. The diameters of the samples were limited to 10 mm, 15 mm, 20 mm, and 25 mm based on the available circular punches used to cut the foams. Composites were prepared using the procedure listed in Table 2.7; cylindrical foam samples were fully saturated in wax baths at temperatures of 82±1°C and allowed to cool at room temperature.

The stress vs. strain data for the 12.54 mm- and 38.1 mm-tall samples are presented in Figure 2.22 and Figure 2.23, respectively.

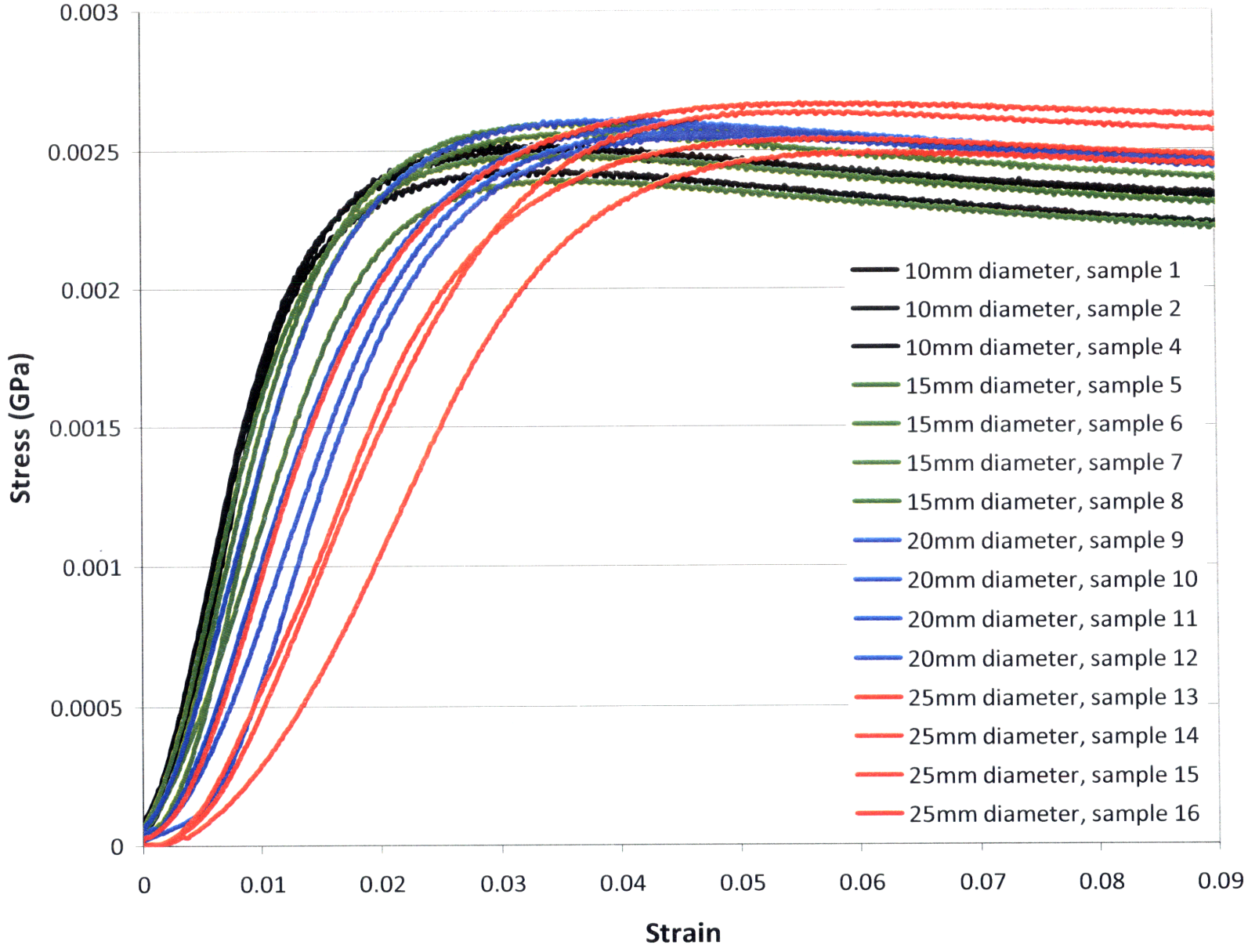

Figure 2.22: Stress vs. strain data for 25.4 mm-tall fully saturated cylindrical composites with varying diameters of 10 mm (black), 15 mm (green) 20 mm (blue), and 25 mm (red).

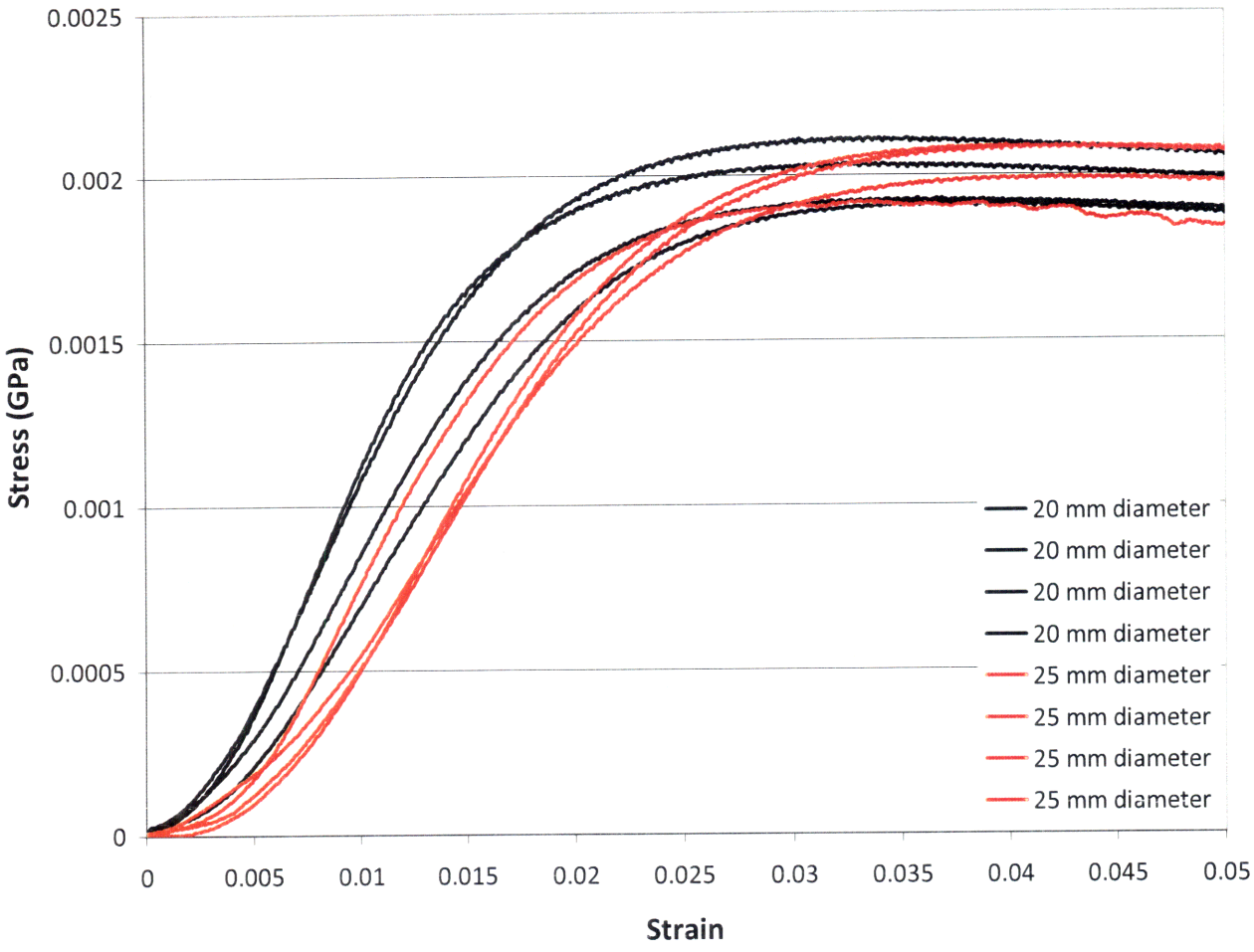

Figure 2.23: Stress vs. strain data for 38.1 mm-tall fully saturated cylindrical composites.

As expected, the data indicated that the proportionality limits (i.e., when the stress vs. strain curve reaches its peak stress in the elastic regime) were comparable to those from the pure wax tests, which can be confirmed from data presented in Figure 2.15 and Figure 2.17. This is important because it ensures that the foam does not diminish the overall strength of the composite. To understand how the calculated moduli of the composites compared with those of pure wax samples (those made with polymer molds, as discussed in the previous section), the data for both composite and wax samples are plotted together in Figure 2.26 and Figure 2.27.

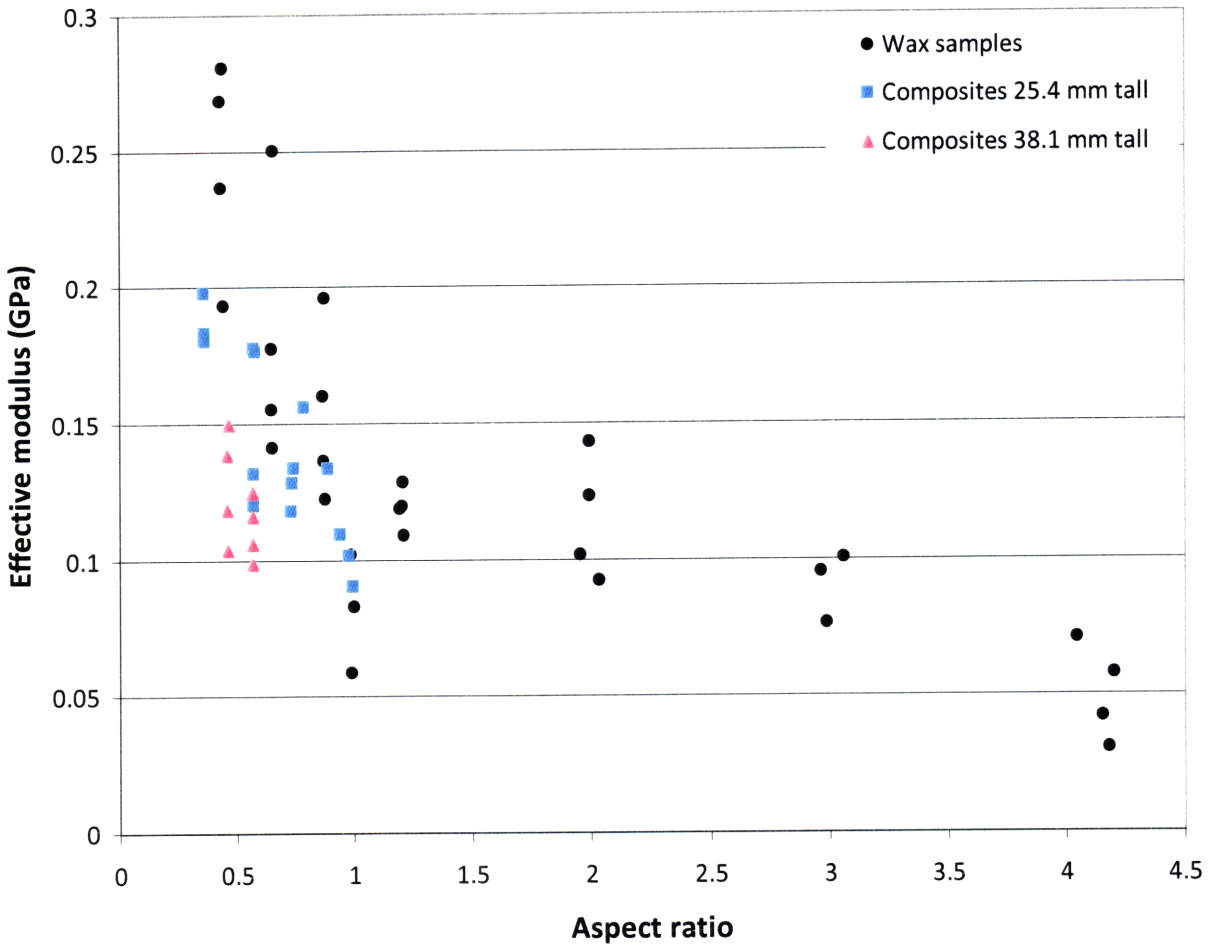

Figure 2.24: Effective modulus vs. aspect ratio data for both composites and wax samples.

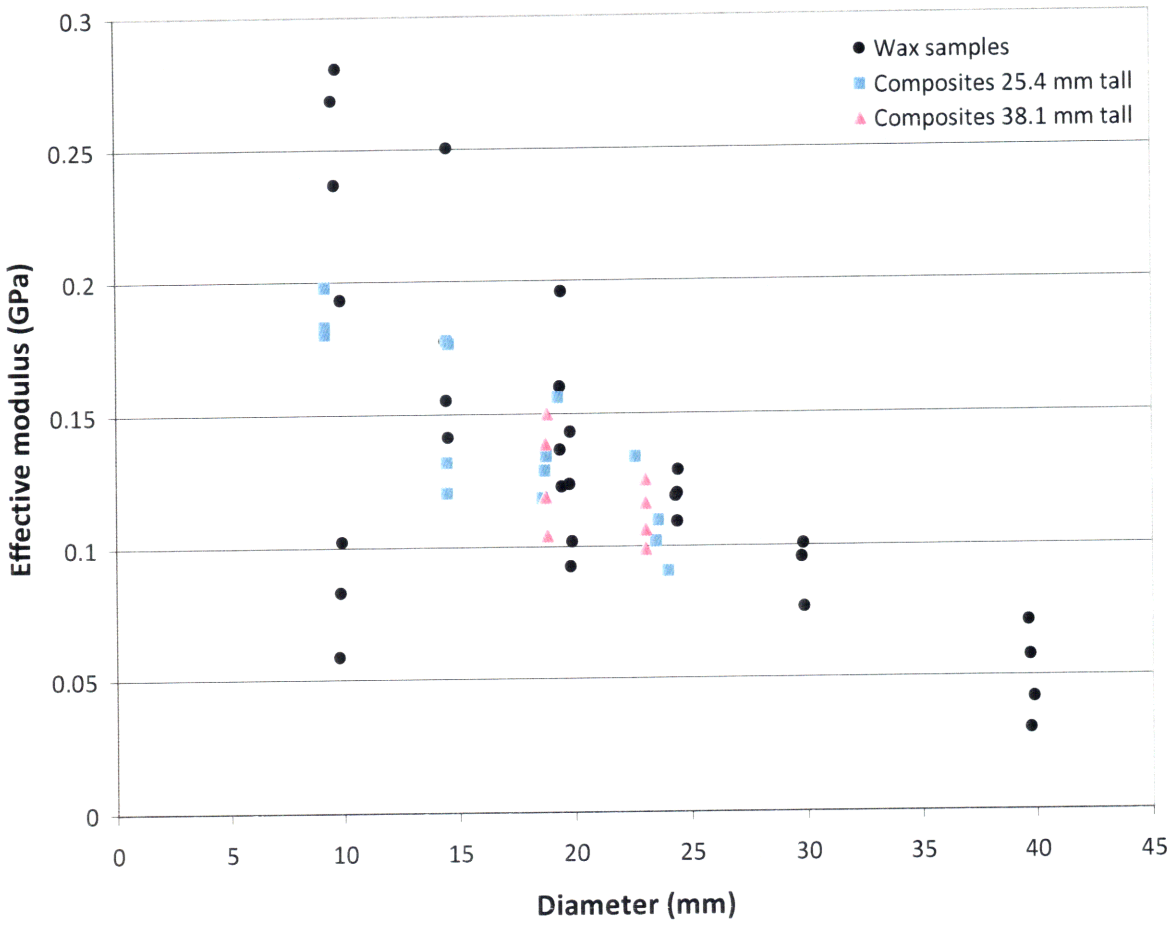

Figure 2.25: Effective modulus vs. diameter data for both composites and wax samples.

These plots indicate that the waxes and composites exhibit similar trends in modulus values. Figure 2.25 is particularly interesting because it suggests that the composites' moduli are highly dependent on cross section, which was not as clearly reflected by the data for the waxes.

Similar to the conclusions drawn from the wax compression tests, the composite samples that were tested might not provide an accurate bulk modulus for the material. However, they are still important to study because the way they are prepared (i.e., as individual samples that are cooled at room temperature) mimics realistic operating conditions if the composites were to be used as robotic components. Future research will involve determining the bulk modulus of the composites by annealing samples before testing them.

2.3.2 Volume fraction dependent tests for 1 cm diameter samples

Experiments were conducted to determine how to repeatably achieve desired volume fractions, or the ratio of the volume of wax to the total volume of the composite. It was also important to determine if there was a correlation between a composite's volume fraction and its modulus so that a composite could be appropriately designed to have a specified modulus. The experiments discussed in this section were performed in one of the earlier phases of the project when super absorbent PU (1) was used for the wax-foam composites.

2.3.2.1 Sample preparation: use of adapted tweezers

Volume fractions were controlled by limiting the amount of wax the foam contained when it was immersed in the molten wax bath. This was done by using custom-made fittings that slid onto the ends of a pair of tweezers to limit the distance the tweezers' ends could be compressed. The tweezers fittings were designed to limit the composites' compressed heights to 0.375 inches, 0.25 inches, and 0.125 inches—which is three quarters, one half, and one quarter of the initial height of each 0.5-inch composite, respectively. A set of these 3D-printed tweezers fittings is shown in Figure 2.26.

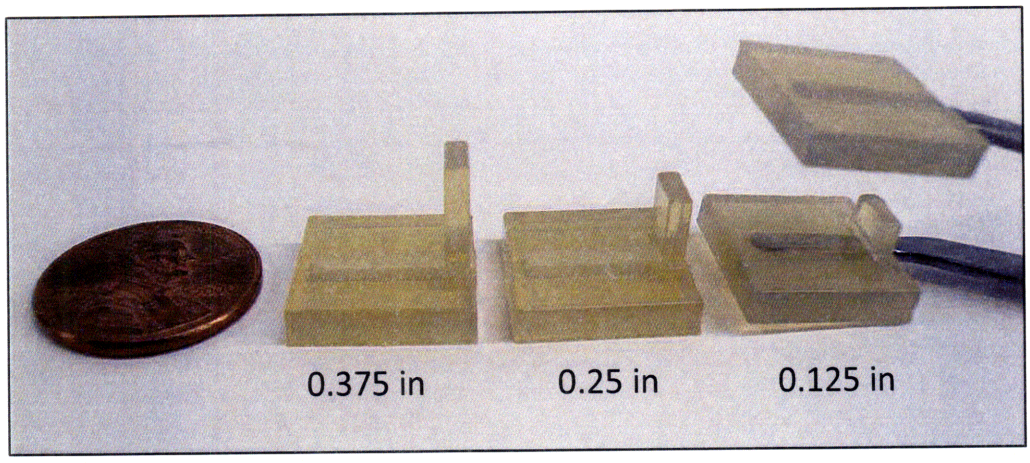

Figure 2.26: 3D-printed tweezers fittings used to limit the distance a pair of tweezers could be compressed to. Fittings were made to limit the compression height to 0.375", 0.25", and 0.125" (the initial height of each composite sample was 0.5").

A detailed description of the sample-preparation process is listed in Table 2.12, with images to accompany several of the steps in Figure 2.27. The samples were chosen to be 10 mm in diameter to be an appropriate size for SQUISHbot.

Table 2.12: Procedure for producing composites with controlled volume fractions

Step no.	Description
1	Cut the foam into cylinders using a 10 mm-diameter circular hole punch on a drill press (the shaft of the hole punch can be fit into the chuck of a drill press). Resulting foam cylinder dimensions: 12.7 mm height, 10 mm diameter.
2	Saturate each foam cylinder sample with wax by immersing the foam samples in a molten wax bath in a glass beaker on a hot plate. With the foam still in the bath, use bare tweezers to force as much air out of the foam as possible. Check that no more air bubbles are leaving the foam.
3	Put the 3D-printed tweezers fittings onto the end of the tweezers. With the saturated foam sample still in the wax bath, slide the tweezers over the foam so that the tweezers are in the position to compress the foam along its length.
4	Compress the saturated foam with the tweezers while the foam is still in the wax bath.
5	Using the tweezers, remove the foam from the wax bath while the foam is still compressed. Immediately allow the tweezers to open once the foam is out of the bath so that the foam can expand to its natural height. It is important for this to be done quickly so that the wax can spread uniformly throughout the foam. Place the samples on a flat surface to cool.

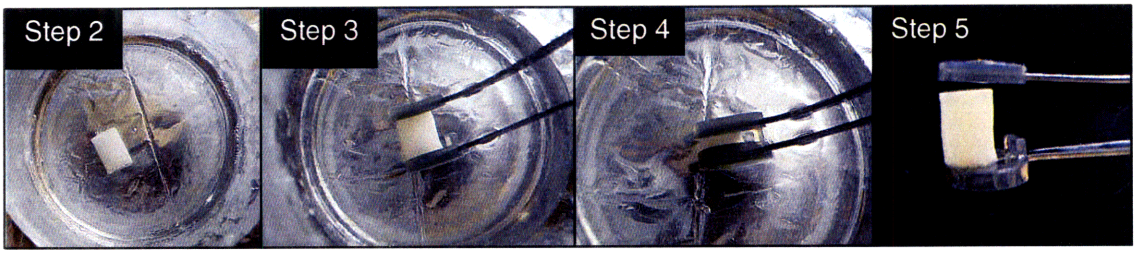

Figure 2.27: Images showing steps for producing composites with controlled volume fractions.

2.3.2.2 Results and analysis

An experiment was performed to determine how consistent the correlation was between the compressed height—of the composite before it was removed from the wax bath (Step 4 in Table 2.12)—and the mass of the final composite. This was done by performing the sample-preparation procedure in Table 2.12 for a single foam sample three times—once for each of the three compressed heights (0.125", 0.25", and 0.375") using adapted tweezers. The mass of the composite was measured after the sample was removed from the bath and cooled. A fourth data point for the same foam sample was taken by measuring the mass of the sample in its fully saturated state. Before a sample could go through another composite-preparation cycle (i.e., repeat the steps in Table 2.12), it was put back into the bath so that the cooled wax in the foam could melt again. Figure 2.28 shows a plot of the compressed heights (of the composites in the bath) vs. the mass of the composites for four different foam samples.

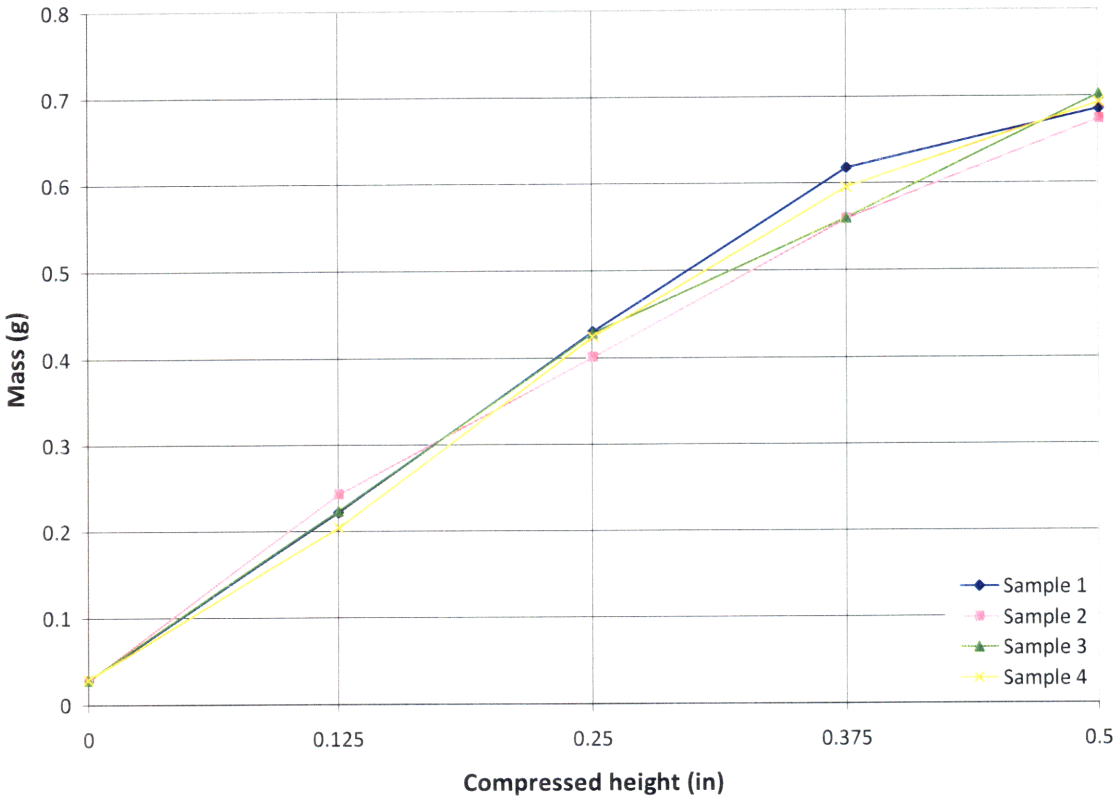

Figure 2.28: Mass vs. compressed height (of saturated foam sample before being removed from wax bath) of final composite. Foam cylinder samples (12.7-mm height, 10-mm diameter) were with of super absorbent PU (1).

The results shown in Figure 2.28 indicated that the mass of a composite was dependent on the height the foam was compressed to in the bath. They also reflected a relatively linear relationship between the compressed height and the resulting mass, as expected. This implies that desired volume fractions, related through mass, could be achieved by specifying the height to which the composite should be compressed to during the sample preparation process. Keep in mind that these relationships do not necessarily hold for samples with different dimensions or samples that are made with materials other than those used to produce the data here.

After verifying that specified volume fractions could be systematically achieved, compression tests were performed to determine if there was a correlation between volume fraction and modulus. The data for twelve samples—three for each compressed heights in addition to three fully saturated composites—is presented in Figure 2.29.

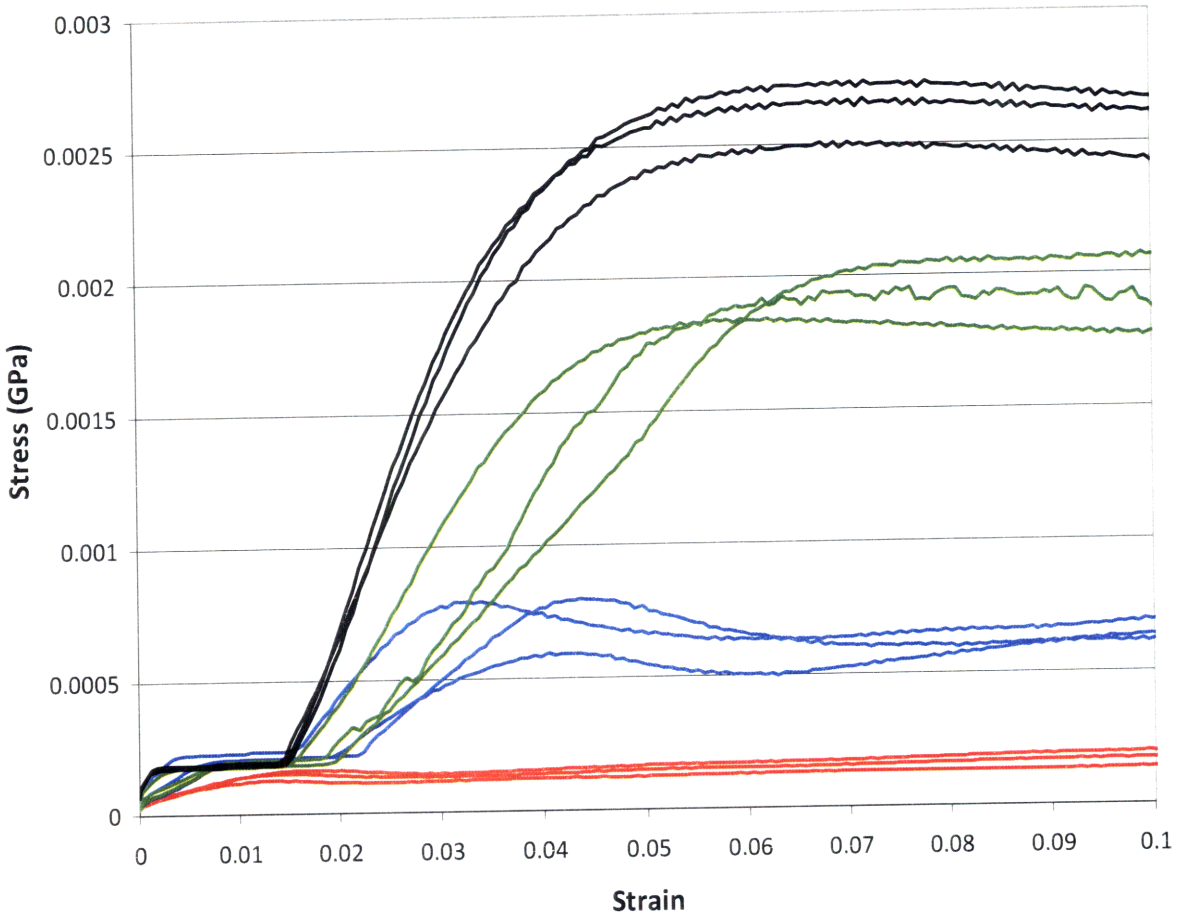

Figure 2.29: Stress vs. strain data for composites with varying volume fractions. The data is color coded as follows: fully saturated composite (black), composite compressed to 0.375" in wax bath (green), composite compressed to 0.25" in wax bath (blue), and composite compressed to 0.125" in wax bath (red).

For all the curves, except those of composites compressed to 0.125" in the wax bath (the lowermost red curves), the data before ~0.015 strain was ignored. The linear stress vs. strain portions of the data used to calculate the moduli of these samples were considered to begin at ~0.015-0.020 strain. The kinks in the curves before this strain range might be due to the machine leveling out the nonparallel surfaces of the composite cylinders, and nonlinearities in the machine. These former effects might be mitigated by controlling the sample preparation process better. For example, rather than using the current adapted-tweezers design with the compression surfaces at a slight angle to each other when the tweezers are open, the compression plates could be designed to be completely parallel during the whole compression and expansion (i.e., releasing the tweezers) process. Because the samples represented by the red curves had minimal

volume fractions, they resembled empty foams and, consequently, returned to their natural shapes with parallel top and bottom surfaces more successfully than the other samples did.

Extracting compression moduli from the data in Figure 2.29, a plot of volume fraction vs. effective modulus is shown in Figure 2.30. The volume fraction was defined as the ratio of the volume of wax in the composite to the volume of the entire composite, and was computed as:

$$\frac{V_{wax}}{V_{composite}} = \frac{\left(\frac{m_{composite} - m_{foam}}{\rho_{wax}}\right)}{V_{composite}} \tag{2.1}$$

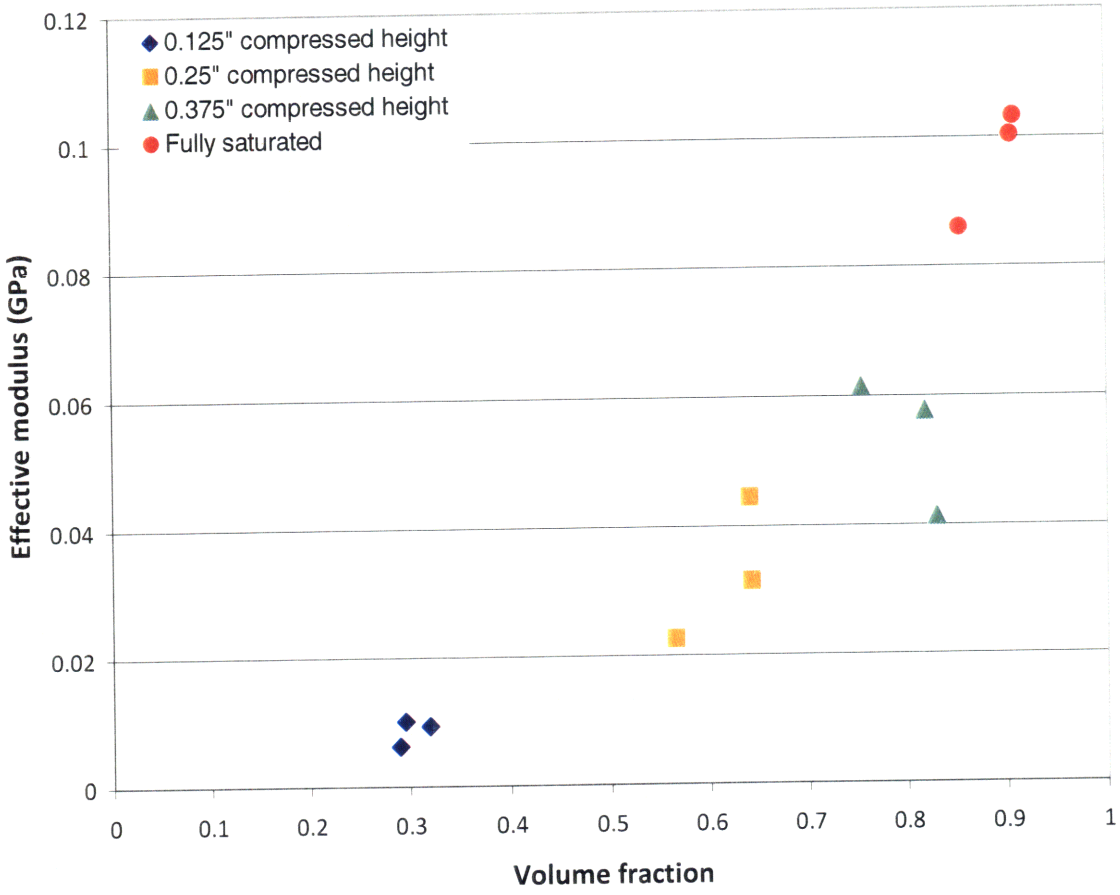

Figure 2.30: Effective modulus vs. volume fraction for foam cylinder samples (12.7 mm height, 10 mm diameter) made with super absorbent PU (1).

The data indicates a relationship between volume fraction and modulus. This relationship can allow a designer to relate compressed height (during the sample preparation

process) to volume fraction to modulus. Even if this data is for samples with a specific geometry, it suggests that similar trends can be realized for samples with other geometries. The correlation between volume fraction and modulus could be further improved with a more controlled sample preparation procedure.

2.3.3 Experimental validation of theoretical model for composites with small volume fractions

While empirical methods are useful for characterizing composites to understand their capabilities as functional components, it is also beneficial to predict the composites' behavior using analytical models. This section describes a theoretical model—developed by fellow SQUISHbot researcher Dr. Arvind Gopinath—that utilizes cellular solids theory to predict the compression modulus of wax-foam composites with small volume fractions. A comparison between the analytic model and test data is also presented.

2.3.3.1 Model description

Table 2.13 lists the variables used in the predictive model in this section.

Table 2.13: Description of variables introduced in the predictive model

Variable	Description
ρ_D^*	Density of the foam
ρ_s	Density of the material that the foam is made of
t_D	Thickness of a typical strut of a foam cell
t_w	Thickness of typical composite strut coated composed of a regular foam strut coated in a thin layer of wax
l	Length of typical strut of a foam cell
ϕ_v^D	Void fraction of a foam in its unfilled state (ratio of volume of air to volume of solid material)
ϕ_s	Ratio of the foam density to the density of the material the foam is made of (i.e., ρ_D^*/ρ_s)
ϕ_w	Volume fraction of the wax in the composite to the total volume of the composite
f	Fraction of the wax that contributes to uniformly coating the cell struts
E_w	Modulus of rigid wax
E_s	Modulus of material foam is composed of
E_{comp}	Effective modulus of a composite strut
E_w^*	Modulus of wax-foam composite

A model for a minimally saturated wax-foam composite was derived from constitutive models that have been previously developed to predict the behavior of open-cell cellular solids. The existing theory treats individual cells of foams as macroscopic structures made of interconnected struts that exhibit the behavior of beams that bend and buckle under loads [14]. These models can be modified to incorporate a thin layer of wax that coats the struts by treating the modified individual struts as composite beams. Figure 2.31 shows images of open-cell polyurethane foam in various states: (from left to right) empty, minimally saturated with wax, and fully saturated wax. As can be seen in the image of the dry foam, the cell geometries of this polyurethane foam are closest to those of a tetrakaidecahderon, or a cell that has 14 faces and an average of 5.14 sides per face. Gibson and Ashby have developed models relating an open cell foam's density to its microscopic cell geometry. All these models assume that the foam is dry, or unfilled. For a foam with a tetrakaidecahederon cell geometry, the following relationship can be assumed [14]:

$$\frac{\rho_D^*}{\rho_s} \sim C_1\left(\frac{t_D}{l}\right)^2\left(1 - D_1\frac{t_D}{l}\right) \tag{2.2}$$

where ρ_D^* is the density of the foam, ρ_s is the density of the foam's material, and t_D and l are the thickness and length of a cell strut, respectively. C_1 and D_1 are constants, the latter of which is only significant for large relative densities.

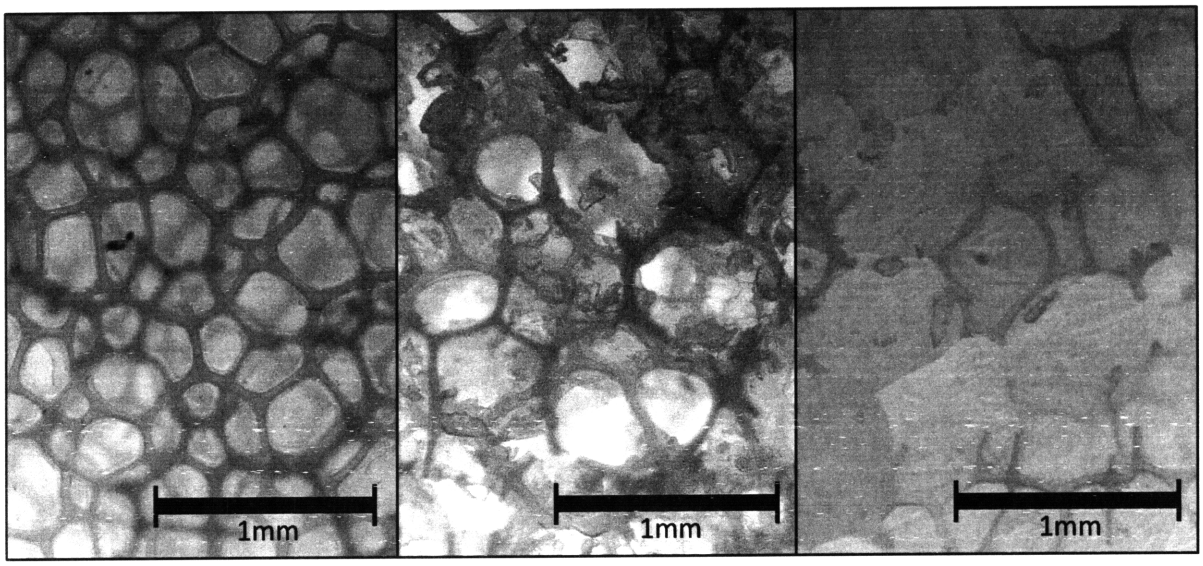

Figure 2.31: Images of PU (2) foam, in various states, taken under an optical microscope.

The porosity, ϕ_v^D, can be expressed in terms of a ratio of densities, ϕ_s, as:

$$\phi_v^D = \left(1 - \frac{\rho_D^*}{\rho_s}\right) = (1 - \phi_s). \tag{2.3}$$

When the PU foam is minimally saturated with wax, it can be assumed that the wax coats the cell struts to form a thin layer of rigid wax on top of the PU scaffold. As seen in the center image of Figure 2.31, some of the wax might not smoothly coat the struts and will, instead, form irregular lumps of wax that occupy parts of the voids. However, this particular image was taken of a minimally saturated composite sample that was sliced using a scalpel to expose an internal

cross section, so some of the wax might have been smeared, thus altering its undisturbed state. In any case, the difference between a minimally saturated sample and a fully saturated sample (which was also sliced using a scalpel and is shown in the right image) is apparent; the minimally saturated samples have significantly less wax in them than the fully saturated ones do. For the purposes of the model presented here, it is assumed that the fraction of the wax that does not contribute to uniformly coating the cell struts does not contribute to bearing the compressive loads for small strains. As discussed in 2.3.1.1, the individual struts are treated as beams in bending during the elastic regime.

The wax volume fraction—or the ratio of the volume of wax to the total volume of the composite—is denoted as ϕ_w, while f is the fraction of the total wax that contributes to coating the cell struts. Let E_s be the modulus of the material the foam is composed of (polyurethane), E_w be the modulus of the solid wax, and t_w be the thickness of a composite strut. If only a thin layer of wax is added to the PU foam struts, (2.2) can be extended to characterize the minimally saturated composites by treating the individual struts as isotropic composite beams. The modulus of the composite material, E_{comp}, for small volume fractions can be approximated as follows:

$$E_{comp} = \frac{\phi_s E_s + f\phi_w E_w}{\phi_s + f\phi_w}. \tag{2.4}$$

The relative densities, ϕ_s, of the empty foam can be reduced to $\phi_s = (t_D/l)^2$ from (2.2) because C_1 is generally unity and D_1 is negligible because the relative densities are small [14]. Extending this relationship to the wax-foam composite becomes

$$\phi_s + f\phi_w \sim (t_w/l)^2. \tag{2.5}$$

For a unit cell of a minimally saturated composite, a stress σ can be approximated to be acting over a cross-sectional area l^2. Each composite strut experiences a deflection of $\delta_w \sim \sigma l^2 \left(l^3/E_{comp} t_w^4\right)$ or $\delta_w \sim \sigma l^5 \left(E_{comp} t_w^4\right)^{-1}$. Therefore, the strain experienced by a unit cell

becomes $\varepsilon_w \sim \delta_w / l \sim \sigma l^4 \left(E_{comp} t_w^4\right)^{-1} = \sigma (l/t_w)^4 E_{comp}^{-1}$. The effective modulus of this unit cell is defined as $E_w^* \equiv \sigma / \varepsilon_w$ and can be written as $E_w^* = E_{comp} (t_w / l)^4$. Substituting in (2.4) and (2.5) gives

$$\frac{E_w^*}{E_s} \sim \left(\frac{t_D}{l}\right)^4 \left[\left(1 + f\frac{\phi_w}{\phi_s}\right)\left(1 + f\frac{E_w}{E_s}\frac{\phi_w}{\phi_s}\right)\right] \sim \phi_s^2 \left(1 + f\frac{\phi_w}{\phi_s}\right)\left(1 + f\frac{E_w}{E_s}\frac{\phi_w}{\phi_s}\right). \qquad (2.6)$$

In the limit of small volume fractions, in which the wax effectively changes the thickness modulus of the struts, this can be simplified to arrive at a linear approximation:

$$\frac{E_w^*}{E_s} \sim \phi_s^2 \left(1 + f\frac{\phi_w}{\phi_s}\left(1 + \frac{E_w}{E_s}\right)\right). \qquad (2.7)$$

2.3.3.2 Sample preparation process

Compression tests were performed on minimally saturated wax-foam composite samples to validate the analytic model described in the previous section. Samples were prepared similarly to how they were for the samples described in 2.3.2, which were purposely constructed to have varying volume fractions. This latter sample preparation procedure, in which customized tweezers were used to limit the amount of wax in a foam sample, is described in Table 2.12. Instead of using adapted tweezers to prepare minimally saturated samples, a pair of large tongs—shown in Figure 2.32—was used to compress the foams as much as possible, after which the compressed sample was immediately removed from the bath and allowed to expand to its natural shape once it left the bath. The sample preparation procedure for making minimally saturated wax-foam composites is listed in Table 2.14, with images from select steps presented in Figure 2.33.

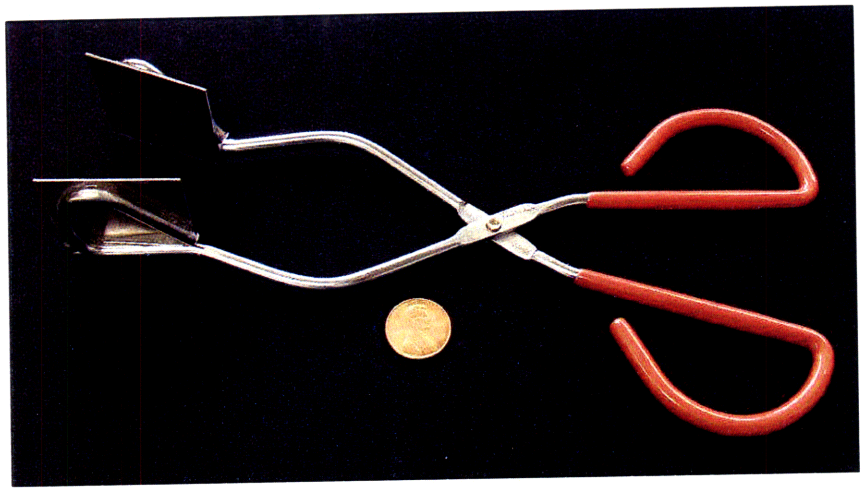

Figure 2.32: Tongs used to prepare minimally saturated composite samples.

Table 2.14: Steps for producing minimally saturated composites.

Step no.	Description
1	Cut the foam into cylinders using circular hole punches (the shaft of the hole punches can be fit into the chuck of a drill press).
2	Saturate each foam cylinder sample with wax by immersing the foam samples in a molten wax bath in a baking pan on a hot plate. With the foam still in the bath, use bare tweezers to force as much air out of the foam as possible. Check that no more air bubbles are leaving the foam.
3	With the saturated foam sample still in the wax bath, position the tongs around the foam so that the tongs are can compress the foam along its length.
4	Compress the saturated foam with the tongs while the foam is still in the wax bath.
5	Using the tongs, remove the foam from the wax bath while the foam is still compressed. Immediately allow the tweezers to open once the foam is out of the bath so that the foam can expand to its natural height. It is important for this to be done quickly so that the wax can spread uniformly throughout the foam. Place the samples on a flat surface to cool.

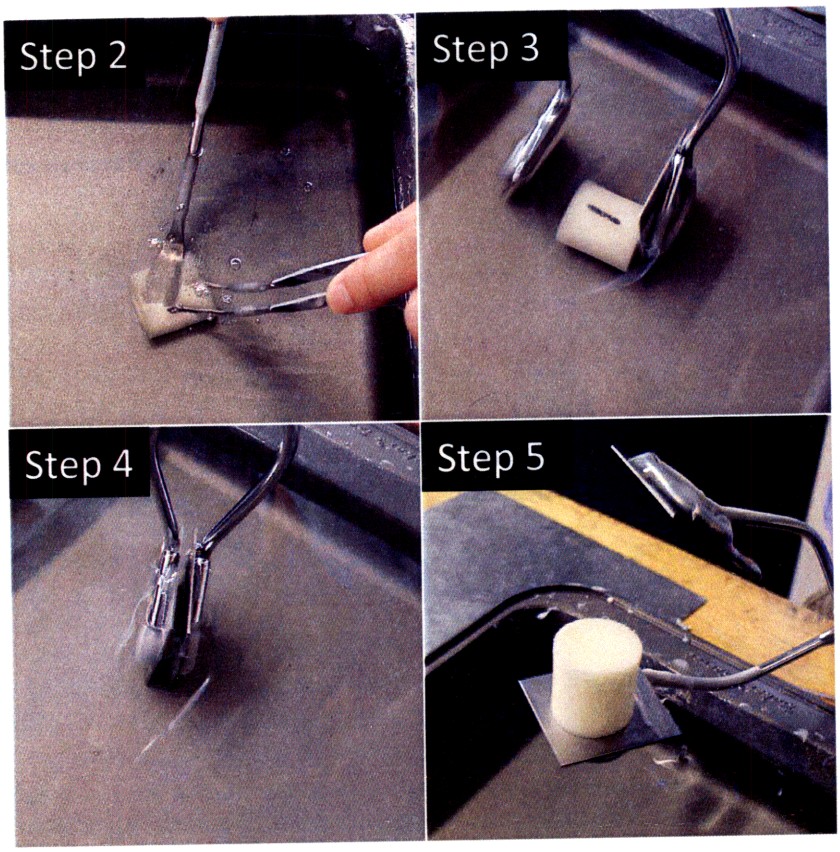

Figure 2.33: Select images from sample preparation process for making minimally saturated wax-foam composites.

2.3.3.3 Test results

The Texture Analyzer was used to perform compression on the minimally saturated composites. The composites were composed of batik wax and PU (1). An initial set of tests was performed on cylindrical samples that were 25.4 mm tall with varying diameters of 10 mm, 15 mm, 20 mm, and 25 mm. A plot of effective modulus vs. volume fraction is presented in Figure 2.34. Volume fraction was defined as the ratio of the volume of the wax to the volume of the entire composite; it is expressed in terms of known parameters in (2.1).

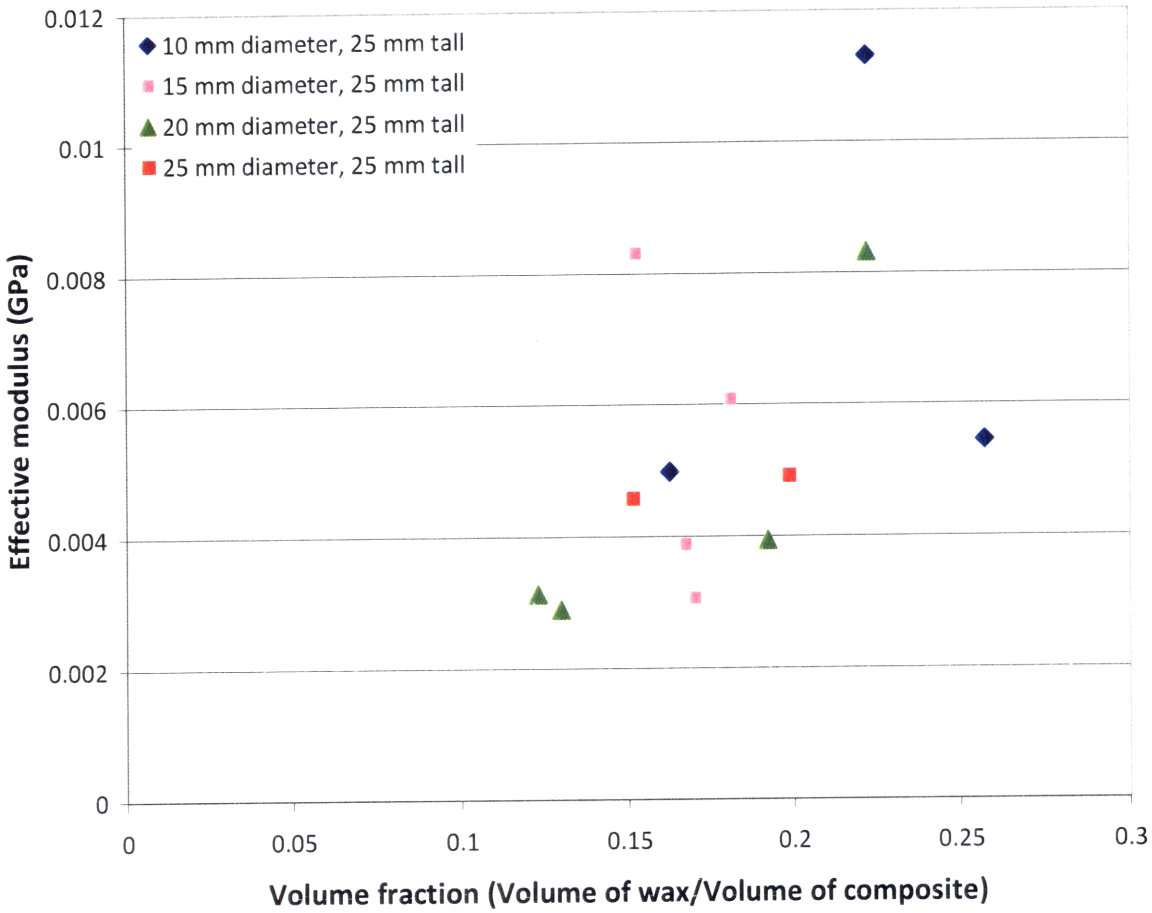

Figure 2.34: Effective modulus vs. volume fraction data for composites with low volume fractions.

The results reflected a general trend of higher volume fractions correlating with higher effective moduli, which was the expected result from earlier studies discussed in 2.3.2. However, the data was considerably inconsistent even for samples with the same dimensions; this is most likely due to the fact that it was difficult to prepare minimally saturated samples whose wax was uniformly distributed throughout the foam. Observations during the sample preparation process indicated that samples that were relatively slender tended to buckle, causing regions along the perimeter of the foam to be fully saturated with wax. This could be visually verified after the samples were cooled, as more saturated regions appeared to be darker than those that were only partially filled with wax. In contrast, the more squat samples with larger aspect ratios—specifically, samples that were 20 mm and 25 mm in diameter—exhibited more true compression so that the wax was more uniformly distributed throughout the sample. These

observations can be inferred by the data; the more slender the samples were, the more randomly distributed their data was.

Because of these inconsistencies, another set of tests was performed on samples that were selected to be 25 mm tall and 25 mm in diameter to minimize the sample variation. Figure 2.35 presents the modulus vs. volume fraction data for these samples. Even though it was likely for the modulus to be geometry-dependent, as demonstrated in 2.3.1.2 and 2.3.1.3, a specific sample geometry was selected to be used to conduct a first-order comparison between empirical data and predicted data generated by the model presented in the previous section.

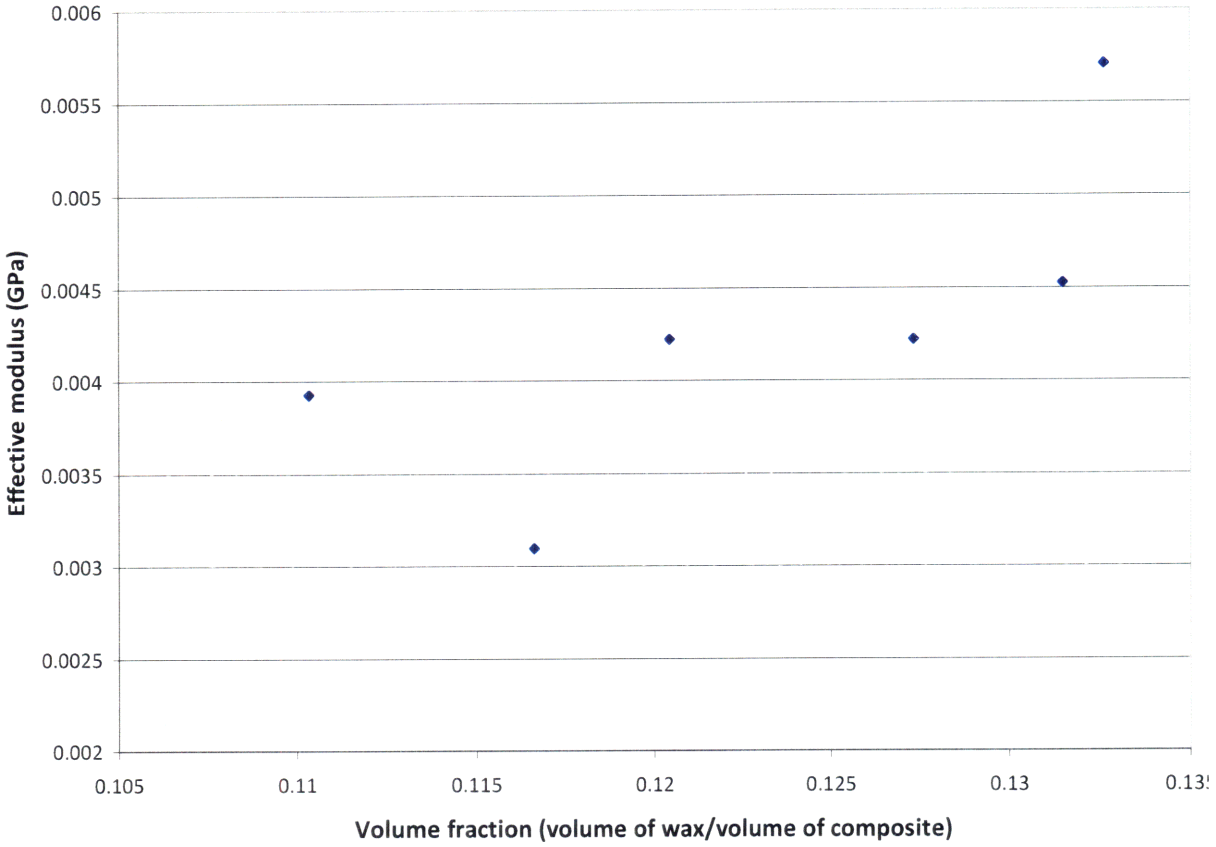

Figure 2.35: Effective modulus vs. volume fraction for composites with low volume fractions. Sample sizes were 25 mm in diameter and 25 mm tall.

Again, the variation across different samples was most likely due to the inconsistent nature of the sample preparation procedure. However, the range of modulus values represented in this recent set of tests is significantly smaller than that of the first test, shown in Figure 2.34.

2.3.3.4 A comparison between the test data and the predicted data

Predicated values for the bulk modulus of composites with small volume fractions were generated using (2.6). Constants used in this equation were ρ_s = 1200 kg/m^3 [14], ρ_D^* = 29.7585 kg/m^3 (calculated from measured parameters), f = 1, E_w = 0.15 GPa (selected as a mean value from data presented in 2.3.1.2), and E_s = 1.6 GPa [14]. Figure 2.36 presents a plot of modulus vs. volume fraction for small volume fractions to compare the empirical values with the predicted ones.

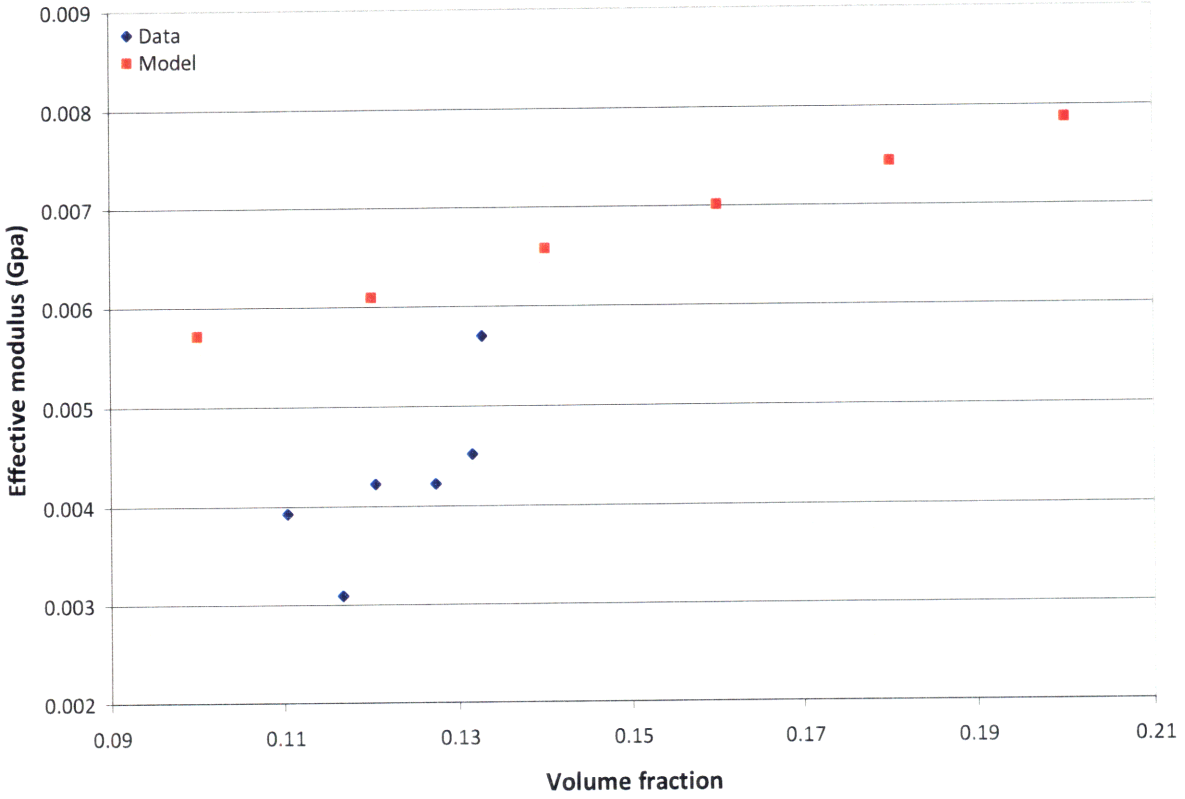

Figure 2.36: Effective modulus vs. volume fraction for composites with low volume fractions to compare empirical data with predicted values.

The two sets of data exhibit modulus values that are within the same order of magnitude. As a preliminary evaluation of the predictive model, this is encouraging, especially because f = 1 was a conservative estimate; Figure 2.31 suggests that f < 1 for small volume fractions, meaning that the predicted modulus values should be closer to the values obtain from the actual

data. In addition to developing a more reliable sample preparation method, future work will be conducted to improve and modify the model to predict the behavior of composites with a larger range of volume fractions. As large volumes of wax begin to dominate the behavior of the composites, simple beam equations are no longer applicable; the composite will more likely resemble a solid piece of wax with structural voids in it.

2.4 Future work for composite characterization

2.4.1 Cyclic testing

It is important to understand that, for the work presented in this thesis, any compression modulus extracted from test data is only an "effective" modulus. Previous sections have demonstrated that the modulus is dependent on a sample's dimensions. In addition, a surprising observation was made while testing a fully-saturated composite sample with a large cross section: although the sample had visibly cracked down its side, the real-time data indicated that the force vs. displacement curve—and, consequently, the stress vs. strain curve—was still in its initial linear elastic regime. While the sample was obviously plastically deforming, the shape of the curve indicated otherwise. Therefore, the modulus obtained by calculating the slope of the assumed elastic regime was not necessarily the true modulus.

To further investigate the aforementioned discrepancies, cyclic compression tests should be performed on samples within what was originally thought to be the elastic regime. Figure 2.37 shows a plot of stress vs. strain data for a single composite sample that had undergone six continuous compression cycles. The sample was a fully saturated wax-foam cylinder, made with PU (2) foam, that was 8.92 mm in diameter and 12.81 in height. The test was performed on the Texture Analyzer with a 30 kg load cell and a test speed of 2 mm/min.

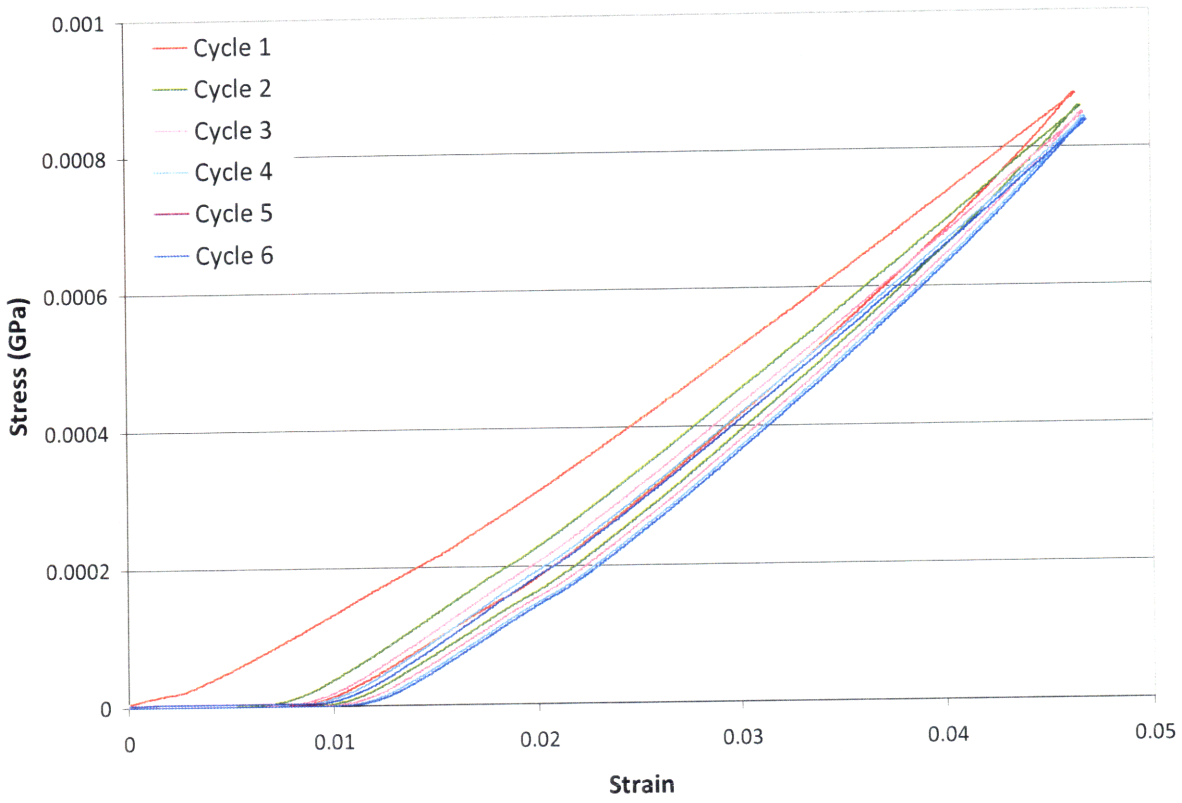

Figure 2.37: Stress vs. strain data for a single composite sample compressed for 6 complete cycles.

Here, zero strain is defined at the initial height of the sample at the beginning of the first compression cycle. The data indicates that the composite did not experience true elastic deformation during any of the six compression cycles even though the curves did not appear to reach the proportionality limit. In other words, after the platen compressed the composite and returned to the height at which it first contacted the sample (at the beginning of the same compression cycle), the sample did not achieve its original height and was therefore plastically deformed. However, the sample did continue to expand between cycles when it was not in contact with the platen. This is indicated in the plot: the strain that each cycle's curve started at was smaller than the strain the previous cycle intersected the horizontal axis at (or when the sample no longer contacted the platen). This viscoelastic effect might suggest that the sample was capable of creep and was more elastic than it appeared to be, as it could expand to a larger height given adequate time. Future cyclic compression tests will need to be conducted with

holding times, during which the platen would remain fixed for a given amount of time at peak amplitudes to allow the sample to achieve its potential dimensions.

The data in Figure 2.37 can be further analyzed by identifying whether there was a quantifiable relationship between how much the sample was plastically and elastically deformed during each cycle. This might be helpful in developing a comprehensive understanding of the performance capabilities of the composites, as they might be expected to experience cyclic loading in robotic applications. Figure 2.38 presents a plot of the ratio of plastic strain to elastic strain vs. the cycle number. Using the curves in Figure 2.37, plastic strain was defined as the difference in strain between the beginning of one compression cycle (when the platen first contacted the sample, denoted by non-zero stress) and the beginning of the following cycle. Elastic strain was defined as the difference between the peak strain for one cycle and the strain at the beginning of the next cycle.

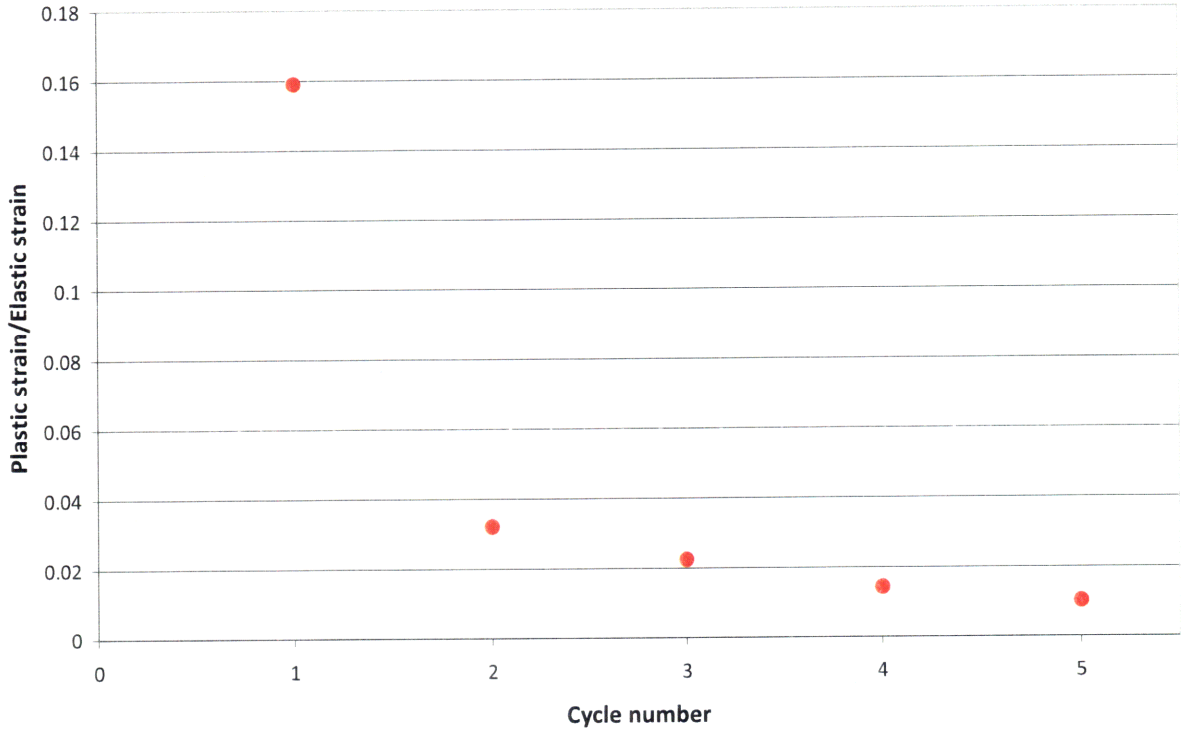

Figure 2.38: The ratio of plastic strain/elastic strain vs. cycle; data was obtained from Figure 2.37.

Only five data points are shown in Figure 2.38 because the amount of plastic or elastic strain for one cycle depended on information about the following cycle; therefore, these

parameters could not be determined for the sixth cycle. This data suggests that the plastic strain converges towards zero, at which tests can be performed to identify a true modulus (though for a sample that had undergone multiple compression cycles). This is supported by the fact that the data for cycles 5 and 6 are nearly identical. This might be difficult to ascertain by looking at the plot in Figure 2.37, though one can verify that the peaks (at maximum strain) of only five different curves can be identified.

A hypothesis for why the supposed elastic regime includes some plastic deformation is that initial loading breaks weaker cell struts, such as those of incomplete cells on the perimeter of the foam.

2.4.2 Bending tests

As discussed earlier, compression testing was selected as the first method used to quantify the material properties of the composites. Other testing methods that would be useful for understanding the capabilities of the composites as structural components include bending tests and tensile tests. However, compression tests were selected over these latter two because compression tests are the most simple of the three to perform. In contrast to simply placing a sample between two large platens for a compression test, bending tests require accurately aligning a sample with the test jig, while tensile tests require adequately clamping a sample without damaging it. It is also much easier to prepare samples for compression tests because they can be relatively small compared to beams that need to be made for bending or tensile tests. Not only is it more difficult to ensure that a foam beam is fully saturated with wax (its volume is relatively large compared to that of a compression test sample), but it is also very difficult to make consistent samples, as the beams tend to warp as they cool; depending on the surface they are cooled on, they usually tend to curve upwards away from the cooling surface.

It might be necessary to perform bending tests on composite beams, especially if the composites are expected to be used as actuatable beam elements in SQUISHbot (examples of how they might be used are discussed in Chapter 3). Some preliminary bending tests have been performed to determine performance metrics such as maximum torque. An image of the test set-up on the Zwick for these tests is shown in Figure 2.39. Each beam was placed on an aluminum rig with fixed-width "L," which defined the beam length for each test. Similar to how the compression tests were performed, the top, moving platen was replaced with a narrow one with a

rounded edge to simulate a point load. Force vs. displacement curves for several of the tests are presented in Figure 2.40, where each colored curve represents a different test sample. All the samples represented in the plot were fully saturated wax-foam beams that consisted of batik wax and PU (2); each beam was roughly 13 mm tall, 10 mm wide, and 38.4 mm long (the latter of which was defined by the test jig). The foam beams, before being saturated with wax, were laser cut from a sheet of foam.

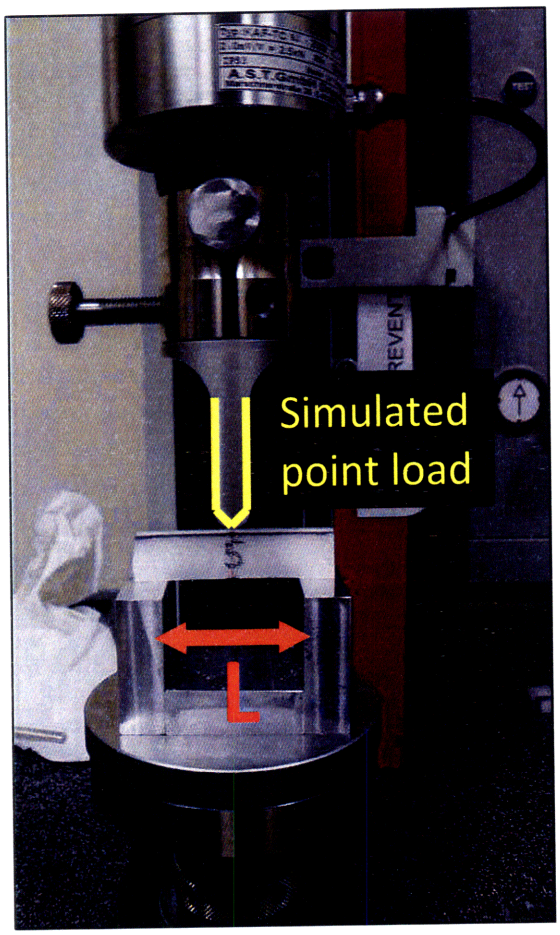

Figure 2.39: Test set-up on Zwick for bending tests on beam samples. A fully saturated wax-foam composite is shown here, with L = 38.4 mm.

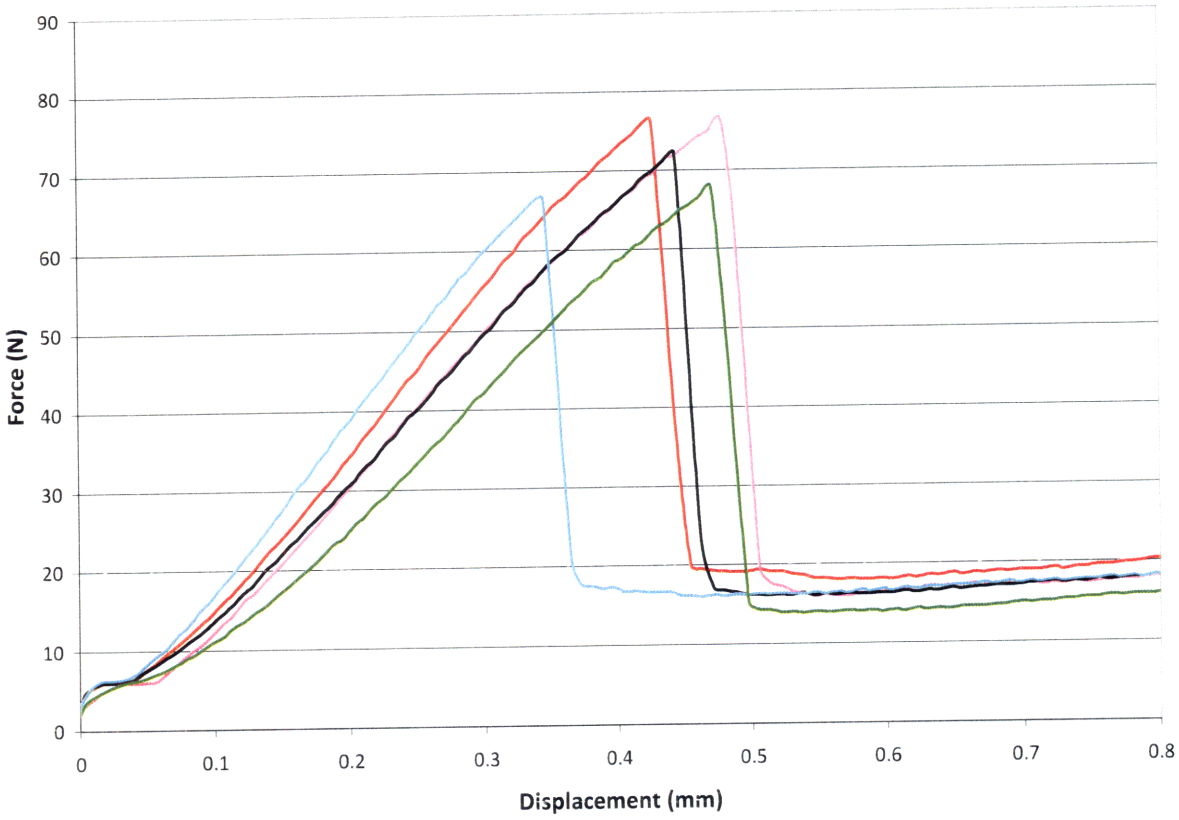

Figure 2.40: Force vs. displacement curves from several preliminary bending tests performed on fully saturated wax-foam composite beams. All the beams were roughly 13 mm tall, 10 mm wide, and 38.4 mm long (the latter of which was defined by the test jig).

As the curves indicated, the tests were very consistent in that the composite beams exhibited brittle fracture upon reaching their maximum load loads. The average maximum torque each of these samples exhibited was 675 N-mm. Because this parameter is geometry-dependent, it is important to perform bending tests on samples with anticipated dimensions for specific applications. In addition to performing bending tests on rigid composites, tests also need to be conducted on thermally activated samples (for instance, by creating a compliant joint by melting a portion of the beam via resistive heating) to determine the relative compliance of the beam in various states. This is necessary, as the composites are to be used as controllable-stiffness structures.

2.4.3 Acquire temperature-dependent data

While this chapter has studied the composites and their components in their solid states in detail, considerable work needs to be done to truly understand the capabilities of using the composites as controllable-stiffness structures. In addition to performing compression and bending tests in which parameters, such as modulus and torque, are functions of temperature, cyclic tests need to be conducted to determine how the composites' performance change over time. These tests would involve cyclic loading as well as cyclic activation and deactivation (i.e., heating and cooling) of the composites.

2.4.4 Developing and validating predictive models using 3D-printed foams

Cellular solids are not limited to commercially available foams. Especially for the active fluid-cellular solid composites being investigated here for soft robotic applications, the functionality of the composites might be improved if the engineer could design the "foam" component to better fulfill performance specifications. For example, if the structure needed to be more stiff in one direction than in others, desired anisotropy could be achieved by designing the cellular architecture of the foam.

Preliminary work has been done to 3D-print polymer anisotropic "foam" structures with macro-scale cell geometries, as shown in Figure 2.41. These printed cellular solids provide a useful platform for developing and validating predictive models for the structural properties of fluid-foam composites, as the engineer has control over individual cell geometries.

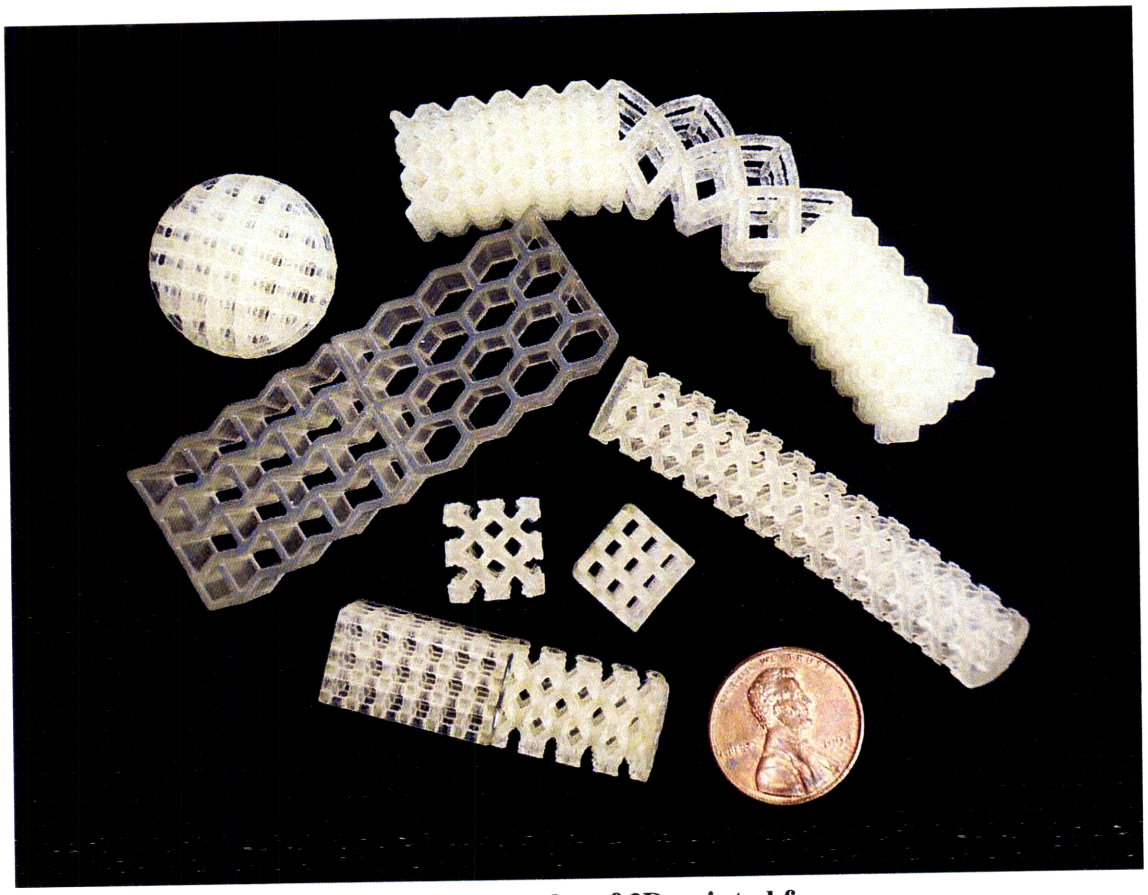

Figure 2.41: Examples of 3D-printed foams.

2.4.4.1 Using 3D-printed foam as platform for developing predictive models

An immediate use of these 3D-printed cellular structures is to validate the model discussed in 2.3.3, which predicts the behavior of foams whose cell walls, or struts, are thinly coated in wax. Though the model assumed that the wax was uniformly distributed throughout the sample, it was extremely difficult to control this property when commercially available polyurethane foams were used. In contrast, and as can be seen in Figure 2.41, it would be much easier to identify how the wax interacts with the printed foams. In the case where the cell struts must be thinly coated with wax, samples could be prepared by dipping the printed foams in a wax bath and immediately removing them so that only a thin layer of wax solidifies on the printed struts. To increase the thickness of a wax layer, this process can be repeated multiple times. This is similar to how candles are made: the candle wick is continuously dipped into and removed from a bath of wax until the candle reaches a desired diameter.

2.4.4.2 Designing anisotropy into foam structures

With the freedom to customize the bulk properties of a foam by designing the architecture of its individual cells, desired anisotropic stiffnesses can be achieved. This might be useful for SQUISHbot as well as other robotic applications in which functional structural components are required. Therefore, rather than relying on a complex actuation system to control an isotropically compliant composite structure, directional properties can be "programmed" into the foam component of the composite. Theoretical models, similar to the one described in 2.3.3.1, can be developed to predict the behavior of—and even optimize—these "designer foams."

Several anisotropic open-cell polymer "foams" that have been 3D-printed are shown below. Figure 2.42 shows two cubes that exhibit different strain characteristics when the same normal force is applied to them; one cube shears while the other one compresses. "Cube 1" tends to shear rather than compress because more force is required to buckle the struts (which would force the structure to compress) than to shear the bulk structure.

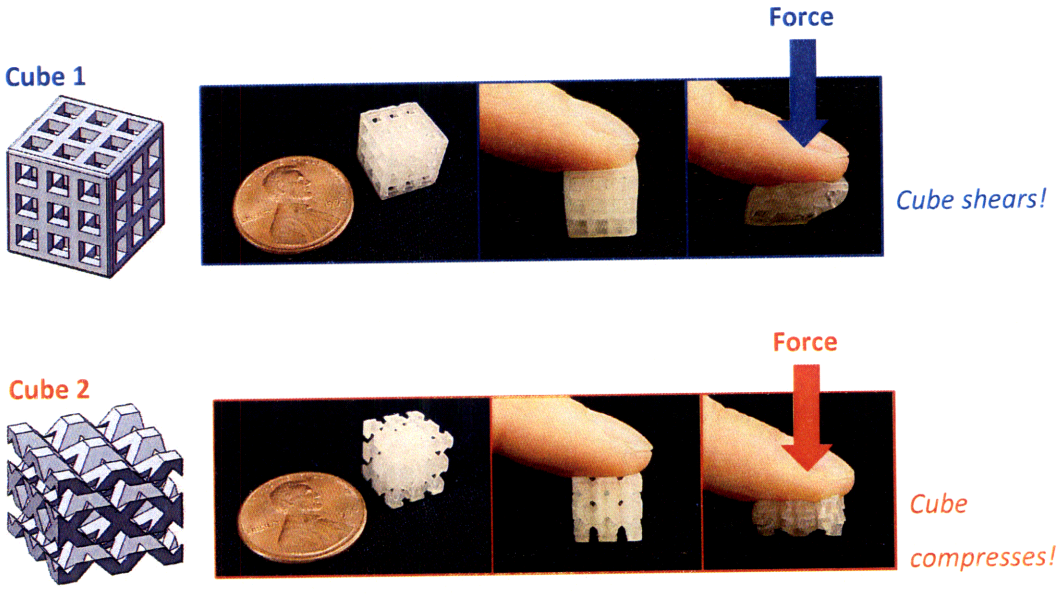

Figure 2.42: Two open-cell 3D-printed foams that respond differently to the same applied force.

These two types of modules—one that tends to shear when acted upon by a normal force and another that tends to compress when acted upon by the same force—can be joined in series

and still provide distinct responses to a centrally applied force. An example of this is shown in Figure 2.43, where half of the length of the printed foam is composed of shearing modules while the other half consists of compression modules. In the diagram labeled "1," the entire structure is shown with no external forces applied to it. In diagram "2," the ends of the structure are pushed together, causing the top half to shear and the bottom half to compress.

This particular example might be useful for a robot's limb, in which bending and extension joints can be decoupled yet still controlled by a central actuator (in this case, the central actuator can be a retractable cable that runs through the length of the structure). The two distinct portions of the limb can be selectively turned "on" or "off" by activating or deactivating the controllable-stiffness fluid that occupies them. This is an excellent example of how anisotropy can be designed into the scaffolding of the fluid-foam composites to improve the performance of functional components.

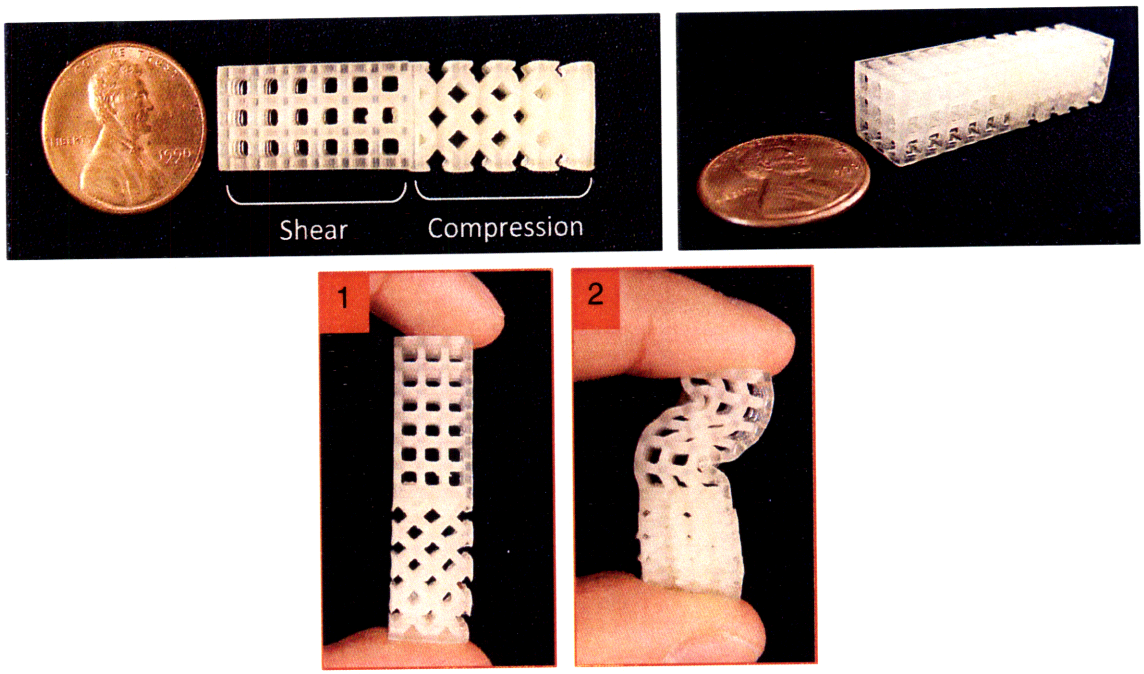

Figure 2.43: Two different anisotropic modules—one that shears and another that compresses when the same normal force is applied—are joined in series.

A demonstration of how these 3D-printed structures can exhibit directional stiffness was conducted by performing compression tests on anisotropic spheres to determine the stiffnesses along different planes. The sphere design that was used for this demonstration is presented in

Figure 2.44. A CAD model is shown on the left; this particular model was created by effectively removing a three-dimensional array of evenly spaced cubes from a solid sphere.

Figure 2.44: 3D sphere design used to demonstrate anisotropic stiffness.

Depending on the direction of the applied force, this sphere exhibits different stiffnesses. When compressed along the direction parallel (or perpendicular) to the straight edges of the removed squares, the structure is very stiff; it requires significant force to buckle the cell struts to cause the structure to compress (as demonstrated by "Cube 1" in Figure 2.42). If the direction of the applied force is rotated 45° relative to the sphere, the structure responds very differently, as it is least stiff along this plane of compression. This is illustrated in Figure 2.45, where each 3D-printed sphere is labeled with a solid line and a dotted line to represent the directions of applied normal forces that produce the maximum stiffness and the minimum stiffness, respectively. The sphere in the right image was rotated 45° relative to the sphere in the left image. In each image, a person's finger was used to apply a normal force to the sphere. The sphere in the right image compressed significantly more than the one on the left did because it was compressed along the direction of the dotted line, or the direction that resulted in the least stiffness. Conversely, the sphere in the left image barely compresses because it was compressed along the direction of the solid line, or the direction of applied force that results in maximum stiffness for this particular structure.

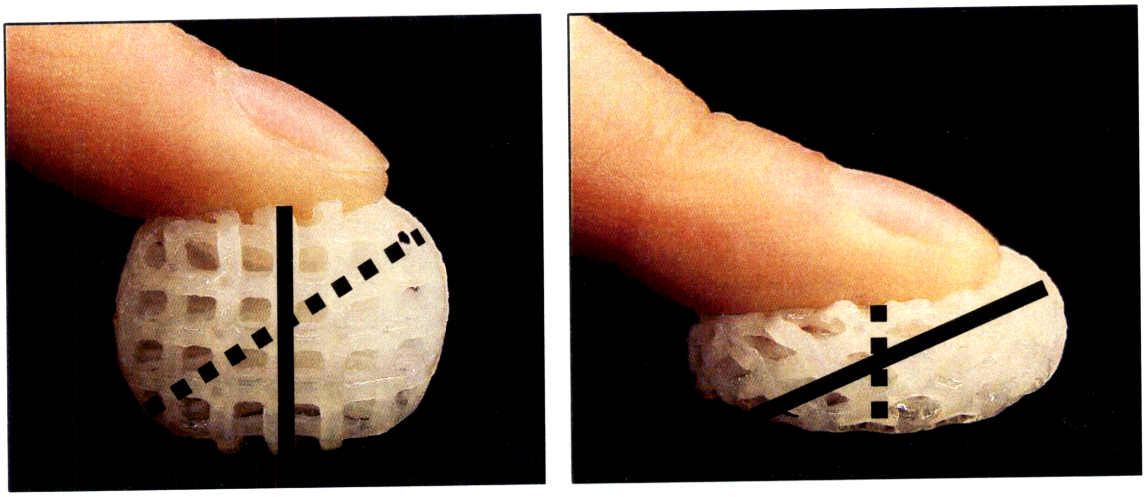

Figure 2.45: 3D-printed anisotropic sphere.

Compression tests were performed on this sphere to determine the difference in bulk stiffness when compressing the sphere along the direction of the solid line (the stiffest direction) versus compressing it along the direction of the dotted line (the most compliant direction). Specifically, one cycle of compression was performed in each direction to identify any hysteresis. The tests were performed on the Texture Analyzer with a 5kg load cell and a test speed of 2 mm/min. The results are presented in Figure 2.46.

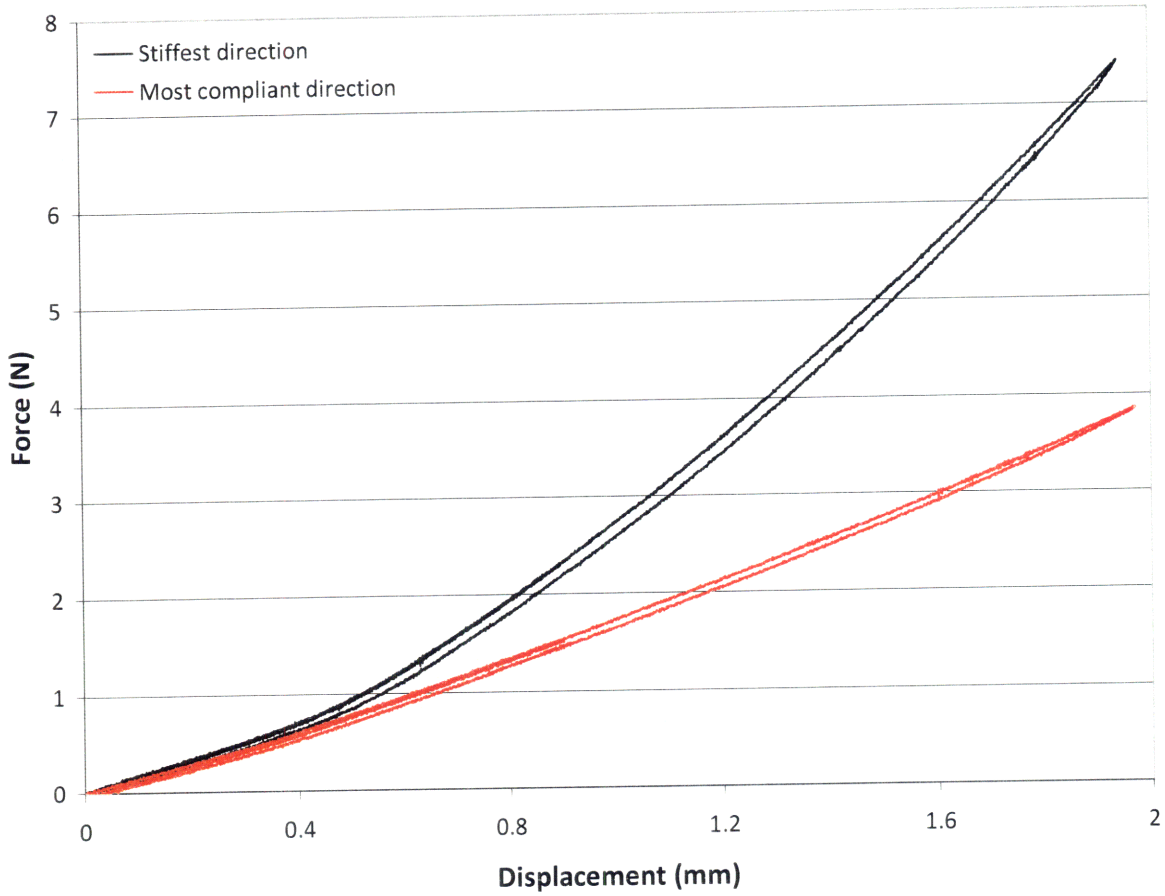

Figure 2.46: Compression tests results for a 3D-printed sphere.

The plot indicates that the sphere can experience different degrees of stiffness depending on the loading direction. As the two plots diverge further apart, the stiffness of the sphere in its stiffest direction is greater than twice the stiffness of the sphere in its most compliant direction. The data also reflects slight hysteresis for loading along both directions; however, the curve representing compression in the stiff direction reflects non-linear elasticity in comparison to the linear elasticity occurring during compression in the compliant direction. This is true because the former becomes stiffer with increased loading as more force is required to deflect the struts (the struts eventually buckle, but the sphere was not compressed enough during the test for this to occur). Because only elastic deformation is occurring here, the 3D-printed foam structures might be more reliable—for quantitative modeling purposes—than the commercially available foams because the latter experience plastic deformation in addition to elastic deformation during initial loading.

In addition to the customizable "foams" having reliable structural behavior, they can also be designed to achieve desired anisotropy. Rather than being limited to commercially available foams that are often isotropic and have fixed bulk properties, the design space for fluid-foam composites can be vastly expanded if the engineer could approach the foam component as a scaffold that can be designed on the cellular level. This section presented several examples of cellular solids whose anisotropy can be designed to contribute to a composite structure's overall functionality. Whether or not these 3D-printed "foams" can be used in fluid-foam composites in the near future (they currently have limited durability and time-dependent stiffness properties as the material becomes brittle over time), they can certainly contribute to developing and validating models used to optimize designable foam structures for applications beyond SQUISHbot.

CHAPTER

3

ROBOTIC APPLICATIONS FOR WAX-FOAM COMPOSITES

Proof-of-concept work has been done to create functional robotic elements using wax-foam composites. Though the components presented in this chapter were primarily inspired by SQUISHbot, they can conceivably be used in broader robotics applications.

3.1 To-date case studies

3.1.1 Universal joints

Perhaps the simplest implementation of a controllable-stiffness structure, a universal joint, could be easily constructed by locally heating a wax-filled foam beam. This was done by wrapping wire around a portion of a composite beam and relying on resistive heating to locally melt the wax so that a compliant joint could be created. An example of a 10 mm diameter wax-filled cylindrical beam (made with batik wax and super absorbent PU (1)) is shown in Figure 3.1. This joint was activated by running 1 amp (at 3.3 volts) through 36 gauge copper wire, which was coiled around a section of the beam 40 times. Figure 3.1 shows the cantilevered beam, with a 100 gram mass hanging from its free end, in both its non-activated (i.e., no heating; rigid joint) and activated (i.e., heated; compliant joint) states. A series of images also shows the beam at several instances throughout the activation process, during which constant current of 1 amp was run through the wire to locally melt the wax to turn a portion of the beam into a compliant joint. It took approximately 70 seconds of constant power input to create the compliant joint.

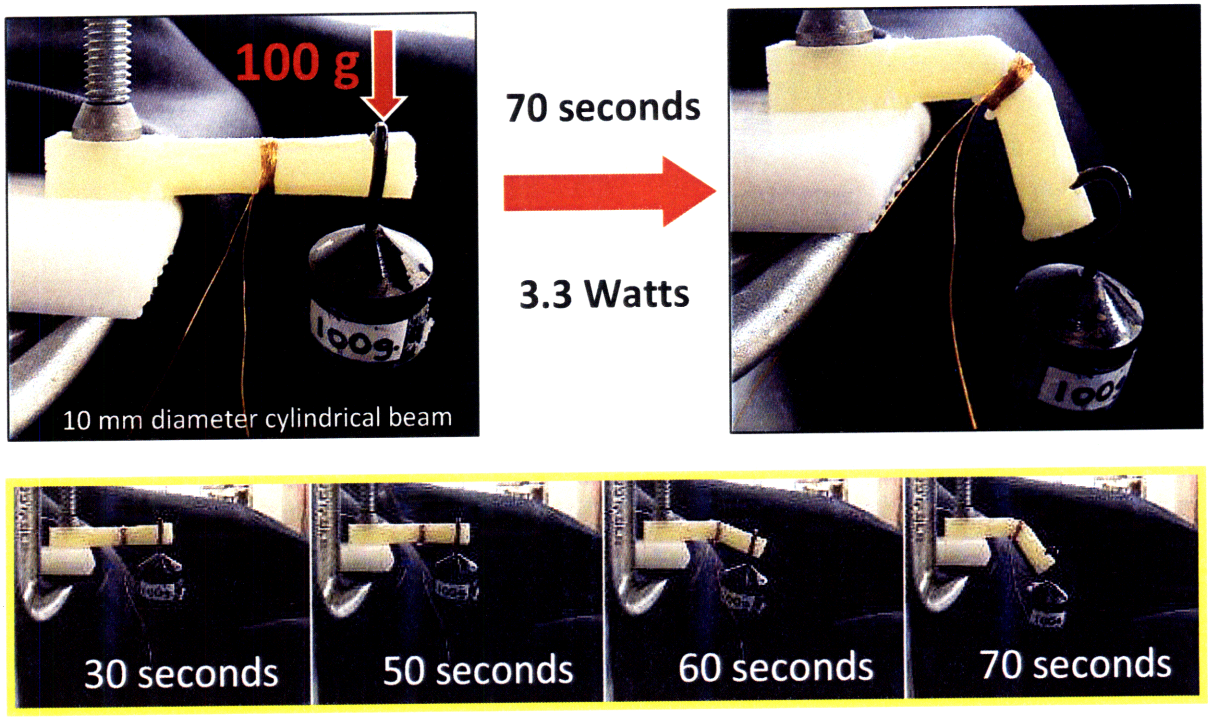

Figure 3.1: A wax-filled cylindrical beam, 10 mm in diameter, in its non-actuated (to left) and actuated (top right) states. A series of images also shows the beam during the activation process, during which the joint transformed from being a rigid to compliant via resistive heating.

Observations indicated that the heating was localized, as only a narrow portion of the beam encompassing the heating element (~1 mm to each side of the wire) was activated, or adequately heated to change states. This was determined by visually identifying which portions of the composite contained melted wax. In other words, the heat did not dissipate along the length of the beam. Therefore, the bending joint was a universal joint that could easily be isolated.

The activated portion of the composite was also extremely compliant; it required minimal force to actuate the joint and to fluidly move the cantilevered end through various positions. Once the joint was allowed to cool in a deflected position, it was able to rigidly maintain its configuration. For example, after the beam shown in Figure 3.1 cooled in its bend position, it was able to rigidly support the 100 gram mass even when the beam was flipped upside down (i.e., rotated 180° about its long axis). After three or so activation and actuation cycles, the foam showed no signs of tearing. However, wax started seeping into the layers of the coiled wire, thus weakening the composite because the foam was no longer fully saturated. This could be

prevented in the future by exploring other heating options or isolating the wire (for instance, by placing an impermeable membrane between the composite and the heating wire).

Because wrapping wire outside of the composite was inefficient, in that it allowed significant heat to dissipate into the air, composite beams were made with wires running through them to create bending joints. In these samples, a single nichrome wire was stitched through a square beam cross section—approximately 5 mm by 5 mm—so that the length of the wire was perpendicular to the length of the beam. A wire could not be weaved through the same cross section many times because it would compromise the strength of the composite. This method of running the heating element through the structure was not as successful as the previous one, in which the wire was wrapped around the outside of the composite. Not only did the former method take more time to adequately heat the areas that strain during bending, but the outer perimeter of the foam tended to tear when the composite was forced to bend. This is most likely because, for a bending element, the outside of the beam strains first and is strained the most. Therefore, it might be efficient to provide the outer perimeter with the most heat to prevent the wax from cooling and causing the foam to tear.

Significant work can be done to improve the efficiency and repeatability of a controllable-stiffness structure, namely one that can be used as a universal joint. Aside from the immediate application of using such a component in SQUISHbot, a continuous universal joint could also replace rigid, traditional ones in general robotic applications.

3.1.2 Three-legged mechanism modeled after Boston Dynamics robot

During Phase I of SQUISHbot, several distinct areas of research were conducted in parallel. Aside from characterizing and developing novel structures for soft robotics, robot prototypes were designed and constructed out of more traditional mechanical components to explore locomotion principles. Specifically, Boston Dynamics developed a concept for a three-legged robot, as shown in Figure 3.2, whose legs had mid-length bending joints that enabled the robot to locomote using an inch-worming gait; the legs bent and extended to allow the two end plates to move relative to each other. Only two legs are necessary for this type of inch-worming motion, though a third leg was added to add another degree of freedom.

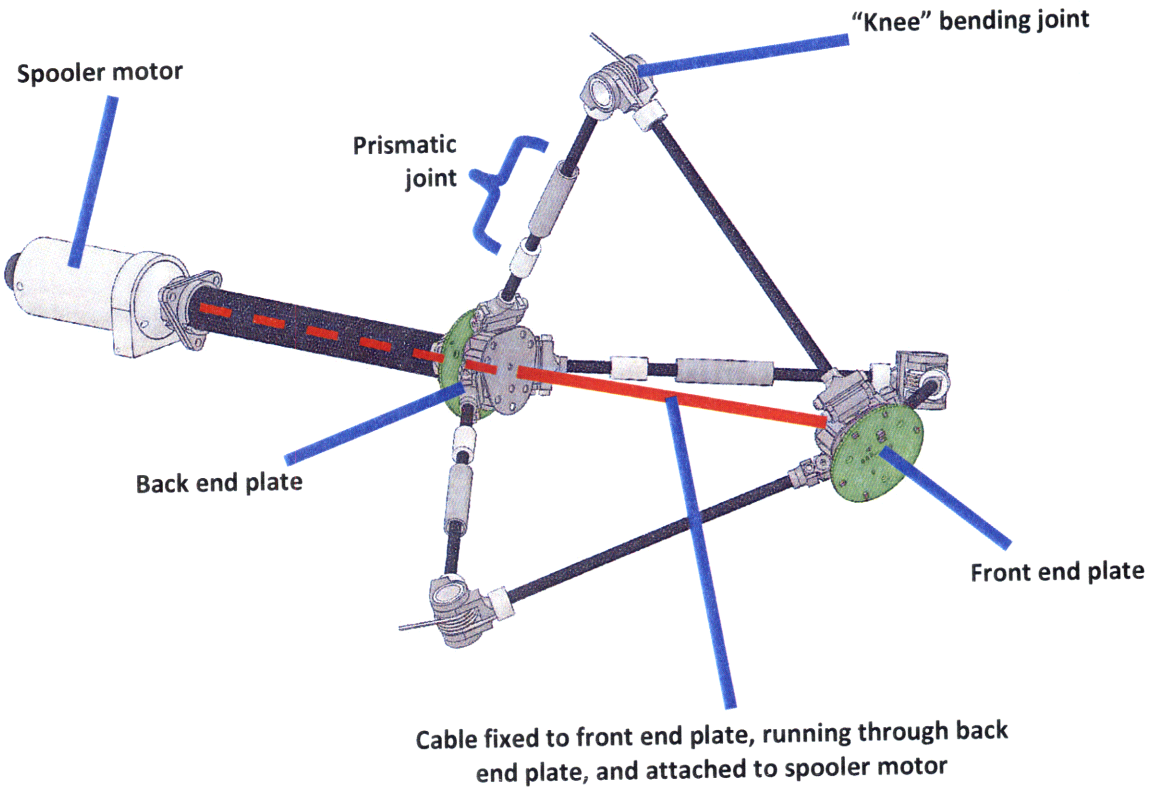

Figure 3.2: Boston Dynamics version of 3-legged robot (CAD model). Image courtesy of Boston Dynamics.

Each of the three legs was composed of: a bending "knee" joint in the middle of its length, a prismatic joint to increase the mechanism's degrees of freedom, and hinged ends that allowed the legs to pivot relative to the end plates. The length of the legs were also designed so that, when bent and completely folded in on themselves, the entire mechanism could achieve a 10:1 reduction in length (and 1:10 expansion in diameter) to fulfill the Phase I dimension-change specifications.

The highlight of this design is that the mechanism can function with only one actuator and multiple "activators." A single cable, running through the two end plates, acts as a tendon that can be pulled in tension or allowed to slack by an actuator, such as spooler motor. Multiple passive joints can be locally activated (i.e., locked or unlocked) to dictate the mechanism's configuration when the tendon is pulled in tension. In this particular design, the knee joints, prismatic joints, and hinges at the ends of the legs can be locally activated to be locked (to prohibit motion) or unlocked (to allow for motion).

While Boston Dynamics built a fully functioning version of this design using traditional rigid components, a simple version of this three-legged mechanism—sans the prismatic components—was constructed using the universal joints described in 3.1.1 as the knee joints. The hinged joints at the ends of the legs were passive pin joints. Because the primary purpose of this version was to test the functionality of fluid-foam composites as tunable bending joints, rigid 3D-printed components were used as the remainder of the mechanism. Figure 3.3 shows the mechanism in its fully elongated state. The blown-up image on the right shows the wax-filled foam joints with copper wire heating elements wrapped around them; the joints were activated through localized resistive heating, as described in 3.1.1.

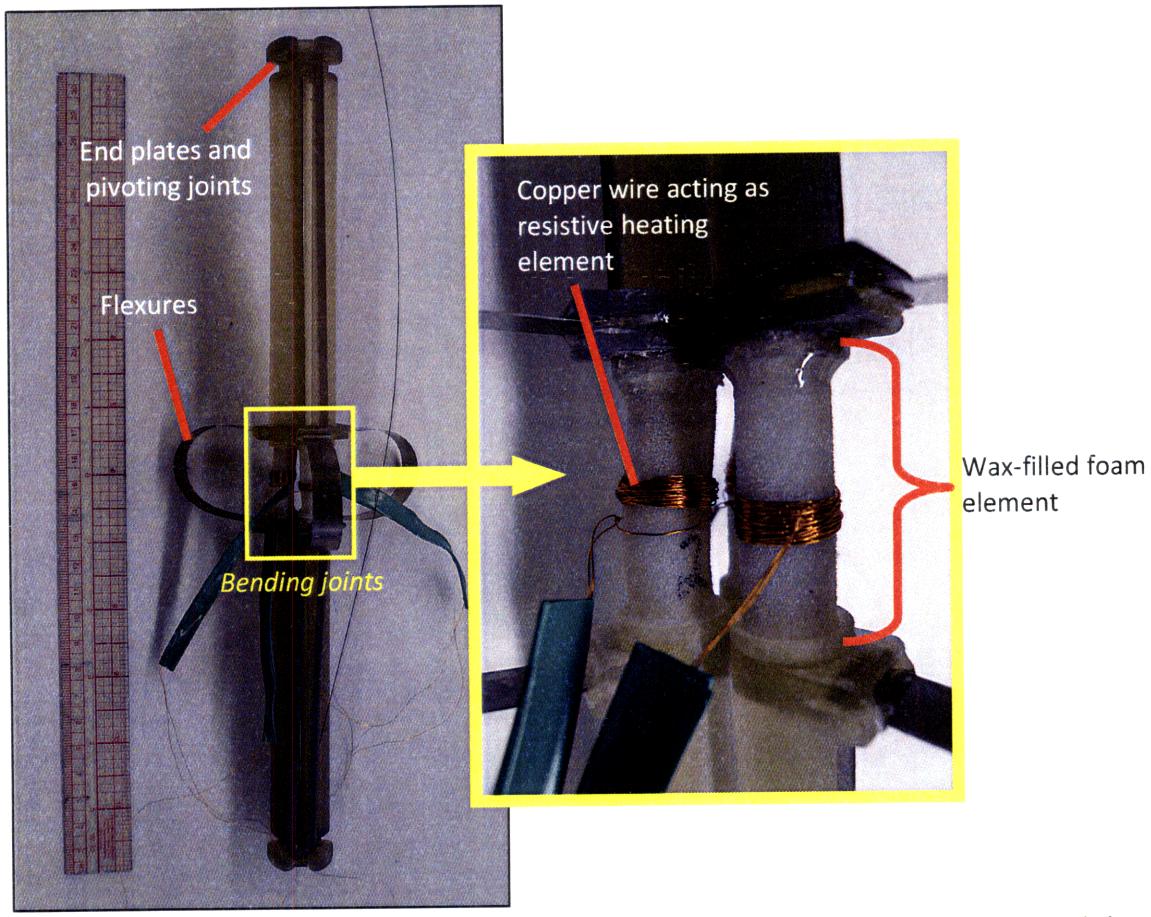

Figure 3.3: 3-legged mechanism with fluid-foam composites acting as bending joints.

The diameter and length of the entire elongated mechanism (as seen in Figure 3.3) was 25.4 mm (1 inch) and 305 mm (12 inches), respectively. The joints in this prototype were 10 mm in diameter, which was arbitrarily selected as a reasonably sized joint to experiment with.

The dimensions of the overall mechanism were chosen based on the assumption that the joints could completely fold on themselves (create a 0° angle) to allow the entire mechanism to achieve at least a 1:10 diameter change.

The metal flexures in this particular version acted as restoring-force structures. Though the three-legged mechanism required an external force to bend the legs once the joints were activated, the flexures provided enough restoring torque to force the legs to passively straighten once the joints were re-activated. Ideally, the composite structure would have adequate stiffness or "shape memory" to passively restore its shape, but the commercially available polyurethane foams used here were incapable of doing so, most likely because they were not stiff enough relative to the softened wax. Figure 3.4 shows the mechanism in its compressed state during a test when the heating elements were activated to locally melt the wax to allow the composites to become compliant bending joints.

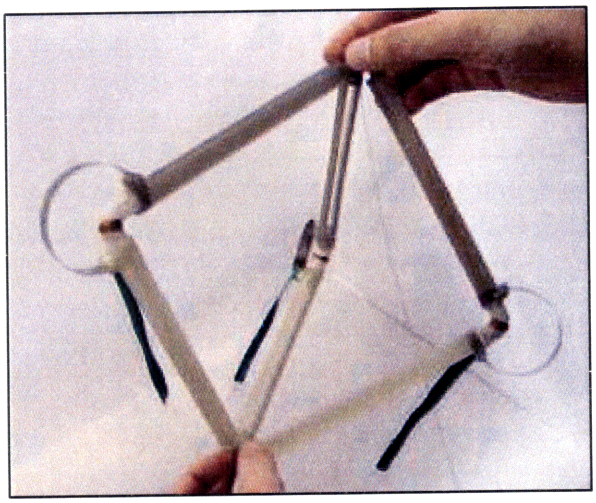

Figure 3.4: 3-legged mechanism with composite bending joints in its maximally compressed state during a test.

The heating element used to activate each wax-foam joint consisted of 36 gauge copper wire wrapped forty times around a 10 mm-diameter composite cylinder. Each joint required 1 amp and 2.2 volts to activate. It only took approximately 30 seconds to activate the joints so that they were compliant enough to be bent by externally pushing the mechanism's end plates towards each other. However, it took approximately 170 seconds for the joints to cool enough to maintain their bent positions after the power was turned off. An external load (here, a person's hands) held the mechanism's end plates relative to each other while the joints were allowed to

cool. This drastic difference between the activation and deactivation times (melting and solidification cycles, respectively) was most likely due to the foam's excellent insulation properties. While the foam efficiently distributed the wires' heat throughout the joint to soften the wax, it also acted an insulator to keep the composite warm even when the power was shut off so that no current was running through the wires. Therefore, future iterations of a similar joint might incorporate a heat sink to expedite the cooling process.

As seen in Figure 3.4, the actuated mechanism with bent legs did not achieve a 10:1 dimension change; with a human in the loop to control how much the joints deflected, the decision to stop bending the legs further was determined by limiting factors that included how stiff the mechanism felt as well has how much wax remained in the composite. Unfortunately, as the wax was melted and the joints were forced to bend during the first activation cycle, some wax was squeezed out of the foam and permanently evacuated from the composite. Despite this, the solidified wax remaining in the composite adequately maintained the joints' bent positions while resisting the restoring forces of the metal flexures. During the second activation cycle, when the power was turned on again so that the heating elements could re-melt the wax in the joints, the preload in the flexures caused the joints to unfold as planned.

Because this prototype of the three-legged mechanism utilized the universal joints discussed in 3.1.1, the challenges it faced were the same as those cited in the previous section. Specifically, wax was squeezed out of the foam when the joints were deflected, which significantly weakened the composite structure after several actuation cycles. However, this problem could be solved by further designing improvements. The time scales associated with operating the joints were also considerably large for robotic applications like SQUISHbot. This drawback might be mitigated, for example, by incorporating a heat sink into the system.

Therefore, while wax is capable of the drastic viscosity and stiffness changes that are desirable for the active-fluid-and-cellular-solid composites being designed, it presents challenges that other fluids with smaller operating time scales, such as MR fluid, might not.

3.1.3 Spine proof-of-concept

One major obstacle of transitioning from traditional robotics to soft robotics is decreasing the number of actuators required in a system, as commonly used actuators—such as motors—are often bulky and unyielding, thus limiting the amount of "softness" and morphability that a robot

is capable of. The spine concept presented in this section can, with just one actuator, achieve what it normally takes multiple actuators to; it elegantly mimics how an octopus—a soft creature that can squeeze itself through tight spaces—operates with a "quasi-articulated structure that resembles the multijointed, articulated limbs of animals with rigid skeletons" [28].

Inspired by the three-legged mechanism's single-actuator design described in 3.1.2, a concept was developed for a multi-degree-of-freedom spine that requires only a single tendon to actuate. Such a mechanism can be useful for not only SQUISHbot—in areas such as steering, manipulation, etc.—but also for general robotics applications, as systems could benefit from decreasing the number of actuators without sacrificing performance. In the medical field, endoscopic devices have largely consisted of systems with multiple actuators to achieve complex maneuverability. A more efficient design might require only one mechanical actuator that is independent of locally tunable areas that determine how the whole structure responds to a central actuation force.

The spine concept presented in this section is shown in Figure 3.5.

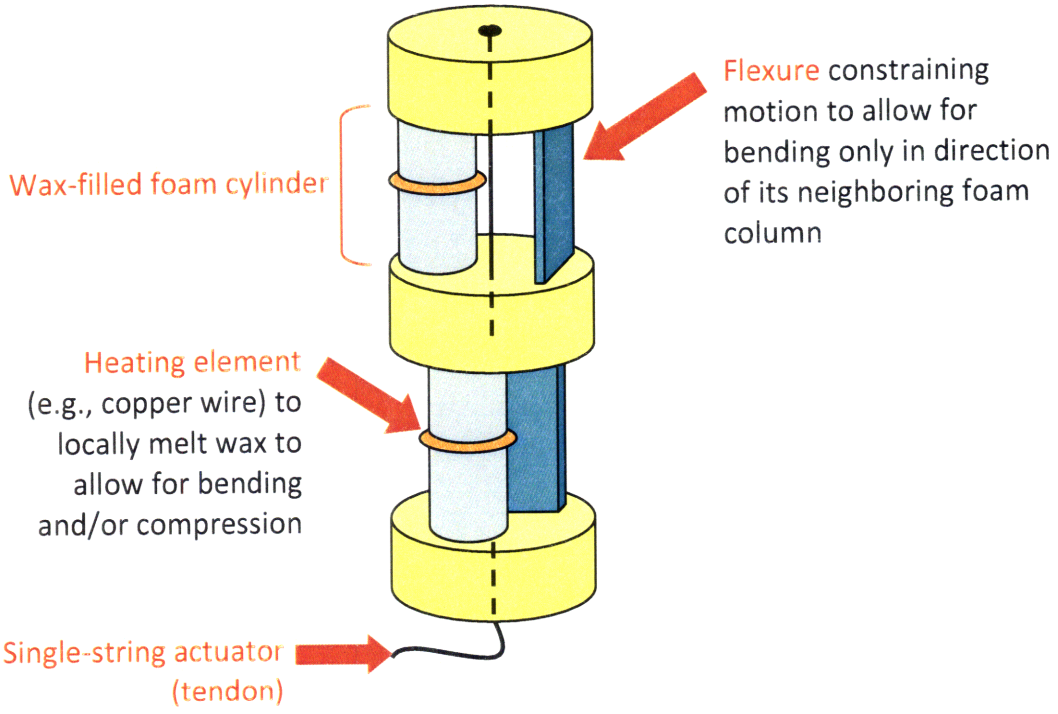

Figure 3.5: Concept for single-actuator, multiple-activators spine.

The design consists of modules that are arranged in series and rotated relative to each other to allow for motion about different axes. Figure 3.5 depicts two modules—each containing a wax-filled foam cylinder and a flexure—rotated 90° relative to each other. Each module has a preferred direction it bends in when the cylinder is compliant. For instance, looking at the top module, if the wax-filled foam cylinder is compliant and the single-string actuator is pulled downwards, the composite cylinder will compress and the top plate of the module will tilt towards the left. This occurs under the assumption that the flexure on the right is stiffer than the activated, compliant wax-foam cylinder. Conversely, if the composite cylinder in the lower module is not activated (or is rigid) when the single-string actuator is pulled, both the composite cylinder and its neighboring flexure should have comparable stiffness to prohibit any motion within that module. A composite can also become rigid in its compressed position so that it can maintain its deformed configuration even when the tendon is released to slack.

The purpose of the flexure is not limited to constraining the direction a module bends in; the flexure also acts as a restoring-force mechanism to return the module to its lengthened position when the composite is compliant and the tendon is allowed to slack.

A result of this spine concept is that multiple decoupled bending directions can be achieved with a single actuator. A demonstration of this concept was fabricated and is shown in Figure 3.6.

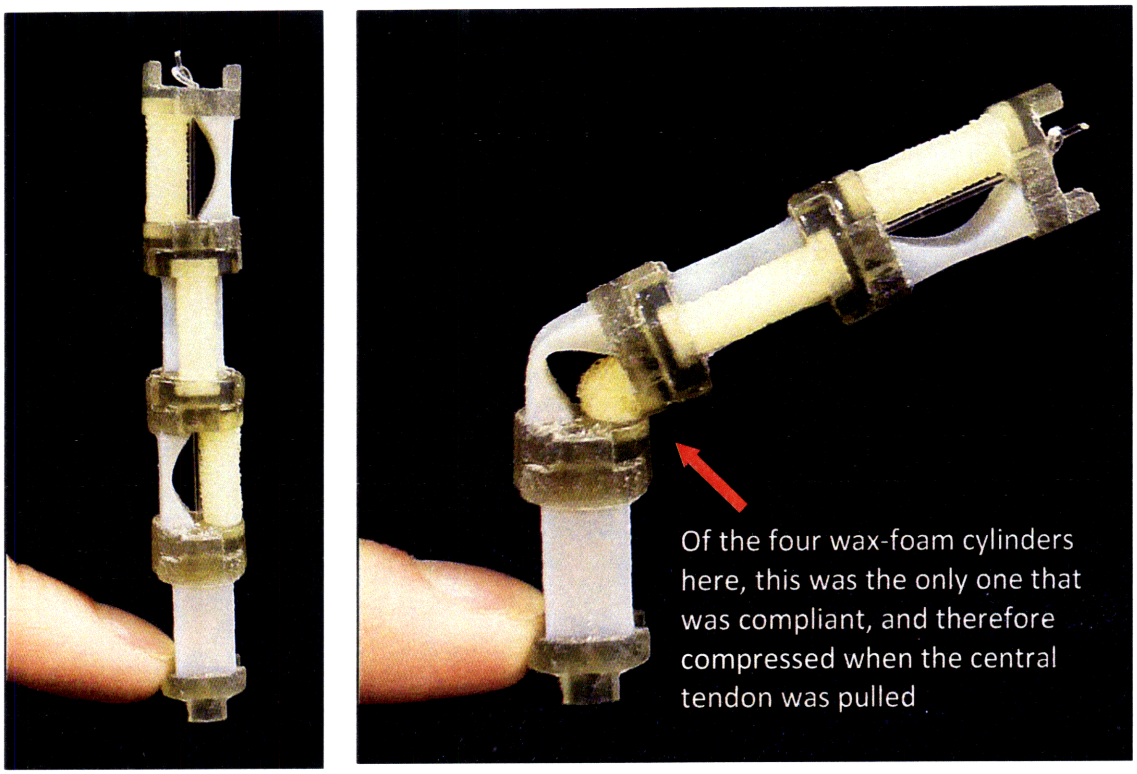

Figure 3.6: Proof-of-concept demonstration of spine.

The spine shown here had four modules oriented 90° relative to one another. The slender yellowish column in each module represented a tunable wax-filled foam element. The grayish curved structure next to each composite element was a 3D-printed contoured flexure made of a polymer with adequate stiffness to restore each module to its elongated position. A piece of fishing line running through the length of the spine was externally accessible and acted as the central tendon.

In this demonstration, the non-activated, rigid composite elements were made of polyurethane foam columns fully saturated with wax, while the activated, compliant composite elements were represented by identical foam columns that were empty (i.e., they had no wax in them). Therefore, rather than heating wax-foam composites to create compliant modules, the activated composites were simulated by using empty foam columns, which are compliant and deformable when the central tendon is pulled. Figure 3.7 shows the spine in a series of configurations created by selectively inserting rigid or compliant foam elements in each module.

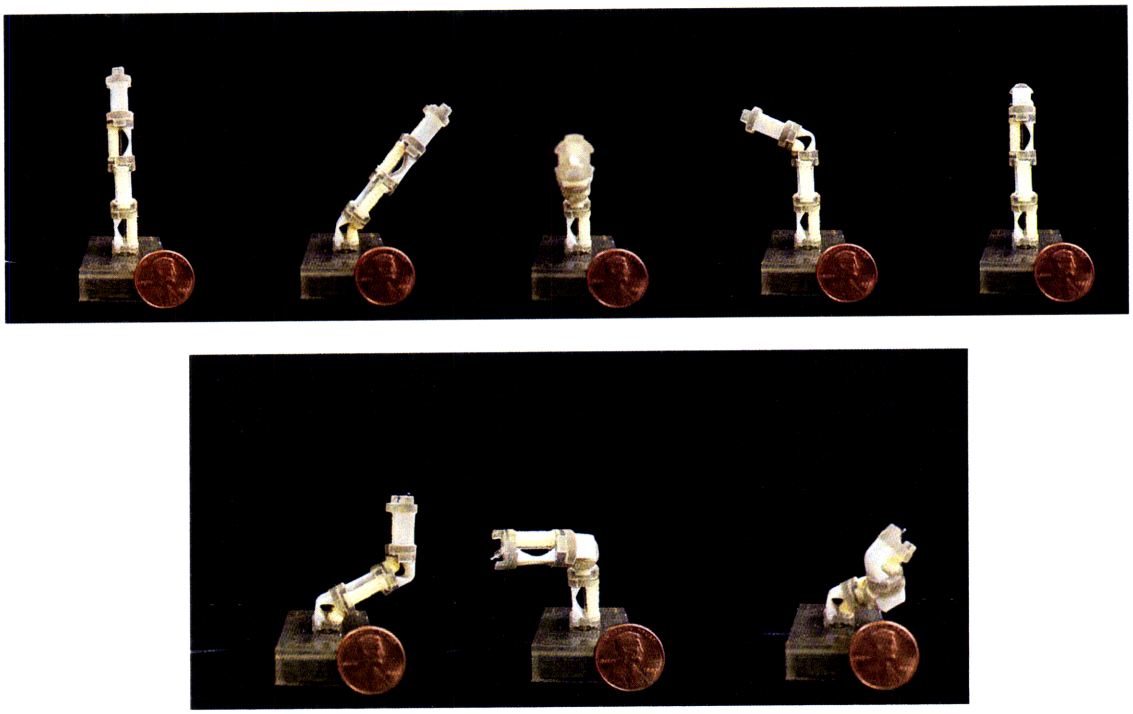

Figure 3.7: Proof-of-concept spine shown in a series of configurations.

Future implementations of this concept can be made of a single anisotropic "foam," similar to those described in 2.4.4.2, that is designed to have the same structural and mechanical properties as the modular mechanism presented here.

3.2 Future work

Future research will primarily be involved with further developing the wax-foam composites that have been the focus of the work presented in this chapter. The development of more advanced composites, such as those utilizing smart fluids and user-designed foams, will require extensive research in the more distant future.

3.2.1 Thermal activation challenges

As previously mentioned, one of the main challenges of the current implementation of the thermally-activated wax-foam composites is to design the system so that the fluid does not leave the composite when it is melted. During an activation cycle for the bending joints, the compressed joints foam tended to squeeze out and permanently evacuate some wax, reducing the amount of wax available to serve as a structural mechanism for future activation cycles. It was

also observed that some of the wax would seep into and stay in the coiled wire heating elements, further reducing the amount of wax available to reinforce the strength of the foam.

These negative outcomes could be mitigated through various methods. First, a sleeve could be integrated into the device to prevent any wax from permanently leaving the composite. Because the foam has favorable wicking properties, it might be more likely to reabsorb the wax if a sleeve contained the entire composite. The wire heating elements could also be wrapped outside of the sleeve so that the melted wax cannot spread between the layers of wire. Research has begun to test the feasibility of using materials like latex sheets and liquid silicone as appropriate containment solutions. Alternatively, other technologies, such as Kapton heaters, can be investigated to serve both as a heating element and a containment mechanism for the composites.

3.2.2 Development of a functioning spine

The spine concept presented in 3.1.3 shows promise for a range of robotic applications. Work will be conducted in the near future to develop a fully functioning spine, with activated fluid-foam composite elements, to evaluate its performance based on metrics such as precision and repeatability. A single cable attached to a spooler motor can serve as the central actuator of the device. To construct a functioning, repeatable system, the previously mentioned fluid-containment issues must be first addressed.

3.2.3 Implementation of a functioning compression module

While 3.1 discussed several designs and methods for constructing bending elements out of fluid-foam composites, little work has been done to develop a functioning compression module. A compression element might be useful as a prismatic mechanism in robotics applications like SQUISHbot, in which a structure might need to contract to perform certain tasks, such as locomotion via an inch-worming gait. One reason why a functioning compression element has not yet been developed is because—unlike for a bending element—a significant volume of fluid might evacuate the foam when a composite structure is compressed. For most applications, the fluid needs to be used for multiple actuation cycles, but storing evacuated fluid is a difficult challenge that has not yet been overcome.

As previously discussed, one can imagine a flexible sleeve containing a fluid-foam composite that stretches to contain any fluid that leaves the foam when the composite is compressed; the sleeve allows the evacuated fluid to be accessible so that the foam can reabsorb the fluid when the composite returns to its elongated state. While this solution seems simple, additional research and testing needs to be performed to successfully develop a functioning fluid-foam prismatic mechanism.

Candidate designs for a compression module have been developed. Figure 3.8 shows a CAD model of a prismatic mechanism that can be integrated into the single-actuator spine concept described in 3.1.3. This prismatic element can be selectively activated or deactivated (like the individual tilting modules in Figure 3.6) to act as a rigid structure or a compliant "joint" that compresses when the single-string actuator is pulled. To constrain the compression to linear motion only, sliding concentric tubes form a linear guide that runs through the center of the module. Also, while the foam component would ideally have enough restoring force to return the module to its elongated state when necessary, a coiled spring might be integrated into this concept as a restoring force mechanism.

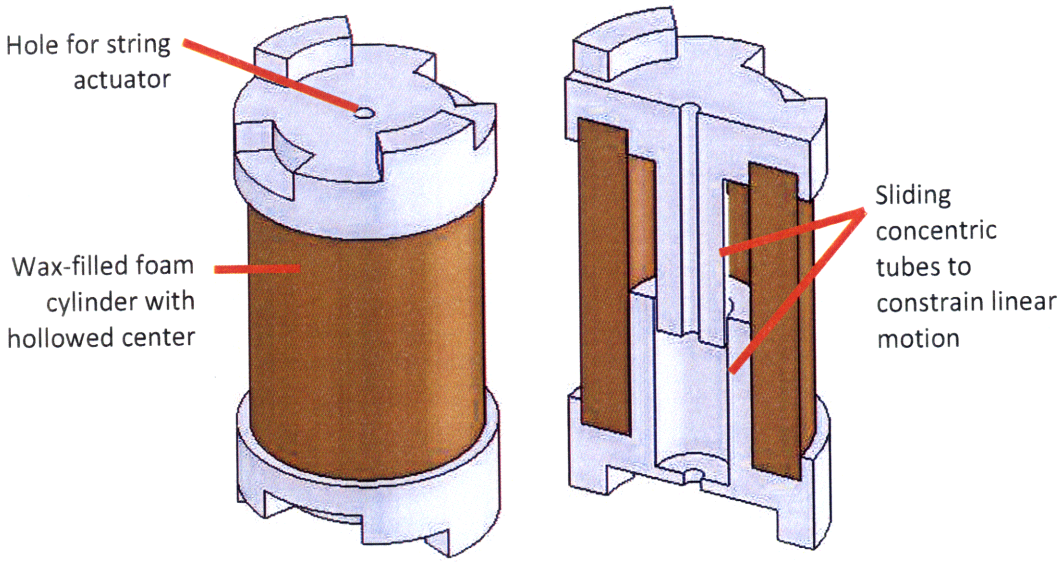

Figure 3.8: CAD model for compression module that can be integrated into spine mechanism.

A simple demonstration—similar to the one depicted in Figure 3.6, where rigid, non-activated elements were represented by fully saturated wax-foam composites while activated, compliant elements were represented by empty foam pieces—of this prismatic mechanism is shown in Figure 3.9. Polyurethane foam was used as the foam component of the composites. Of the three modules shown, only the middle one represented an activated, compliant module because its foam component was not saturated with wax . Therefore, when the actuation cable (a fishing line running through all three modules) was pulled, only the middle module compressed, as seen in the image on the right.

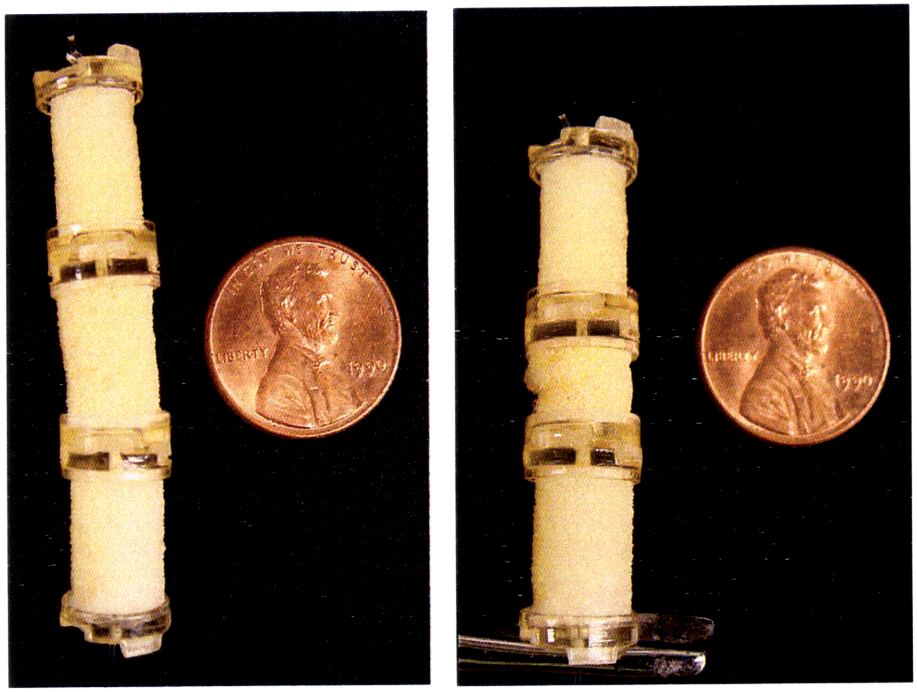

Figure 3.9: A demonstration of a prismatic element that can be integrated into the single-actuator spine concept.

CHAPTER 4

CONCLUSIONS

The aim of the work presented in this thesis was to establish a novel approach for realizing soft robotics. Most attempts to create soft robots have involved adopting the infrastructure of modern-day robots—which often rely on multiple fixed actuators to drive discrete elements—and replacing rigid components with soft ones. Unfortunately, there has been minimal success in developing soft actuators that even approach the performance capabilities of traditional robotic components. Therefore, rather than modifying the design of a current robot to produce a soft one, the approach taken in this thesis was to investigate a new class of meso-scale fluid-foam composites that have controllable stiffness, so that a continuous structure can take the form of a single robot.

Meso-scale composites allow for a large design space, as multiple components can be individually selected to contribute to an overall architecture. The research described in this thesis focused on a specific controllable stiffness composite: an open-cell polyurethane foam saturated with wax. The advantage in studying a composite like this is that both classes of materials are widely commercially available and can be easily experimented with. Because wax can take the form of both a liquid with low viscosity as well as a solid with high stiffness, the composite was capable of being thermally activated to transition from a stiff, load-bearing structure to a morphable, compliant one. The primary drawback of using wax in robotic applications is that it takes a significant amount of time to activate (melt) and deactivate (cool), thus limiting the operating speed of a robot, which is often a crucial performance metric. In addition to the wax component, the purpose of the foam was to act as a shape-memory scaffold in which the wax naturally wicked into, thus maintaining the form of the composite even as it transforms between different states and configurations.

This thesis focused on two main areas to investigate the potential of these wax-foam composites. The majority of the research involved characterizing the mechanical properties of the composites to understand their capabilities as structural elements. Composites were also used in proof-of-concept implementations to explore innovative methods of utilizing controllable stiffness materials in robotics. In the first part of the research, compression tests were performed on rigid samples to characterize their empirical modulus. Significant research needs to be conducted in the future to quantify how well the composites can transition between stiff and compliant states. This might involve thermally activating and deactivating samples during cyclic compression and bending tests. In the second portion of the research, several challenges arose in the promising yet rudimentary proof-of-concept work. For instance, there was no trivial method for packaging the composites so that they could be robust elements with repeatable performance capabilities. Future work will also involve developing creative solutions to solve these types of problems.

Research will be conducted in parallel to continue to explore the design space for this novel class of controllable stiffness composites. Smart fluids, such as electrorheological and photorheological ones, can be used to further the possibilities of these materials. While the wax-foam composites that have been developed might not be ideal for robotics—mostly because of their significant activation and deactivation times—they still play an important role in demonstrating how similar combinations of materials can transcend the current state of soft robotics.

REFERENCES

[1] Hakozaki, M., H. Oasa, and H. Shinoda. "Telemetric robot skin." *Robotics and Automation, 1999. Proceedings. 1999 IEEE International Conference on.* 1999, 957-961 vol.2.

[2] Hirzinger, G., N. Sporer, A. Albu-Schaffer, M. Hahnle, R. Krenn, A. Pascucci, and M. Schedl. "DLR's torque-controlled light weight robot III-are we reaching the technological limits now?." *Robotics and Automation, 2002. Proceedings. ICRA '02. IEEE International Conference on.* 2002, 1710-1716 vol.2.

[3] Sasaki, D., T. Noritsugu, and M. Takaiwa. "Development of Active Support Splint driven by Pneumatic Soft Actuator (ASSIST)." *Robotics and Automation, 2005. ICRA 2005. Proceedings of the 2005 IEEE International Conference on.* 2005, 520-525.

[4] Sugiyama, Y. and S. Hirai. "Crawling and jumping of deformable soft robot." Intelligent Robots and Systems, 2004. (IROS 2004). Proceedings. 2004 IEEE/RSJ International Conference on. 2004, 3276-3281 vol.4.

[5] Hunter, I. W. and S. Lafontaine. "A comparison of muscle with artificial actuators." *Solid-State Sensor and Actuator Workshop, 1992. 5th Technical Digest., IEEE.* 1992, 178-185.

[6] Caldwell, D. "Natural and artificial muscle elements as robot actuators." *Mechatronics* 3 (June 1993): 269-283.

[7] Herr, Hugh, R. Dennis. "A swimming robot actuated by living muscle tissue." *Journal of NeuroEngineering and Rehabilitation* 1 (2004).

[8] Grissom, Michael D., et al. "Design and experimental testing of the OctArm soft robot manipulator." SPIE, 2006.

[9] Trimmer, Barry A., A. Takesian, B. Sweet, C. Rogers, D.Hake, D.Rogers. "Caterpillar locomotion: A new model for soft-bodied climbing and burrowing robots." *7th International Symposium on Technology and the Mine Problem.* Monterey, CA. May 2-5, 2006.

[10] Crespi, A., A. Badertscher, A. Guignard, and A. Ijspeert. ": an amphibious snake-like robot." *Robotics and Autonomous Systems* 50 (March 2005): 163-175.

[11] Ginder, John M., M. Nichols, L. Elie, and S. Clark. "Controllable-stiffness components based on magnetorheological elastomers." SPIE, 2000, 418-425.

[12] Kornbluh, Roy D., H. Prahlad, R. Pelrine, S. Stanford, M.. Rosenthal, and P.von Guggenberg. "Rubber to rigid, clamped to undamped: toward composite materials with wide-range controllable stiffness and damping." SPIE, 2004, 372-386.

[13] Defense Sciences Office, "Defense Sciences Research and Technology Special Focus Area: Chemical Robots," accessed May 4, 2009, <http://www.darpa.mil/dso/solicitations/baa07-21mod2.html>.

[14] Gibson, Lorna J., M. Ashby. *Cellular Solids: Structure and Properties.* 2 edition. Cambridge University Press, 1999.

[15] Warner, M., B. Thiel, and A. Donald. "The elasticity and failure of fluid-filled cellular solids: Theory and experiment." *Proceedings of the National Academy of Sciences of the United States of America* 97 (February 2000): 1370-1375.

[16] Georget, D. M. R., A. C. Smith, and K. W. Waldron. "Modelling of carrot tissue as a fluid-filled foam." *Journal of Materials Science* 38 (May 2003): 1933-1938.
[17] Boomsma, K. "On the effective thermal conductivity of a three-dimensionally structured fluid-saturated metal foam." *International Journal of Heat and Mass Transfer* 44 (February 2001): 827-836.
[18] Lu, T. "Heat transfer in open-cell metal foams." *Acta Materialia* 46 (June 1998): 3619-3635.
[19] J. R. Ehrlich, "Pore-Filled, Open-Cell Foam," U.S. Patent No. 3,471,419, Oct. 7, 1969.
[20] R. Harvey, William H. Harvey Company, "Sealing Gasket Means," U.S. Patent No. 3,400,411, Sept. 10, 1968.
[21] Suh, J. W., S. Homans, and M. Yim. "Telecubes: mechanical design of a module for self-reconfigurable robotics." *Robotics and Automation, 2002. Proceedings. ICRA '02. IEEE International Conference on.* 2002, 4095-4101 vol.4.
[22] Kajita, S., O. Matsumoto, and M. Saigo. "Real-time 3D walking pattern generation for a biped robot with telescopic legs." *Robotics and Automation, 2001. Proceedings 2001 ICRA. IEEE International Conference on.* 2001, 2299-2306 vol.3.
[23] Chan, B., T. Guo, and A. Hosoi. "Snail-Inspired Biomimetic Devices." *APS Meeting Abstracts* (November 2006).
[24] Ewoldt, Randy H., C. Clasen, A. Hosoi, and G. McKinley. "Rheological fingerprinting of gastropod pedal mucus and synthetic complex fluids for biomimicking adhesive locomotion." *Soft Matter* 3 (2007): 634-643.
[25] Carlson, J. D., D. Catanzarite, and K. St. Clair. "Commercial Magneto-Rheological Fluid Devices." *5th Int. Conf. on Electro-Rheological, Magneto-Rheological Suspensions and Associated Technology.*
[26] Jolly, Mark R., J. Bender, and D. Carlson. "Properties and Applications of Commercial Magnetorheological Fluids." *SPIE 5th Annual Int. Symposium on Smart Structures and Materials,.* March 1998.
[27] Carlson, J. "MR fluid, foam and elastomer devices." *Mechatronics* 10 (June 2000): 555-569.
[28] Sumbre, German, G. Fiorito, T. Flash, and B. Hochner. "Neurobiology: Motor control of flexible octopus arms." *Nature* 433 (February 2005): 595-596.
[29] Elliott, J., et al. "In-situ deformation of an open-cell flexible polyurethane foam characterised by 3D computed microtomography." *Journal of Materials Science* 37 (April 2002): 1547-1555.